

*Synthesis and Characterisation of Visible Light
Responsive Photocatalysts for Solar Fuel Production and
Synthesis of Fine Chemicals*

A Thesis Submitted

In Partial Fulfillment of the Requirements for the Degree of

DOCTOR OF PHILOSOPHY

In

Chemistry

By

Sandeep Kumar

Reg. No. 2020098002

Under the Supervision

Prof. Rajesh Kumar Yadav



Department of Chemistry & Environmental Science

Madan Mohan Malaviya University of Technology, Gorakhpur (U.P.),

INDIA

January, 2024

© M. M. M. University of Technology, Gorakhpur, (U.P.) – 273010,

INDIA

ALL RIGHTS RESERVED

Certificate

Certified that *Sandeep Kumar* has carried out the research work presented in this thesis entitled “*Synthesis and Characterisation of Visible Light Responsive Photocatalysts for Solar Fuel Production and Synthesis of Fine Chemicals*” for the award of Doctor of Philosophy in Chemistry from Madan Mohan Malaviya University of Technology, Gorakhpur under my supervision. The thesis embodies result of original work and studies carried out by student himself and the contents of the thesis do not form the basis for the award of any other degree to the candidate or to anybody else.

Signature of Supervisor(s)

Name: Dr. Rajesh K. Yadav

(Professor)

Department of Chemistry & Environmental Science

Madan Mohan Malaviya University of Technology,

Gorakhpur-273010

India(U.P.)

Date: .././....

Candidate's Declaration

I declare that this written submission represents my work and ideas in my own words and where other ideas or words have been included, I have adequately cited and referenced the original sources. I also declare that I have adhered to all principles of academic honesty and integrity and have not misrepresented or fabricated or falsified any idea/data/fact/source in my submission. I understand that any violation of the above will be cause for disciplinary action by the University and can also evoke penal action from the sources which have thus not been properly cited or from whom proper permission has not been taken when needed.

(Signature)

Sandeep Kumar

(Name of the student)

2020098002

(Roll No.)

Department of Chemistry & Environmental Science

(Name of Department)

Date: ../.. /.....

Approval Sheet

This thesis entitled “*Synthesis and Characterisation of Visible Light Responsive Photocatalysts for Solar Fuel Production and Synthesis of Fine Chemicals*” by Sandeep Kumar is approved for the degree of Doctor of Philosophy in Chemistry.

Examiner

Supervisor (s)

Head of Department

**Dean, Research & Development or
Other Dean/Professor to be nominated
by the Vice Chancellor in his absence**

Date: _____

Place: _____

Acknowledgement

First and foremost, I would like to express my sincerest thanks to my supervisor **Prof. Rajesh Kumar Yadav** (DST Ramanujan Fellow, Department of Chemistry and Environmental Science, Madan Mohan Malaviya University of Technology, Gorakhpur) for their unwavering support, guidance, and encouragement throughout the research process. Their knowledge, experience, and insights have been invaluable in shaping the direction of this thesis, as well as providing feedback and constructive criticism that has helped me to improve my work. I am indebted to them for their mentorship, and I am grateful for the time and effort they have invested in me.

I would also like to extend my thanks to **Prof. Poran Prakash Pande** (Professor, Department of Chemistry & Environmental Science Department M. M. M. University of Technology, Gorakhpur), **Prof. Tae Wu Kim** (Department of Chemistry, Mokpo National University, South Korea) for their input on this Ph.D. journey. Their expertise and guidance have been instrumental in shaping the theoretical framework and research methodology used in this thesis. Their attention to detail, valuable insights, and constructive feedback have been extremely helpful in improving the quality of my work. I am honored to have had such a knowledgeable co-supervisor.

Also, I pay my sincere gratitude to another co-supervisor **Prof. Atul Pratap Singh** (Department of Chemistry, Chandigarh University) for his unwavering support and inspiration during my research period.

In addition, I would like to express my appreciation to **Prof. Dilip Kumar Dwivedi** (Department of Physics and material Science, M. M. M. University of Technology, Gorakhpur), **Dr. Vitthal L. Gole** (Professor, Department of Chemical Engineering, M. M. M. University of Technology, Gorakhpur), **Dr. Navneet Kumar Gupta** (Department of Chemistry, Indian Institute of Science, Bangalore) and who have provided me with valuable feedback, insights, and support throughout the research process. Their contributions have been instrumental in shaping and improving this thesis, and I am grateful for their time and expertise. Their willingness to answer my questions, provide feedback, and offer insights has significantly contributed to the quality of my work. I am grateful for their patience, kindness, and dedication to their profession. Special thanks to **Mrs. Reema Yadav** for their constant support.

I must also acknowledge and thank my colleagues, **Dr. Satyam Singh, Dr. Pooja Singh, Dr. Shivani Singh, Dr. Chanadni Singh, Mr. Ravindra K. Shukla, Mr. Rajat Singhal**, who have provided me with support and encouragement throughout the research process. Their feedback and insights have been invaluable in shaping my understanding of the research topic and refining my ideas. Their support and encouragement have made this process much more enjoyable, and their willingness to share their knowledge and expertise has been significant in shaping my research ideas.

Finally, I would like to extend my heartfelt thanks to my family members My father **Shri Subhash Chand** and my mother **Smt Kamlesh Devi**, My Dearest Wife **Mrs. Seema Devi** and Son **Master. Avindra Rajput** who have supported me throughout this journey. Their unwavering love, encouragement, and support have been invaluable in helping me to stay motivated and focused on completing this thesis. They have been my source of inspiration and motivation throughout this journey, and I am grateful for their unwavering support. Their sacrifices and love are the bedrock of my success.

I would like to express my sincere gratitude to all the individuals who have supported and guided me throughout the research process. Their contributions have been invaluable, and I am grateful to have had the opportunity to work with such a talented and dedicated group of individuals. I am honored to have had their guidance and support throughout this journey, and I hope to continue to make them proud in my future endeavors.

By Sandeep Kumar

List of Figures

Figure 1. 1 Several technique employed for the tranformation of CO ₂ in to different useful chemicals/fuels.....	23
Figure 2. 1 Anthropogenic pollutants and their origins. Carbon dioxide (CO ₂), carbon monoxide (CO), nitrogen dioxide (NO ₂), polycyclic aromatic hydrocarbons (PAHs), particulate matter (PM), and volatile organic compounds (VOCs).....	30
Figure 2. 2 An overview illustrating the synthesis of organic compounds utilizing carbon dioxide.	31
Figure 2. 3 Illustrative depiction of the synthesis of g-C ₃ N ₄ photocatalyst as a foundational material through thermal polymerization using different precursors.	35
Figure 2. 4 Photocatalysts derived from g-C ₃ N ₄ for various photocatalytic reactions.	36
Figure 2. 5 Categorization of polymers based on their structures.	37
Figure 2. 6 Several excellent properties of Bakelite	39
Figure 2. 7 Development of Eosin-Y as catalyst in different type reactions	40
Figure 2. 8 Several uses of nicotinamide cofactor (a) 1,4-NADH (b) 1,4-NADPH.....	42
Figure 2. 9 Different uses and their application of solar light produced fine chemical (HCOOH).....	43
Figure 2. 10 Different type medicinal drug molecules and natural products was synthesized by C-H bond generation	44
Figure 2. 11 Various metal catalysed and photocatalyzed protocols for C-H bond formation.....	45
Figure 3. 1 Synthesis of S-g-C ₃ N ₄ photocatalyst.....	51
Figure 3. 2 UV-visible absorption spectra of PDA@S-g-C ₃ N ₄ (red) and S-g-C ₃ N ₄ (blue) photocatalysts.....	53
Figure 3. 3 FTIR spectra of PDA@S-g-C ₃ N ₄ (red) and S-g-C ₃ N ₄ (blue) photocatalysts.	54
Figure 3. 4 Powder X-ray diffraction (PXRD) analysis of as-synthesized P@SGCN photocatalyst.	55

Figure 3. 5 Transmission electron microscopy (TEM) measurement of P@SGCN photocatalyst. (a) TEM image of P@SGCN photocatalyst. (b) Selected area electron diffraction (SAED) image. (c) The one-dimensional profile of the area indicated by the magenta rectangle in the SAED image. The lattice spacing (d-spacing) of 0.333 nm (=1/3.002 nm) corresponds to the (002) planes in the SGCN medium. (d) Elemental mapping measured by the energy dispersive spectroscopy (EDS) for P@SGCN photocatalyst. Left figure shows the target range for the EDS mapping and right figures show the element-specific mapping images. The existence of oxygen element (red color) in the measured range implies that the polydopamine moieties are well doped onto the SGCN medium.....	56
Figure 3. 6 Particle size analysis of (a) S-g-C ₃ N ₄ and, (b)PDA@S-g-C ₃ N ₄ photocatalysts.	57
Figure 3. 7 Zeta potential analysis of (a) S-g-C ₃ N ₄ (-3.39 mV), and (b) PDA @S-g-C ₃ N ₄ (-13.4 mV) photocatalysts.....	58
Figure 3. 8 Photocatalytic activities using polydopamine (P), pristine SGCN, and P@SGCN photocatalysts. Catalytic tests for (a) NADH regeneration and (b) production of HCOOH from CO ₂	59
Figure 4. 1 UV-visible absorption spectra of bromophenol (red colour), bakelite (blue colour) and BPB-composite photocatalyst (black colour).....	68
Figure 4. 2 Fourier-transform infrared (FTIR) spectra of bromophenol and BPB-composite (black colour) photocatalyst.	69
Figure 4. 3 Field emission scanning electron microscopy (FESEM) images of a) bromophenol and b) BPB-composite photocatalyst.	70
Figure 4. 4 Particle size of bromophenol and BPB-composite photocatalyst.....	71
Figure 4. 5 Zeta potential plots of a) bromophenol and b) BPB-composite photocatalyst.	71
Figure 4. 6 EDS of (a) Bromophenol and (b) BPB-composite photocatalyst.....	72
Figure 4. 7 DSC of bromophenol and BPB-composite photocatalyst.	72

Figure 4. 8 Photocatalytic activity of bromophenol and BPB-composite photocatalyst for (a) NADH regeneration and (b) artificial photosynthetic production of formic acid from CO ₂	74
Figure 4. 9 Reusability and stability test of BPB-composite photocatalyst for 1,4-NADH regeneration.....	75
Figure 4. 10 Chromatogram of HPLC	76
Scheme 1. 1 Schematic illustrations of natural photosynthesis. In natural photosynthesis photoexcited electrons are transferred through Photosystem II (PS II) and I (PS I) for the reduction of oxidized NADP ⁺ into NADPH cofactors. (PQ = plastoquinone, PC = plastocya	24
Scheme 1. 2 Illustrative depiction of a photocatalytic-biocatalytic artificial photosynthetic system for regenerating 1,4-NADH/NADPH and formic acid from CO ₂ . This process involves the formate dehydrogenase enzyme and operates through an electron transfer mechanism	27
Scheme 2. 1 Illustration of natural and artificial photosynthetic system process.	32
Scheme 3. 1 Artificial photosynthesis process based on P@SGCN photocatalyst/biocatalyst coupled process for the generation of HCOOH from CO ₂ under the irradiation of solar light.	50
Scheme 3. 2 Schematic diagram of the preparation of the PDA@S-g-C ₃ N ₄ photocatalyst.	52
Scheme 4. 1 Schematic illustrations of Z-scheme in natural photosynthesis. The absorption of solar light energy by chlorophyll in the leaves of plants causes electrons to excite. NAD ⁺ is reduced to NADH as a result of a sequential multi-electron transfer. The	

cofactor thus formed is used to produce carbohydrates in the Calvin cycle (PC = plastocyanin, PQ = plastoquinone, FR = ferredoxin and Cyt = cytochrome complex) [146][148]	64
Scheme 4. 2 Synthesis of BPB-Composite.	65
Scheme 4. 3 Schematic illustration of a BPB-composite photocatalyst-enzyme coupled system for formic acid production from CO ₂	68
Scheme 4. 4 Plausible NAD ⁺ reduction for the production of ‘enzymatically active/inactive’ isomers of NADH via free radical intermediates.	77
Scheme 5. 1 Diagrammatic illustration of: (a) Photocatalytic electronic structure and Gibbs free energy change in photocatalytic process. (b) UP-hill of photocatalytic reactions.	82
Scheme 5. 2 (a) Schematic illustration of HCOOH production from CO ₂ via the route of photo&biocatalyst integrated system. (b) Synthesis of EY@DEHB photocatalyst via Pd-catalyzed.	83
Scheme 5. 3 Synthetic scheme of EY@DEHB photocatalyst via coupling of EY and DEHB at 90oC temperature for 72h.	85
Scheme 5. 4 Three-dimensional structure of EY@DEHB photocatalyst.....	85
Scheme 5. 5 Synthesis of organometallic rhodium complex.	86
Scheme 5. 6 Plausible electrochemical reduction of NAD ⁺ via free radical intermediates to be formed ‘enzymatically active/inactive’ NADH isomers.....	97
Scheme 6. 1 Polydopamine modified photocatalyst catalyzed the artificial photosynthesis process for the generation of HCOOH from CO ₂ under sun ray irradiation.....	101
Scheme 6. 2 Grafting of Polymer Brushes onto SGCN under Visible- Light Irradiation	103

List of Symbols

G	Gibbs free energy
ζ	Zeta potential
λ	Wavelength
$^1\text{O}_2$	Singlet oxygen
$^3\text{O}_2$	Triplet oxygen
$\text{O}_2^{\bullet-}$	Superoxide radical anion
δ	Chemical shift
s	Singlet
m	Multiplet
$^1\text{PC}^*$	Excited singlet state of photocatalyst
$^3\text{PC}^*$	Excited triplet state of photocatalyst
mmol	Millimole
μL	Microliter
μmol	Micromole
U	Unit
nm	Nanometer
1D	One-dimensional
2D	Two-dimensional
3D	Three-dimensional
eq./equiv.	Equivalent
MHz	Megahertz
eV	Electron volt

List of Abbreviations

HOMO	Highest occupied molecular orbital
LUMO	Lowest unoccupied molecular orbital
PS II	Photosystem II
PS I	Photosystem I
ATP	Adenosine triphosphate
Pc	Plastocyanin
Fd	Ferredoxin
FNR	Ferredoxin–NADP ⁺ oxidoreductase
AsA	Ascorbic acid
TEOA	Triethanolamine
ET	Electron transfer
NAD ⁺	Nicotinamide adenine dinucleotide (oxidized form)
NADH cofactor	Reduced 1,4-dihyronicotinamide adenine dinucleotide
NADP ⁺ form)	Nicotinamide adenine dinucleotide phosphate (oxidized
NADPH	Reduced 1,4-dihyronicotinamide adenine dinucleotide phosphate cofactor
ADPR	Adenosine diphosphate ribose
VB	Valence band
CB	Conduction band
PC	Photocatalyst
CTFs	Covalent triazine frameworks
COF	Covalent organic framework
GDH	L-glutamate dehydrogenase
F _{ate} DH	Formate dehydrogenase
UV-Visible	Ultraviolet–Visible
FT-IR	Fourier transform infrared
FE-SEM	Field emission scanning electron microscopy
AFM	Atomic force microscopy
BET	Brunauer–Emmett–Teller
DSC	Differential scanning calorimetry

DLS	Dynamic light scattering
PXRD	Powder X-ray diffraction
NMR	Nuclear magnetic resonance
TD-DFT	Time-dependent density-functional theory
MOs	Molecular orbitals
ICT	Intramolecular charge transfer
CV	Cyclic voltammetry
TGA	Thermogravimetric analysis
DTA	Differential thermal analysis
DTG	Derivative thermogravimetric
SET	Single electron transfer
PT	Proton transfer
ISC	Inter system crossing
RH	Relative humidity
CO ₂	Carbon dioxide
N ₂ O	Nitrous oxide
CH ₄	Methane
PFCs	Perfluorocarbons
HFCs	Hydrofluorocarbons
SF ₆	Sulfur hexafluoride
g-C ₃ N ₄	Graphitic carbon nitride
P	Polydopamine
P@SGCN carbon nitride	polydopamine (P) modified sulfur-doped graphitic carbon nitride
T	Thiourea
D	Dopamine
S-gC ₃ N ₄	Sulfur doped graphitic nitride
B	Bromophenol blue
BPB	Bromophenol bakelite composite
F	Formaldehyde
EY	Eosin-Y
DEHB	3, 5-diethynyl-4-hydroxybenzaldehyde
PVDHFP	Poly (vinylidene fluoride- <i>co</i> -hexafluoropropylene-)

Abstract

Name of the Student	Sandeep Kumar
Roll No.	2020098002
Degree	Doctor of Philosophy in Chemistry
Thesis title	Synthesis and Characterisation of Visible Light Responsive Photocatalysts for Solar Fuel Production and Synthesis of Fine Chemicals
Name of the Supervisor	Prof. Rajesh Kumar Yadav
Month and Year	January- 2024

The transformation of carbon dioxide (CO₂) into chemicals and fuels with added value stands out as a significant innovation in addressing both energy needs and the challenge of global warming. Among the notable approaches, an artificial photosynthetic system emerges as a leading strategy for converting CO₂ into solar chemicals and fuels, including formaldehyde, formic acid, methanol, ethanol, methane, and more. In this context, an efficient photocatalyst must possess a broad solar light absorption range, effective space-charge separation, high physico-chemical stability, and strong redox ability. In the contemporary landscape, various innovative, cost-effective, and robust semiconductor photocatalysts like carbon nitride, functionalization of Bakelite polymer, and Eosin -y functionalised materials have garnered significant attention. These materials demonstrate substantial potential for diverse photocatalytic applications, gaining particular importance in medicinal chemistry and various industries. Graphitic carbon nitride-based materials stand out as excellent candidates for studies in photocatalysis, thanks to their exceptional thermal, mechanical, electrical, and optical properties. Notably, they boast a high specific surface area, superior charge mobility, high thermal conductivity, and robust chemical and electrochemical stability. Additionally, Bakelite composite materials are recognized as significant photocatalysts, showcasing excellent characteristics such as physicochemical stability, a tunable band gap (approximately 2.02 eV), high chemical resistance, and outstanding electronic properties. Furthermore, the research significance

of two-dimensional Eosin-Y has garnered widespread attention due to their compelling features. In addition to this, the synthesis of several type photocatalyst has garnered increased attention due to their distinctive properties, including excellent thermal stability, chemical stability, high mechanical strength, superior chemical resistance, lower production costs, and solar light harvesting capabilities. These exceptional properties position photocatalysts to be proficient in solar chemical production and organic transformation when exposed to solar light irradiation.

In pursuit of this objective, I have formulated solar light-harvesting photocatalysts using diverse synthetic methods, outlined as follows:

- Calcination
- Condensation reaction
- Sonogashira–Hagihara cross-coupling reaction

The current thesis is structured into 7 chapters:

Chapter one serves as the introduction, offering motivation and outlining the research objectives. It covers the contemporary CO₂ levels, natural photosynthesis, artificial photosynthesis, and organic transformations.

Chapter two is discussed about literature review on artificial photosynthesis, photoresponsive systems, and organic transformations. Herein, I have discussed about existing challenge to develop artificial photosynthetic systems, design strategies of photocatalysts, and applications of newly design photocatalysts. Further, describe the mechanistic pathway of artificial photosynthetic systems for NADH/NADPH regeneration and solar chemicals production. In this chapter also discuss the various applications of photogenerated nicotinamide cofactors (NADH/NADPH) and synthesised solar chemicals carbon dioxide redction reaction (CO₂RR) into formic acid and organic transformation such as 1, 3-oxathiolane-2-thiones production.

Chapter three of this thesis continues by detailing the synthesis of a light-harvesting photocatalyst, polydopamine (P) modified sulfur-doped graphitic carbon nitride (P@SGCN), and its applications. Here we employing the direct chemical doping of polydopamine to the SGCN. In the as-synthesized photocatalyst, polydopamine (P) can efficiently transfer the photoinduced electrons for the artificial photocatalytic process in

order to suppress the fast electronhole recombination [37]. The polydopamine (P) shows an outstanding adhesion capability which is readily modified on the surface of SGCN. The P@SGCN photocatalyst exhibited outstanding photocatalytic efficiency in regenerating NADH and in the highly selective production of formic acid, HCOOH, from CO₂. The newly design P@SGCN photocatalyst is show excellent photocatalytic efficiency in solar chemical production due to it high light harvesting capability, high BET surface area, high molar extinction coefficient, and suitable band gaps.

In the ongoing progress chapter fourth of the thesis research on bakelite polymer a for regeneration of NADH, formation of formic acid from CO₂ under solar light. Bromophenol dye enhance the high molar excitinction cefficient with slow charge recombination of the bakelite polymer. A novel Bromophenol-Bakelite (BPB) composite with bromophenol blue dye-doped inside the Bakelite matrix that is visible light active photocatalyst in an artificial photocatalyst-enzyme couple set up for the production of formic acid from carbon dioxide The results show enhancement in photocatalytic properties of BPB- composite in comparison to pure bromophenol blue dye. Additionally, systematic spectroscopic measurements provide the mechanistic insights for the NADH regeneration and solar fule formation via bromophenol doped bakelite photocatalyst.

In the next fifth chapter, we discuss about the metal free work, the newly bottom-up construction of novel yne-linked Eosin-Y functionalized (EY@DEHB) photocatalyst coupled with a formate dehydrogenase enzyme to establish this system, To the best of our knowledge, the yne-linked Eosin-Y functionalized photocatalyst for the production of highly selective HCOOH from CO₂ under the irradiation of visible light using a photo&biocatalyst integrated system has not been constructed earlier to this research. Eosin-Y is a well-known organic dye of the fluorescein family which got more attention due to its eco-friendly, easy handling, and also have great potential for visible-light mediated applications. Eosin-Y is a promising photosensitizer that reveals better yield for solar chemicals/fuels. Here, Eosin-Y coupled with DEHB as a photosensitizer to enhance the visible light absorption ability of EY@DEHB photocatalyst and also for highly selective photocatalytic HCOOH production.

In the continuation of research work, we discuss in chapter sixth the design and development of new class of metal free polymer photocatalyst. The grafting method is utilized to graft Poly (vinylidene fluoride-co-hexafluoropropylene-) polymer brush onto s-doped graphitic carbon nitride (PVDHFP@SGCN) for CO₂ reduction. The

PVDHFP@SGCN was analysed via UV spectroscopy, thermal gravimetric analysis (TGA), and Fourier transforms infrared spectroscopy (FT-IR). PVDFP increase the photocatalytic efficiency of SGCN after the grafting. Here, PVDHFP coupled with SGCN as a photosensitizer to enhance the visible light absorption ability of PVDHFP@SGCN photocatalyst and also for highly selective photocatalytic HCOOH production.

Chapter eighth is the summary of all the chapters which gives a major conclusion about artificial photosynthesis along with organic transformations and its applications. In this chapter, I have discussed about synthesis, characterization techniques, and various applications of newly design photocatalysts such as NADH/NADPH regeneration, formic acid production along with organic transformations). Also, briefly discuss about future scope of my research work in field of artificial photosynthesis and organic transformations such as 1, 3-oxathiolane-2-thiones production.

Contents

Certificate	ii
Candidate's Declaration	iii
Approval Sheet	iii
Acknowledgement	iv
List of Figures	v
List of Schemes	Error! Bookmark not defined.
List of Symbols	ix
List of Abbreviations	xi
Abstract	xiii
CHAPTER- 1	21
1.1 Introduction.....	22
1.2 Aim of research work	28
CHAPTER- 2	29
2.1 Consequence of environmental carbon dioxide (CO ₂)	30
2.2 Existing Challenges	31
2.3 Artificial photosynthesis vs Natural photosynthesis.....	31
2.4 Proposal tactics of photocatalyst.....	33
2.4.1 Carbon nitride based photocatalysts.....	34
2.4.2 Polymer doped Photocatalyst	37
2.4.3 Eosin-Y functionalized Photocatalyst.....	39
2.4.4 Artificial photosynthetic system for 1,4-NADH/ NADPH regeneration and solar fuel generation	41
2.5 Application of photogenerated solar chemicals.....	41
2.5.1 Application of NADH and NADPH.....	41
2.5.2 Application of formic acid.....	42
2.6 Organic transformations reactions	43
2.6.1 C-H bond generation	43
2.6.2 1, 3-oxathiolane-2-thiones.....	45
2.6.3 β -keto Sulfoxidation	46
CHAPTER-3	47
3.1 Introduction.....	48
3.2 Experimental Section	50

3.2.1 Materials Used.....	50
3.2.2 Instruments and measurements.....	50
3.2.3 Preparation of SGCN.....	50
3.2.4 Preparation of the P@SGCN.....	51
3.2.5 Photoregeneration of NADH.....	52
3.3 Result and Discussion.....	52
3.3.1 UV-Visible spectroscopy.....	52
3.3.2 FTIR spectroscopy.....	53
3.3.3 X-ray diffraction Analysis.....	54
3.3.4 HR-TEM Analysis.....	55
3.3.6 Zeta potential.....	57
3.4 A Photoinduced regeneration of NADH and production of HCOOH from CO ₂ .	58
3.4.1 Reusability and Chemical Stability.....	59
3.5 Photocatalyst/biocatalyst coupled process for the generation of HCOOH from CO ₂	60
CHAPTER-4.....	61
4.1 Introduction.....	62
4.2 General remarks.....	64
4.3 Instruments and Measurement.....	64
4.4 Synthesis of BPB-composite photocatalyst.....	65
4.5 Process of photocatalytic NADH regeneration.....	66
4.6 Procedure to produce Formic Acid from CO ₂	66
4.7 Results and Discussion.....	66
4.7.1 Design an artificial enzyme-coupled photocatalytic system.....	66
4.7.2 Characterisation of N-EGQD photocatalyst.....	68
4.8 Photocatalytic studies of NADH and formic acid yield.....	73
4.8.1 Reusability and Chemical Stability.....	74
4.8.2 HPLC chromatogram for Formic acid.....	75
4.9 During the reduction of NAD ⁺ , the possibility of producing different NADH isomers.....	76
CHAPTER-5.....	79
5.1 Introduction.....	80
5.2 Experimental Section.....	83
5.2.1 General remarks.....	83
5.2.2 Instruments and measurements.....	84
5.2.3 Synthesis of EY@DEHB photocatalyst.....	84
5.2.4 CpM synthesis.....	85
5.2.5 Proton nuclear magnetic resonance (1H-NMR) spectra of rhodium complex.....	86

5.3 Results and Discussion	87
5.3.1 Artificial AQBCN photocatalyst-biocatalyst coupled system	87
5.4 Mechanism of NADH regeneration	96
CHAPTER- 6.....	98
Creating effective and cost-efficient photocatalysts for CO ₂ fixation, inspired by nature, poses a significant challenge in material chemistry. The photoinduced polymer grafting of metal-free sulfur-doped graphitic carbon nitride (SGCN) has recently gained substantial attention due to its diverse applications spanning photocatalysis, energy conversion and storage, and biomaterials. In this research study, we delve into the development of a light-harvesting photocatalyst synthesized through the grafting of Poly (vinylidene fluoride-co-hexafluoropropylene) polymer brush onto sulfur-doped graphitic carbon nitride (PVDHFP@SGCN) using visible light irradiation. Subsequently, PVDHFP@SGCN films can be produced through spin coating on glass substrates. The investigation highlights the exceptional properties of the newly formulated photocatalysts, including outstanding solar light-harvesting capability, optimal optical band-gap suitability, and highly structured π -electron pathways facilitating efficient charge migration. These attributes position the photocatalyst as a highly promising candidate for various photocatalytic applications, particularly in utilizing solar energy for diverse chemical reactions. Moreover, the current PVDHFP@SGCN photocatalyst demonstrates remarkable efficiency as a catalyst in CO ₂ fixation, resulting in the production of formic acid as a green solar chemical.	99
6.1 Introduction.....	99
6.2 Experimental Section	102
6.2.1 General remarks	102
6.2.3 Preparation of the SGCN.....	102
6.2.4 Preparation of the PVDHFP@SGCN.....	102
6.2.5 Photochemical Cofactor Regeneration of NADH	103
6.3 Results and discussion	103
6.3.1 Photo regeneration of NADH and generation of HCOOH from CO ₂	103
6.3.2 Optical Properties of Highly Efficient PVDHFP@SGCN Photocatalyst for CO ₂ Fixation	105
6.3.3 Tauc plot of PVDHFP@SGCN photocatalyst.....	106
6.3.4 Cyclic voltammetry studies	106
6.3.5 EIS electrochemical studies.....	107
6.3.6 Tafel plot studies.....	108
6.3.7 FTIR studies	109

6.3.8 XRD pattern studies	110
6.3.9 EDS analysis and SEM analysis.....	111
6.3.10 The average particle Size.....	112
CHAPTER-7.....	114
7.1 Conclusion	115
7.2 Future Scope	117
References.....	118
Curriculum Vitae.....	142

CHAPTER- 1

Introduction

1.1 Introduction

Recently, the excessive presence of carbon dioxide (CO₂) in the environment has become a paramount concern, serving as the primary contributor to global warming and related issues [1], [2], [3]. Each day witnesses a significant release of CO₂ into the atmosphere through various means, with the combustion of fossil fuels being the most prevalent. The reliance on burning fossil fuels exacerbates this challenge.

To sustain the carbon cycle, atmospheric CO₂ naturally transforms into carbohydrates through the process of photosynthesis in green plants. However, natural photosynthesis is significantly impacted by deforestation, urbanization, industrialization, and the excessive use of fossil fuels [4], [5], [6]. Some estimates suggest that anthropogenic CO₂ levels could reach 590 ppm by the year 2100, resulting in a projected 1.9°C increase in global temperature[7].

In response to the energy crisis and global warming, recent research has predominantly focused on capturing and effectively utilizing CO₂ to produce valuable, clean, and non-polluting chemicals and fuels a scientifically challenging endeavor [8], [9], [10]. Consequently, the utilization of CO₂ for the synthesis of solar chemicals and fuels has gained importance, as it not only mitigates the adverse effects of global warming but also addresses the global fossil fuel shortage [11], [12], [13]. The 2021 global average atmospheric carbon dioxide, as per NOAA's Global Monitoring Lab analysis, stood at 414.72 parts per million. Many scientists, climate experts, and government officials concur that 350 ppm represents the deemed "safe" threshold for carbon dioxide levels.

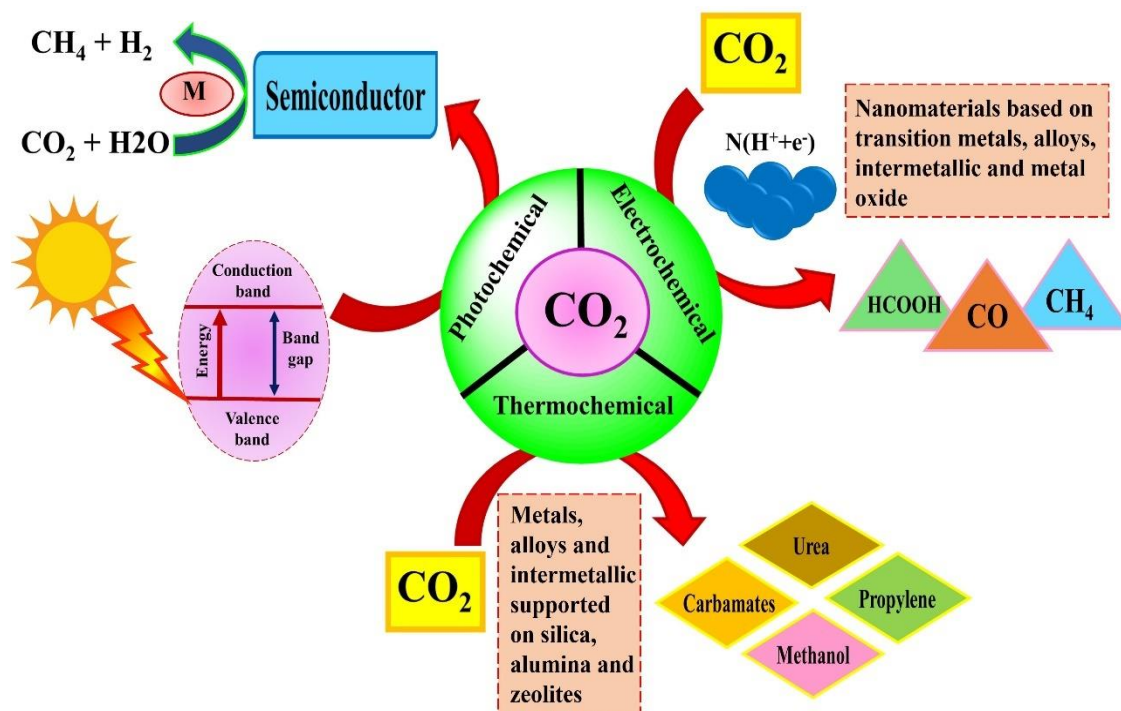
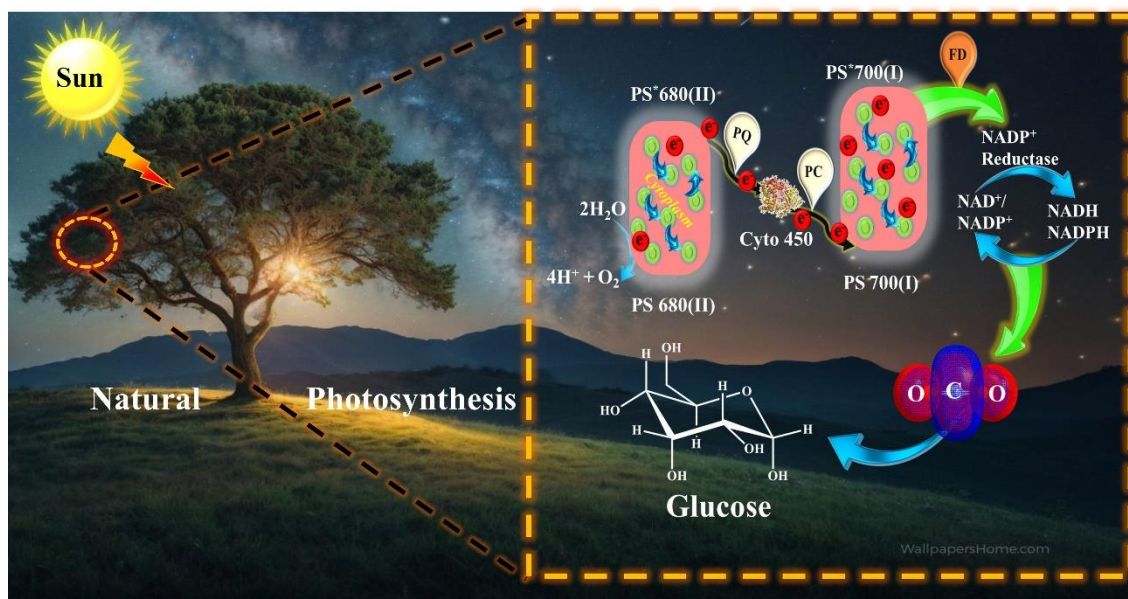


Figure 1. 1 Several technique employed for the tranformation of CO₂ in to different useful chemicals/fuels.

Various techniques, including photochemical, electrochemical, and thermochemical processes, can be employed to transform CO₂ into chemicals and fuels (Figure 1.1) [2]. The choice of catalysts and technological processes is crucial, given their strong dependence on the selected methods. The concept of utilizing CO₂ in renewable energy sources is inspired by the emulation of natural photosynthesis. Natural photosynthesis serves as an efficient pathway for converting solar energy into chemical energy in the presence of CO₂ and H₂O. This occurs through a photo-induced electron transfer series involving photon-capturing complexes, protein-metal clusters, and redox biocatalysts, as illustrated in Scheme 1.1.



Scheme 1. 1 Schematic illustrations of natural photosynthesis. In natural photosynthesis photoexcited electrons are transferred through Photosystem II (PS II) and I (PS I) for the reduction of oxidized NADP^+ into NADPH cofactors. (PQ = plastoquinone, PC = plastocya

The process of photosynthesis in green plants involves both light-dependent and light-independent (dark) reactions, as depicted in Scheme 1.1. During the light-dependent reaction, photo-induced electrons are transferred from photosystem II (PS-II) to photosystem I (PS-I) through the Z-scheme. In PS-II, Chlorophyll (P680) absorbs solar energy and becomes excited (P680^*). To create photoexcited electrons, P680^* generates a driving force that facilitates the extraction of electrons from water (H_2O) molecules, with the presence of a water-oxidation catalyst [14].

These photoexcited electrons undergo transfer to the light-harvesting complex of PS-I (P700) via the electron-transport chain, which includes plastoquinone (PQ), cytochrome complex (Cyt.), and plastocyanin (PC). Subsequently, the transferred electrons are re-excited by P700^* and conveyed to ferredoxin (FD), followed by the reduction of the oxidized form of the nicotinamide cofactor NADP^+ to NADPH through the enzyme ferredoxin NADP^+ -reductase (FNR). The produced NADPH cofactor is subsequently employed in the redox enzymatic reactions of the Calvin cycle as a reducing agent to convert CO_2 into carbohydrates during the light-independent reaction (Scheme 1.1). [15]. The Z-Scheme-based natural photosynthesis serves as an elegant model for establishing synergy between photocatalysis and biocatalysis.

In the last few decades, significant efforts have been dedicated to the pursuit of artificial photosynthesis, drawing inspiration from natural photosynthesis, with the aim of converting solar energy into valuable chemical energy. Consequently, research focusing on the eco-friendly and green artificial photosynthesis pathway for fixing the rapidly increasing CO₂ into essential chemicals and fuels has seen exponential growth. In contemporary times, the artificial photosynthesis process has been acknowledged as the most environmentally benign and potentially beneficial method for converting solar energy into chemical energy (Scheme 1.2). The drive towards selectively reducing CO₂ into chemicals and fuels has resulted in the development of various solar light-harvesting semiconductor photocatalysts. Both organic and inorganic semiconductors, as well as transition-metal complexes, have been extensively utilized as potential photocatalysts for the conversion of direct solar energy into value-added chemicals through artificial photosynthetic systems. However, they face challenges such as low conversion efficiency, poor photostability, limited solar light harvesting ability, and rapid charge recombination. To address these issues and enhance photocatalytic stability and efficiency, there is a need to develop solar light-active photocatalysts capable of driving the reduction of CO₂ through a photoelectrochemical route under solar light.

Moreover, photocatalysis has emerged as an economical and valuable alternative for organic transformations, conducted under mild reaction conditions. These transformations involve the use of photocatalysts, including costly transition metal complexes and organic-inorganic composite materials, to facilitate reactions via radical intermediates. Transition metal complexes, such as ruthenium and iridium, have been extensively explored in numerous synthetic protocols under solar light irradiation [28-33]. However, these transition metal complexes suffer from drawbacks like low efficiency and poor selectivity, influenced by factors such as photo-stability, multielectron transfer capability, reusability, suitable band gap, and cost-effectiveness.

In an effort to address these challenges, I have developed cost-effective metal-free photocatalysts that are active under solar light for solar chemical production. These photocatalysts have been utilized in various applications, including the production of regeneration of NADH/NADPH, formic acid generation from CO₂, and organic transformations involving 1,3-oxathiolane-2-thiones. Consequently, efficient solar light-active photocatalysts, such as carbon nitride, bakelite, and Eosin-Y, play a crucial role in facilitating the production of chemicals and fuels through diverse reaction protocols. The

constituents of an artificial photosynthetic system responsible for transferring photoinduced electrons and protons to facilitate the conversion of solar energy into chemical energy include:

- Photocatalyst
- Sacrificial agent: Ascorbic acid (AsA)
- Electron mediator: Rhodium complex [Cp*Rh(bpy)Cl] Cl/Methyl viologen (MV)
- Oxidized nicotinamide adenine dinucleotide/nicotinamide adenine dinucleotide phosphate (NAD⁺/NADP⁺)
- Enzyme

In terms of mechanism, the photocatalyst initiates electron transfer following the photoexcitation of electrons from the valence band (VB)/highest occupied molecular orbital (HOMO) to the conduction band (CB)/lowest unoccupied molecular orbital (LUMO) under solar light irradiation. The energy levels of the HOMO and LUMO of the photocatalyst are determined by the provided formula, using ferrocene as a reference:

$$E(\text{HOMO}) = -e [E_{\text{ox}} + 4.5]$$

$$E(\text{LUMO}) = -e [E_{\text{red}} + 4.5]$$

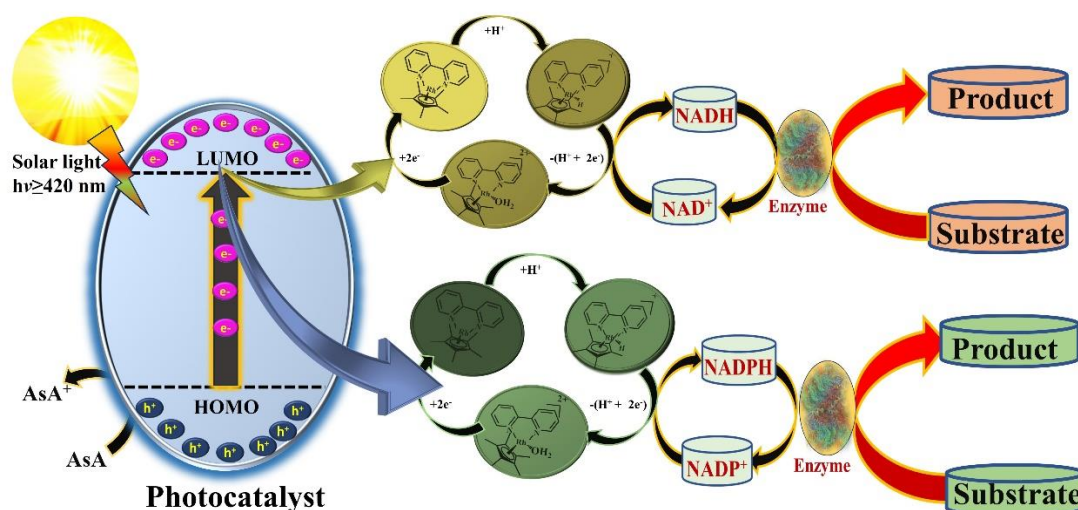
The photo-excited electrons originating from the valence band (VB) of the photocatalyst generate holes (h⁺), which are subsequently quenched by ascorbic acid serving as a sacrificial agent, as illustrated in Scheme 1.2. These photo-generated holes and electrons act as charge carriers, participating in oxidation and reduction reactions. The band gap of photocatalytic materials is defined as the potential difference between the valence band (VB)/highest occupied molecular orbital (HOMO) and the conduction band (CB)/lowest unoccupied molecular orbital (LUMO) respectively. The optical band gap of photocatalytic materials is calculated using the reported equation [16]:

$$\text{Optical band gap} = 1240/\lambda$$

Moreover, the photo-excited electrons move from the conduction band (CB) of photocatalytic materials to the electron mediator (Rh-complex/MV) to regenerate NAD(P)H and facilitate the production of solar chemicals/fuels, as illustrated in Scheme 1.2. Rh-complex is chosen as the preferred electron mediator over MV due to the toxic

nature of MV.[17] Consequently, Rh-complex is employed as the electron mediator for NADH regeneration and solar chemical production.

Scheme 1.2 illustrates artificial photosynthesis, incorporating a photocatalyst-biocatalyst integrated system for the production of solar chemicals and fuel, such as NADH/NADPH regeneration, and formic acid. The solar light-harvesting photocatalyst captures incident photons, becoming excited and transferring photo-generated electrons to reduce the rhodium complex/MV. Subsequently, the reduced rhodium complex/MV abstracts a proton from an aqueous solution and converts $\text{NAD}^+/\text{NADP}^+$ to NADH/NADPH after the transfer of a hydride ion, thereby completing the photocatalytic cycle.[18]



Scheme 1. 2 Illustrative depiction of a photocatalytic-biocatalytic artificial photosynthetic system for regenerating 1,4-NADH/NADPH and formic acid from CO_2 . This process involves the formate dehydrogenase enzyme and operates through an electron transfer mechanism

During this process, the rhodium complex/MV serves as an electron mediator between the photocatalyst and the NAD^+/NADP cofactor, facilitating the regeneration of NADH/NADPH. Subsequently, the regenerated NADH/NADPH cofactor is used to produce valuable solar chemicals like L-glutamate and formic acid with the help of specific enzymes. Formate dehydrogenase is employed to convert CO_2 into formic acid. [19].

1.2 Aim of research work

Artificial photosynthesis and processes for organic transformation are increasingly recognized as highly convenient methods for producing organic compounds and converting solar energy into solar chemicals. The research initiatives strive to achieve the following goals:

- The creation of a novel Bromophenol-Bakelite (BPB) composite with bromophenol blue dye-doped inside the Bakelite matrix that is visible light active photocatalyst in an artificial photocatalyst-enzyme couple set up for the production of formic acid from carbon dioxide. The results show enhancement in photocatalytic properties of BPB-composite in comparison to pure bromophenol blue dye.
- The synthesis of a metal-free the newly bottom-up construction of novel yne-linked Eosin-Y functionalized (EY@DEHB) photocatalyst coupled with a formate dehydrogenase enzyme to establish this system focused on achieving NADH/NADPH regeneration and formic acid production.
- Development efforts are directed towards a cost-effective and metal- the grafting method is utilized to graft Poly (vinylidene fluoride-co-hexafluoropropylene-) polymer brush onto s-doped graphitic carbon nitride (PVDHFP@SGCN) for CO₂ reduction and organic transformations.

CHAPTER- 2

Literature Review

2.1 Consequence of environmental carbon dioxide (CO₂)

In the current situation, the continuous rise in the release of greenhouse gases such as carbon dioxide (CO₂), nitrous oxides (N₂O), and methane (CH₄) resulting from activities like burning fossil fuels and deforestation has given rise to environmental challenges, including global warming, ocean acidification, and an increase in sea levels [20], [21]. Among these greenhouse gases, particular attention is directed towards CO₂, a significant emission originating from the combustion of fossil fuels, biomass (coal/wood), kerosene heaters, and tobacco smoke, all of which contribute to anthropogenic pollutants (Figure 2.1).

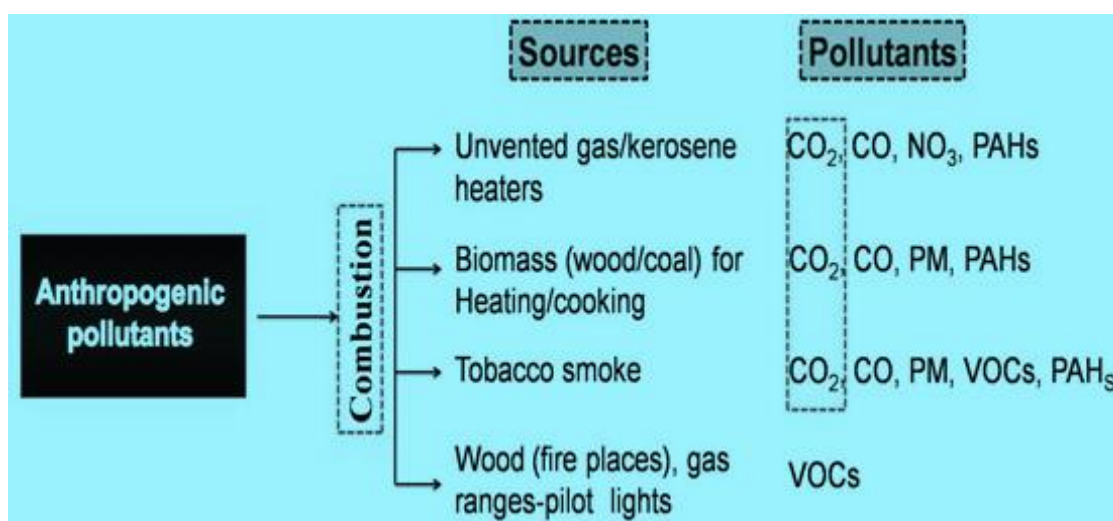


Figure 2. 1 Anthropogenic pollutants and their origins. Carbon dioxide (CO₂), carbon monoxide (CO), nitrogen dioxide (NO₂), polycyclic aromatic hydrocarbons (PAHs), particulate matter (PM), and volatile organic compounds (VOCs).

In recent times, researchers have shown a keen interest in developing effective environmentally friendly strategies for utilizing CO₂, recognizing it as the greenhouse gas contributing to adverse climate change. From a chemical standpoint, CO₂ represents an inexpensive, abundantly available, and renewable carbon feedstock suitable for conversion into value-added chemicals and fuels. Consequently, there is a growing body of research aimed at transforming CO₂ into a clean, non-polluting, sustainable, and abundant energy source using solar energy. Moreover, various pieces of literature also highlight the fixation of CO₂ through the synthesis of organic compounds, as illustrated in Figure 2.2 [22], [23], [24].

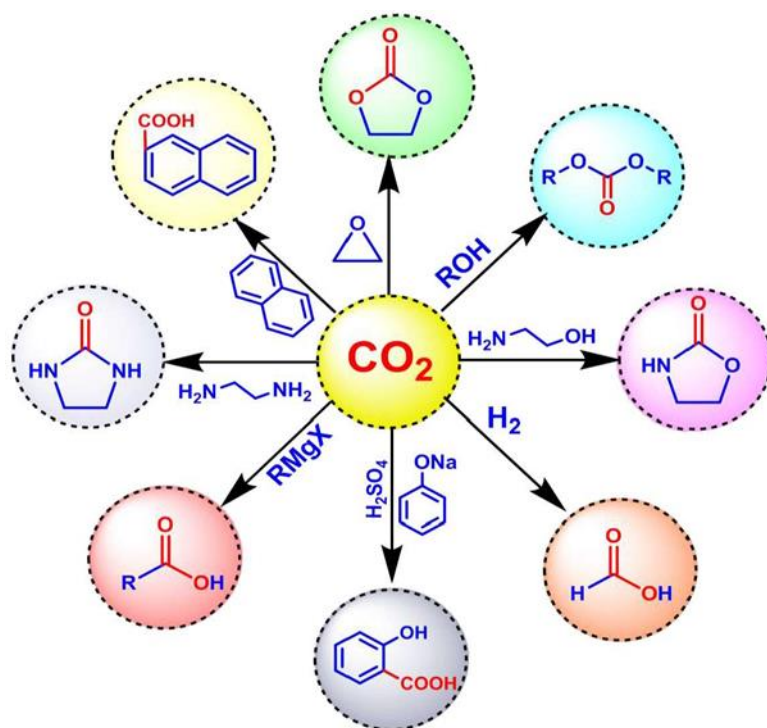


Figure 2. 2 An overview illustrating the synthesis of organic compounds utilizing carbon dioxide.

2.2 Existing Challenges

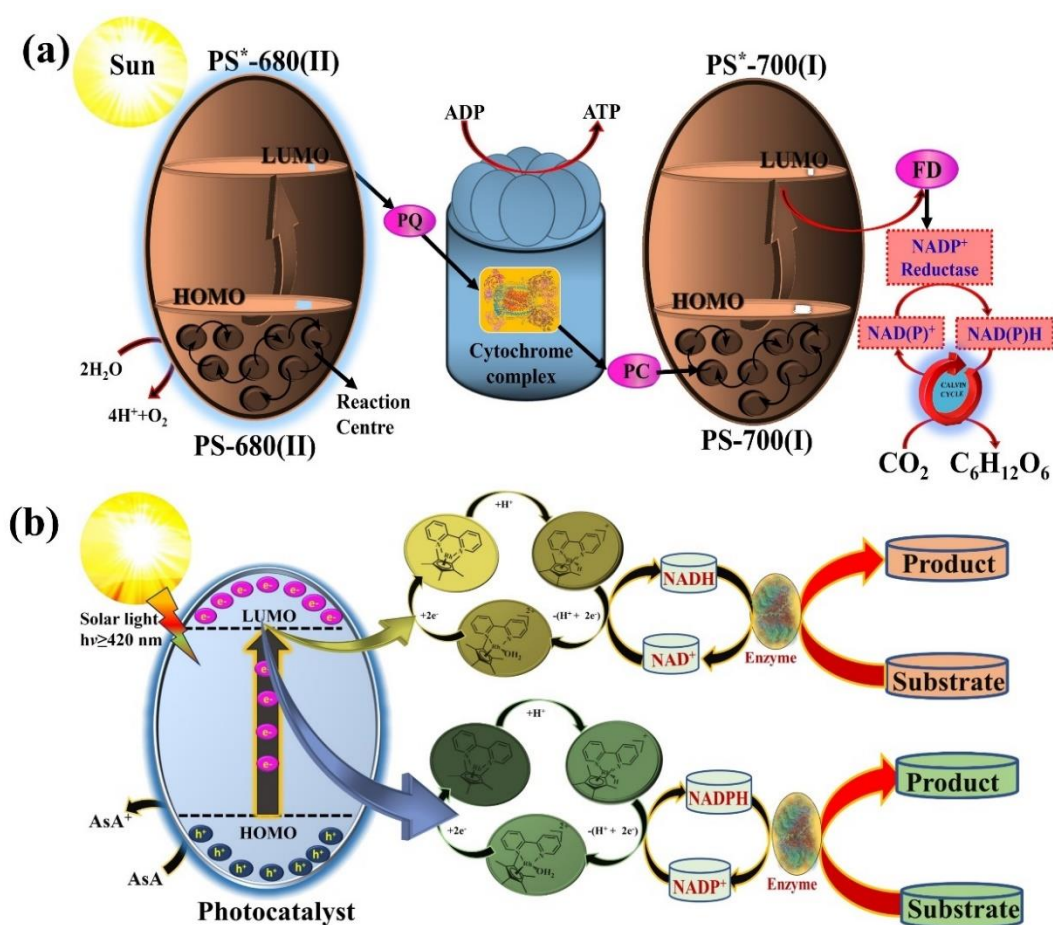
Transforming CO₂ into value-added chemicals and fuels poses a significant challenge. Numerous transition-metal catalysts, including palladium (Pd), copper (Cu), ruthenium (Ru), nickel (Ni), iron (Fe), zinc (Zn), and others, have been employed in many studies to convert atmospheric CO₂ into organic compounds through synthetic approaches under demanding conditions [25], [26], [27]. However, transition-metal catalysts have drawbacks such as high cost, toxicity, and low efficiency. Consequently, the quest for producing clean and renewable chemicals and fuels from CO₂ using metal-free photocatalysts remains a formidable challenge. In this context, the exploration of novel, eco-friendly, and green strategies involving artificial photosynthetic systems becomes desirable for manufacturing value-added chemicals/fuels under solar light irradiation.

2.3 Artificial photosynthesis vs Natural photosynthesis

The development of the artificial photosynthetic system has been prompted by the escalating environmental concerns and the growing need for sustainable and renewable energy solutions—a significant challenge in meeting current energy demands. Recognition of solar energy's potential for environmental remediation and the production of chemicals/fuels through artificial photosynthesis has gained prominence [28], [29],

[30]. Artificial photocatalysis mimics the natural photosynthesis process, transforming solar energy into chemical energy and chemical bonds [28], [29], [30]. This process involves the use of photocatalysts as light-harvesting materials or photosensitizers, as illustrated in Scheme 2.1.

In the natural photosynthesis process, electrons are liberated from sacrificial H_2O molecules (oxidized) under solar light irradiation. These electrons then reduce CO_2 molecules into hydrocarbons through a photoinduced electron transfer (PET) chain, facilitated by a biocatalyst (Scheme 2.1). The transfer of electrons from H_2O to CO_2 occurs through multiple steps, leading to an increase in the energy of electrons (i.e., uphill reactions). In this way, photosynthesis converts solar energy into stored chemical energy, specifically carbohydrates (Scheme 2.1). Similarly, artificial photosynthesis can convert solar energy into value-added chemical energy through the mechanism of a photoinduced electron transfer chain, as depicted in Scheme 2.1.



Scheme 2. 1 Illustration of natural and artificial photosynthetic system process.

In the context of artificial photosynthesis, the fundamental mechanism illustrates that a solar light-active photocatalyst captures photons, generating electron-hole pairs that actively participate in uphill reactions. Subsequently, electrons are excited from the valence band (VB) to the conduction band (CB), leaving behind holes [31]. In a photocatalytic reaction, the alteration in Gibbs free energy (ΔG) is determined by the difference between the reduction potential (P_{red}) and oxidation potential (P_{ox}). A positive or negative ΔG value signifies uphill or downhill reactions, respectively. The reduction of CO_2 involves an uphill reaction, whereas the degradation of organic compounds under solar light corresponds to a downhill reaction[32]. Additionally, photo-generated electrons are directed towards the production of solar chemicals through the photoinduced electron transfer (PET) chain, which incorporates an electron mediator and enzyme.

2.4 Proposal tactics of photocatalyst

Semiconductor photocatalysts have attracted considerable attention because of their varied applications, which encompass the degradation of environmental pollutants, the generation of solar fuels, and organic transformations. [33], [34]. Over the past few decades, metal oxide semiconductors have demonstrated remarkable capabilities, superior stability, and efficient solar light harvesting for various photocatalytic processes [35]. The n-type TiO_2 semiconductor, pioneered by Fujishima and Honda in 1972, marked a milestone for solar fuel production in a photoelectrochemical cell[36]. Subsequently, Halmann and Inoue explored the use of inorganic semiconductors such as GaP, TiO_2 , ZnO, SiC, and CdS for the reduction of CO_2 a few years later [37], [38]. The research landscape has witnessed extensive activities in the last few decades, involving the development of other inorganic semiconductors, including oxides, nitrides, sulfides, and more, for solar-to-fuel photocatalytic conversion. [39], [40]Despite yielding various promising results, inorganic semiconductors face challenges such as poor optoelectronic properties and limited flexibility.

For this purpose, polymeric semiconductor materials have gained popularity due to their abundance on the planet (mostly consisting of C, H, O, N, and S) and their extraordinary structural and functional diversity. Since Yanagida and co-workers first reported on poly(p-phenylene) for the photocatalytic evolution of hydrogen in 1985 [41]research on the photocatalytic generation of solar fuel using organic semiconductors has rapidly expanded [66, 67]. Numerous researchers have explored the reduction of CO_2 or water

splitting using various materials, including conjugated microporous polymers (CMPs), graphitic carbon nitride (g-C₃N₄) [42], [43], [44], graphene-based materials [45], covalent organic polymers (COPs)[46], covalent organic frameworks (COFs) [47], [48], covalent triazine frameworks (CTFs) [49], [50], and linear conjugated polymers.[51], [52] As a result, throughout my research, I have developed several solar light-active photocatalysts, which are listed below.

- Carbon nitride based photocatalysts
- Bakelite based Photocatalyst
- Eosin-Y functionalized Photocatalyst
- grafting of Poly (vinylidene fluoride-*co*-hexafluoropropylene-) polymer on SGCN

2.4.1 Carbon nitride based photocatalysts

Graphitic carbon nitride (g-C₃N₄) represents a 2D semiconductor material comprising interconnected tri-s-triazine units linked through tertiary amines. The crystallinity, morphology, and photoactivity of various allotropic forms of carbon nitride, including -C₃N₄, C₃N₄, g-o-triazine, g-h-triazine, g-h-heptazine, cubic C₃N₄, and pseudo cubic C₃N₄, are determined by the monomer and linkage pattern. The g-C₃N₄ is comprised of more stable tri-s-triazine units with a crystalline nature, demonstrating remarkable chemical stability (resistant to both acid and base media) and thermal endurance (up to 600 °C) owing to its high degree of polymerization. The synthesis of g-C₃N₄ entails the calcination of nitrogen-rich compounds such as urea, thiourea, melamine, cyanamide, dicyandiamide, and others (refer to Figure 2.3). Noteworthy is that g-C₃N₄ absorbs light in the blue region of the solar spectrum (420-450 nm) and has a medium band gap of approximately 2.8 eV, which is attributed to the alternating presence of carbon and nitrogen. [53], [54].

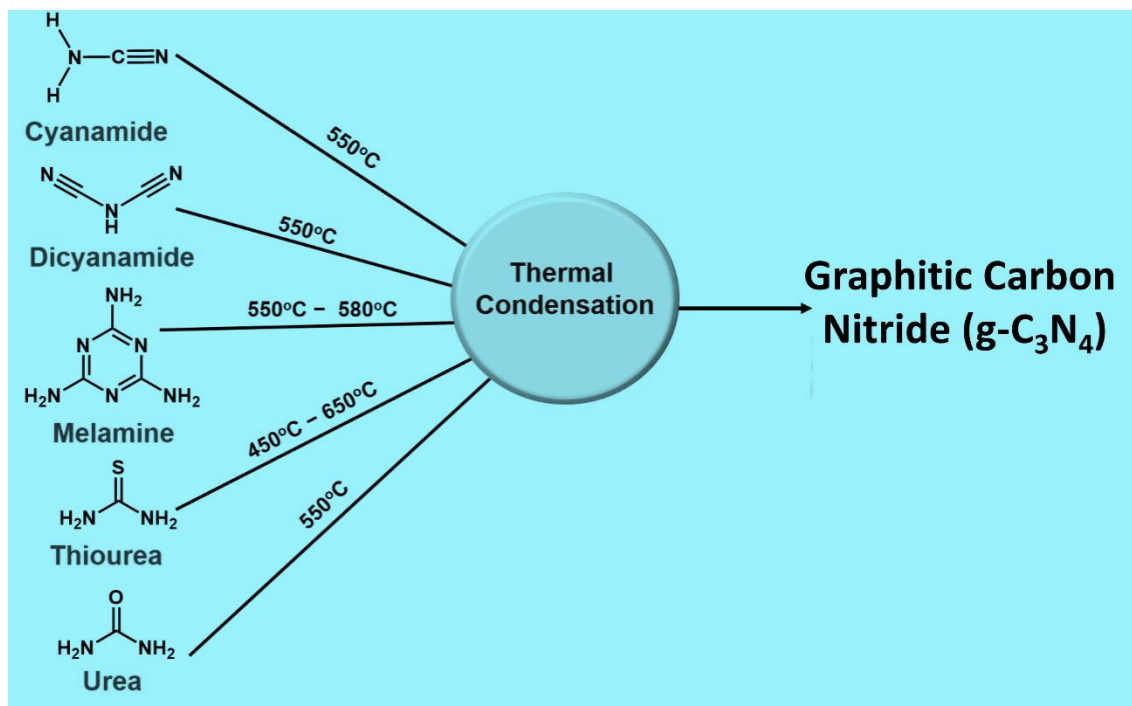


Figure 2. 3 Illustrative depiction of the synthesis of g-C₃N₄ photocatalyst as a foundational material through thermal polymerization using different precursors.

A novel metal-free g-C₃N₄ semiconductor has garnered significant attention due to its affordability, non-toxic nature, high stability, and impressive electronic and optical properties [55], [56]. This semiconductor, with a medium band gap, has found widespread applications in degrading organic pollutants and water splitting[57], [58]. However, it faces challenges such as moderate absorption of solar light, rapid charge recombination, limited surface areas, and low carrier charge mobility. To overcome these drawbacks, various strategies have been employed to modify g-C₃N₄, including the decoration of metal nanoparticles, coupling [59], [60], element doping[61], exfoliation methods, and the incorporation of organic dyes[62].

On the contrary, due to rapid recombination of charge carriers, limited surface area, and low absorption coefficient, g-C₃N₄ exhibits insufficient photocatalytic efficacy [63]. Various approaches have been explored to overcome these limitations, including doping with different metals like Fe [64] or Ag [65], and introducing non-metal elements such as S or B [66],[67] into the bulk g-C₃N₄. A comprehensive review by certain researchers outlines diverse modification methods aimed at improving the photocatalytic efficiency of g-C₃N₄ [68]. Furthermore, the development of composites using other semiconductor materials presents an innovative strategy to enhance the photocatalytic effectiveness of

g-C₃N₄ [69]. In a review conducted by Wen and colleagues[70], a range of enhancement techniques such as nano-carbon loading, band gap engineering, and defect controls are discussed to elevate the performance of metal-free g-C₃N₄ in photocatalysis and related fields. Additionally, the combination of g-C₃N₄ with CdS quantum dots (QDs) emerges as a novel method to enhance g-C₃N₄ performance under visible light [71]. An alternative and effective strategy for enhancing the activity of g-C₃N₄ in the visible spectrum is to reduce the reliance on metal-based light-harvesting materials and instead apply organic dye onto the surface of g-C₃N₄. Moreover, strategies like manipulating the morphology of the g-C₃N₄ structure and employing plasma-based surface modification to augment the BET surface area have arisen as appealing methods for adjusting the photocatalytic activity within the visible spectrum. [72]. The resulting modified g-C₃N₄ materials showcase outstanding photocatalytic capabilities across diverse domains, as illustrated in Figure 2.4.

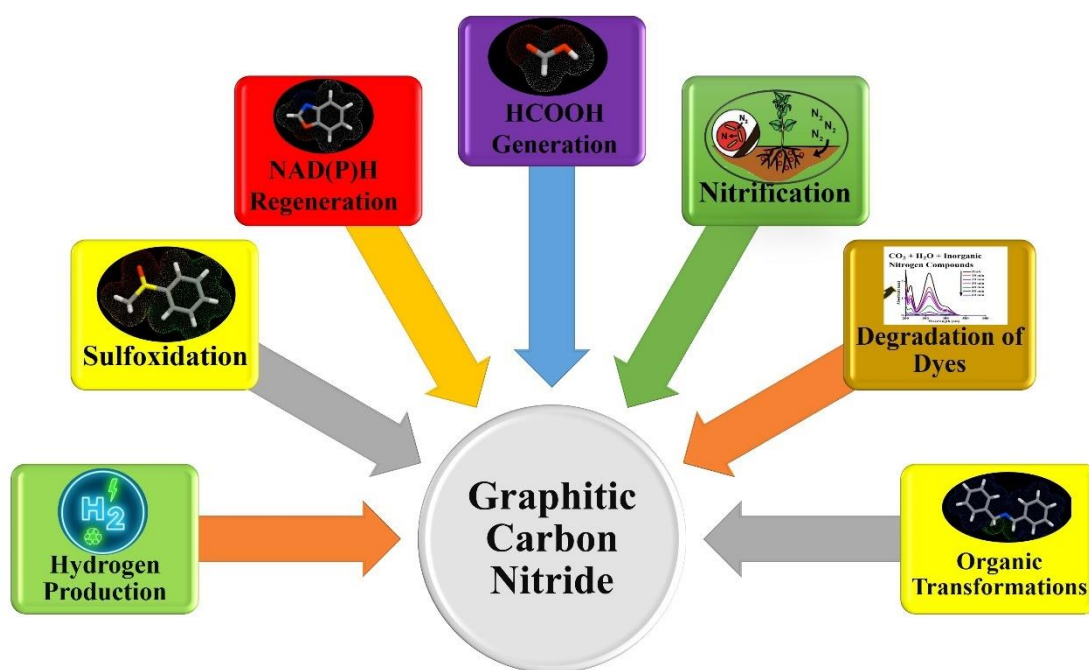


Figure 2. 4 Photocatalysts derived from g-C₃N₄ for various photocatalytic reactions.

Some researchers have proposed using expensive metal-based g-C₃N₄ photocatalysts, which involve modifications like incorporating gold nanoparticles onto g-C₃N₄ [73] and creating ternary nanocomposites consisting of g-C₃N₄-black phosphorus-gold nanoparticles [74] for various photocatalytic applications. Considering the observations mentioned above, it is evident that employing non-metal doping and surface modification of g-C₃N₄ through composite formation or functionalization with cost-effective

chromophores could be an effective strategy for developing solar light-harvesting photocatalysts. In the constituent element of P@SGCN, Dopamine is a biopolymer that has been used in the various fields, including biomedicine, environment, and energy. Because of its excellent biocompatibility and hydrophilicity [37] as well as its varied adhesion ability, dopamine is a significant organic material that shows the excellent ability for the surface functionalization. The polymeric form of dopamine called as polydopamine (P) has a high UV and visible-light absorption properties and can be readily used for the surface modification .

2.4.2 Polymer doped Photocatalyst

Polymeric materials possess a range of properties that make them well-suited as catalyst supports, effectively boosting efficiency in various applications. Figure 2.5 illustrates the application of polymer-supported photocatalysts in numerous photocatalytic reactions, leveraging their high surface area, reusability, and stability [75], [76].

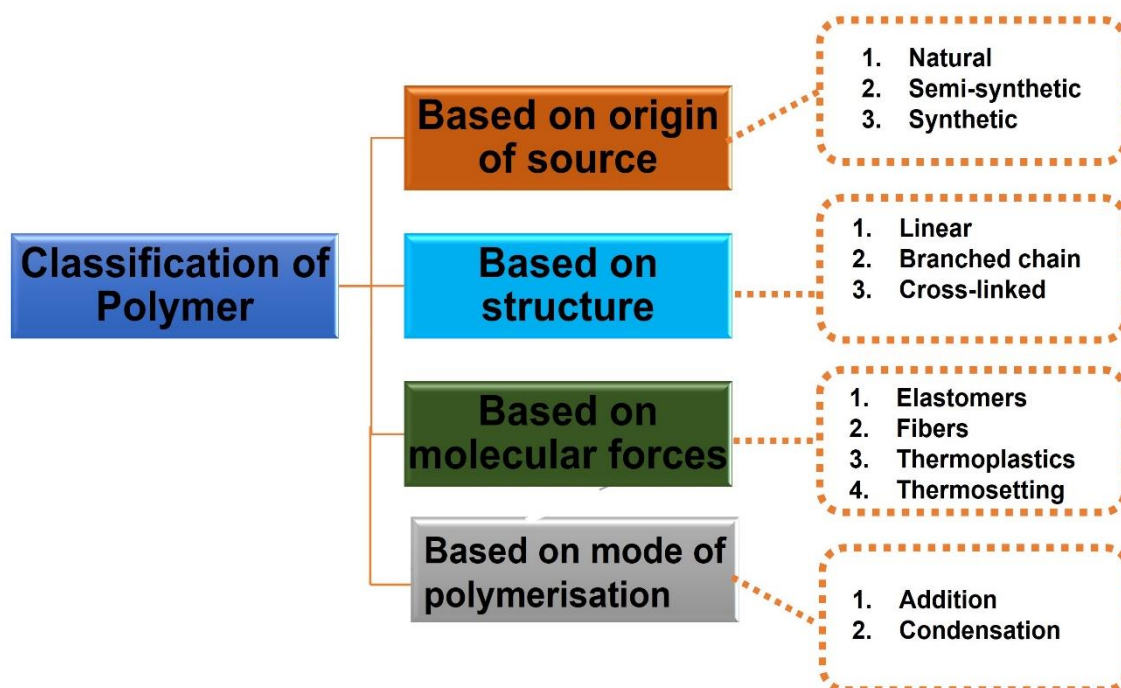


Figure 2. 5 Categorization of polymers based on their structures.

Figure 2.5 illustrates that the integration of polymeric materials consistently enhances the photocatalytic activity of inorganic-organic compounds [77]. As a result, various reports emphasize the development of metal-based polymeric materials tailored for photocatalytic reactions. Although these photocatalysts have demonstrated significant

advancements in the field, their composition heavily depends on noble or rare elements and metal/metal oxides [77]. Consequently, the pursuit of an environmentally friendly, durable, and cost-effective polymer-based photocatalyst remains a challenging undertaking. Bakelite, an early phenol/formaldehyde resin, is a thermoset material with high crosslinking. It is produced through a condensation reaction between phenol and formaldehyde, catalyzed by either a basic or acidic catalyst. Invented by the Belgian-American chemist Leo Baekeland in New York in 1907, Bakelite is notable for being among the earliest synthetic plastics. Its popularity soared due to its electrical non-conductivity and heat-resistant characteristics, making it a favored material for electrical insulators, radio and telephone casings, and a wide array of products including kitchenware, jewelry, pipe stems, children's toys, and firearms. Overall, phenolic resins [78], [79] are prominent thermosetting resins extensively employed across various industrial sectors. Their applications encompass molding compounds, coatings, structural adhesives, thermal insulation materials, and composites. Their prevalence in these areas is attributed to their outstanding thermal and chemical resistance [78]. However, due to their high crosslinking density, phenolic resins exhibit brittleness, posing a challenge in their industrial use. To address this drawback, several research endeavors have been undertaken to modify phenolics by incorporating elastomers or thermoplastics. Polymer nanocomposites have garnered significant attention in polymer science research due to their ability to enhance various properties. This includes improvements in mechanical properties, as demonstrated in studies by [79]. Additionally, these nanocomposites show promise in areas such as scratch and abrasive-resistant hard coatings, as well as improvements in barrier properties and fire resistance, as indicated by [80]. In broad terms, the upcoming generation of composite structures needs to exhibit enhanced stiffness, strength, toughness, lightness, durability, and intelligence, incorporating multifunctionality. While the choice of nanomaterial, polymer matrix, and incorporation method usually determines mechanical properties, a novel approach has surfaced to notably augment not just the mechanical attributes but also the electrical and thermal properties of composites. This is achieved by strategically introducing a small quantity of dye (Bromophenol) was added into the polymeric matrix, resulting in composite materials with the targeted properties [81]. Some important properties of bakelite based materials in Figure 2.6.

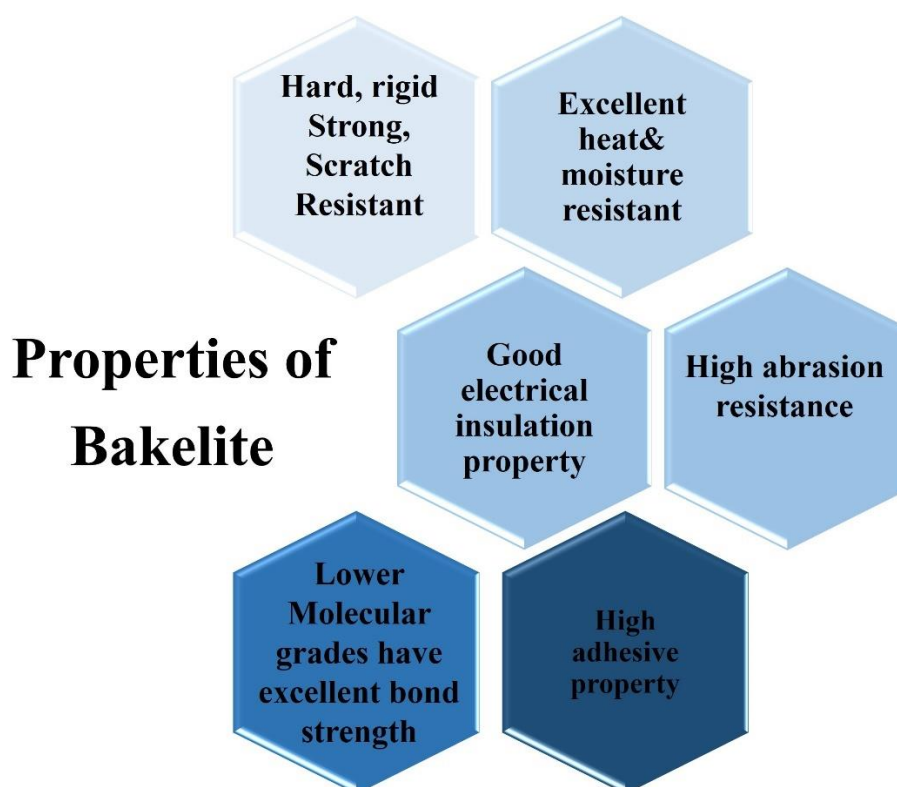


Figure 2. 6 Several excellent properties of Bakelite

Consequently, I formulated and created a novel Bromophenol-Bakelite (BPB) composite, incorporating bromophenol blue dye into the Bakelite matrix. The BPB-composite functions as a visible light-harvesting photocatalyst in a photocatalyst–enzyme coupled artificial photosynthetic system. Compared to bromophenol, the BPB-composite photocatalyst has shown a seven-fold increase in NADH and formic acid yields and remarkable thermal stability. In conclusion, an efficient photocatalyst has been created for the selective production of solar chemicals directly from CO₂ in an artificial photosynthetic process.

2.4.3 Eosin-Y functionalized Photocatalyst

In recent times, Eosin Y, a widely recognized dye molecule, has been increasingly employed as a photoredox catalyst in organic synthesis [84]. Its cost-effectiveness and easy accessibility make Eosin Y an attractive alternative to conventional inorganic transition metal photocatalysts. [82] Despite the outstanding photophysical properties exhibited by ruthenium and iridium polypyridyl complexes in visible light photocatalysis, their high cost and potential toxicity present drawbacks on a larger scale. [83]

Organic dyes have emerged as a compelling solution to transition metal complexes in photoredox catalysis. These dyes are generally more cost-effective and less toxic, offering ease of handling and, in some cases, surpassing the performance of organometallic and inorganic catalysts. Eosin Y, in particular, has become widely utilized as an organophotocatalyst in synthetic transformations. This renowned dye boasts a rich history, having been employed in various applications such as cell staining, pH indication, aiding in analytical halide determination by Fajans, and serving as a dye pigment in products like lipsticks. [84] The aim of this article is to explore recent applications of eosin Y as a visible light photocatalyst in organic synthesis.[85]

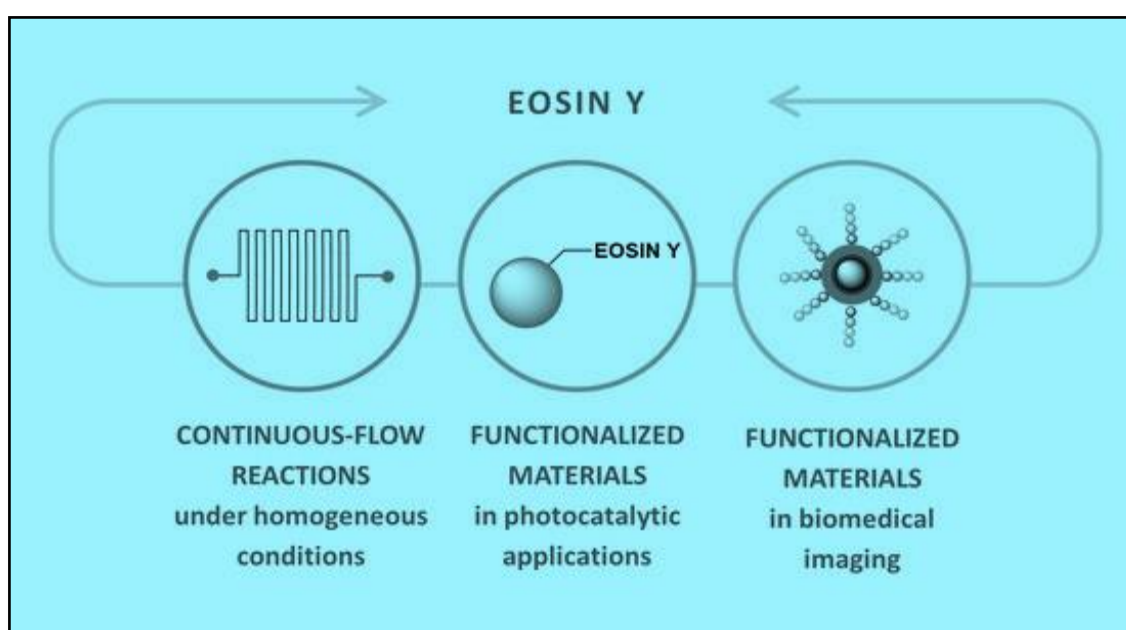


Figure 2. 7 Development of Eosin-Y as catalyst in different type reactions

The photochemistry of eosin-Y has been thoroughly examined in Figure 2.7. Under visible light exposure, eosin-Y quickly undergoes intersystem crossing to the lowest energy triplet state, with a lifetime of 24 μs [89]. Eosin Y selectively absorbs green light, as shown in its UV-Vis spectrum, which exhibits a distinct peak at 539 nm with a molar extinction coefficient (ϵ) of 60,803 $\text{M}^{-1} \text{cm}^{-1}$. Upon excitation, eosin-Y demonstrates enhanced reducing and oxidizing properties compared to its ground state. The redox potentials of the excited state can be estimated using the standard redox potentials of the ground state, determined through cyclic voltammetry, and the energy of the triplet excited

state. Eosin-Y offers the measured ground state and the estimated excited state oxidation and reduction potentials. [85], [86]

2.4.4 Artificial photosynthetic system for 1,4-NADH/ NADPH regeneration and solar fuel generation

Scheme 2.1 provides an illustrative representation of the photocatalytic system responsible for generating formic acid from CO₂. In the initial step, incident photons are absorbed by the photocatalyst, inducing an electron transition from a localized orbital in its valence band to the conduction band. These electrons are subsequently transferred to the rhodium complex (Rh) [87]. Through the reduction of the electron mediator, the rhodium complex gains a proton from the aqueous solution. Subsequently, it transfers a hydride ion to NAD⁺, converting it into NADH and finalizing the photocatalytic cycle. The Rh complex serves as an electron mediator between the photocatalytic material and the nicotinamide cofactor (NAD⁺), thereby facilitating the regeneration of 1,4-NADH. Ultimately, the reduced form of the nicotinamide cofactor participates in the enzymatic (F_{ate}DH) conversions of CO₂ into formic acid. Consequently, formic acid is produced as the final product from the CO₂ substrate through the photocatalytic-biocatalytic system.

2.5 Application of photogenerated solar chemicals

2.5.1 Application of NADH and NADPH

NADH: NADH plays a crucial role as a redox cofactor in various metabolic reactions, showcasing diverse physiological functions in its reduced form [88], [89]. Its antioxidative properties make it particularly valuable in addressing skin conditions like dermatitis and underscore its exceptional efficacy as a biological reducing agent [90]. In its reduced state, this form of the nicotinamide cofactor effectively safeguards cells and cell membranes from generated free radicals, contributing to the prevention of numerous diseases [91]. 1,4-NADH is applied in the treatment of conditions such as Alzheimer's disease, Parkinson's disease, chronic fatigue syndrome, and dementia. Additionally, it functions as an energy supplement, enhancing mental clarity, memory, alertness, and athletic performance, as depicted in Figure 2.8a [92].

NADPH:

NADPH is actively involved in biosynthetic and redox reactions, serving a vital function in protecting against detrimental reactive oxygen species and aiding in the regeneration of glutathione [93]. Additionally, NADPH is utilized in anabolic pathways, including cholesterol synthesis, steroid synthesis, ascorbic acid production, and cytosolic fatty acid synthesis, as illustrated in Figure 2.8b [88].

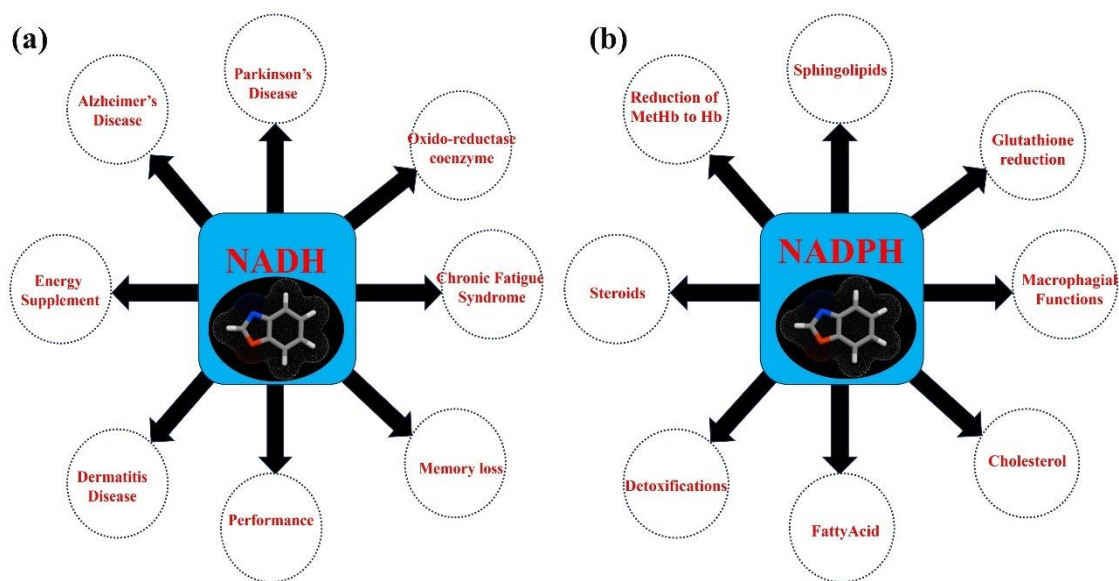


Figure 2. 8 Several uses of nicotinamide cofactor (a) 1,4-NADH (b) 1,4-NADPH.

2.5.2 Application of formic acid

Formic acid has demonstrated numerous industrial and pharmaceutical applications, as illustrated in Figure 2.9 [94]. It serves as an antibacterial agent in livestock feed and preservatives. Furthermore, formic acid facilitates quick fermentation at low temperatures, minimizing the loss of nutritional value. Due to its acidic nature, formic acid is extensively employed in tanning, dyeing, finishing textiles, and leather production. In rubber production, it functions as a coagulant [94], and it finds application in various cleaning products as a substitute for mineral acids. Formic acid has been reported for its use in treating warts, and it can also be utilized as a fuel in fuel cells, both directly in formic acid cells and indirectly in hydrogen fuel cells.

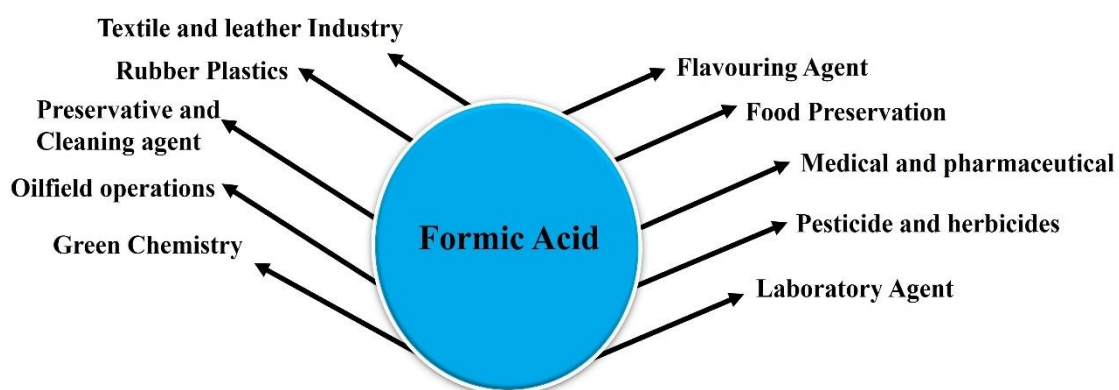


Figure 2. 9 Different uses and their application of solar light produced fine chemical (HCOOH).

2.6 Organic transformations reactions

The field of transformative science is advancing the synthesis of organic compounds, enabling selective assembly, molecular engineering, and architectural design with significant applications in material sciences, biochemistry, pharmaceutical industries, agrochemicals, and other domains. Photoredox-catalyzed organic transformations operate based on radical intermediates. The excited state of the photocatalyst facilitates the activation of organic substrates through a single-electron transfer (SET) reaction. Utilizing this potent synthetic tool, the development of various organic compounds from simple substrates has been achieved, encompassing the functionalization of C-H bonds, C-S bonds, keto sulfoxidation, and 1,3-oxathiolane-2-thiones.

2.6.1 C-H bond generation

C-H bond activation stands out as a potent tool in organic synthesis, boasting remarkable applications in drug discovery, crop protection, and the agrochemical and pharmaceutical industries, as depicted in Figure 2.10 [95].

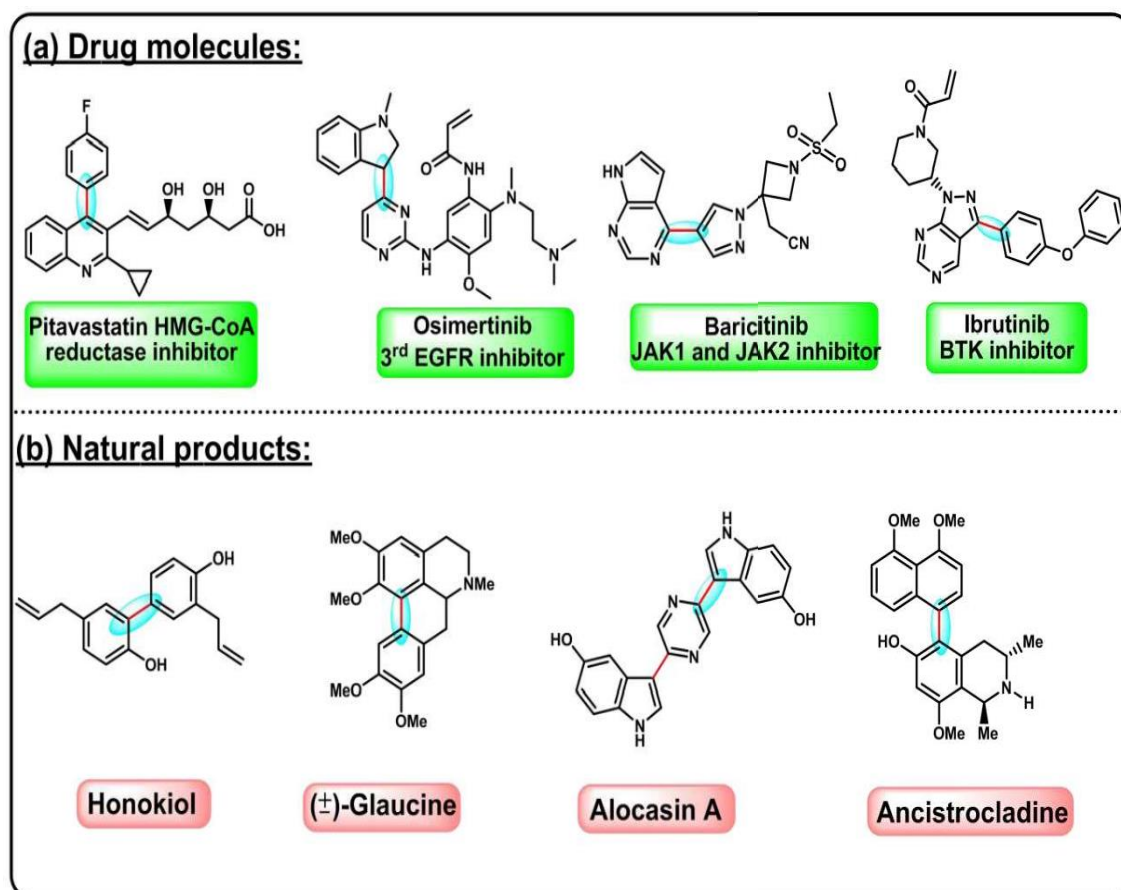


Figure 2. 10 Different type medicinal drug molecules and natural products was synthesized by C-H bond generation

Literature reports indicate that C-H bond activation has been achieved using various costly transition metals such as iridium, palladium, ruthenium, and rhodium as catalysts, as shown in Figure 2.11 [96]. Unfortunately, these transition metals are both toxic and expensive. Consequently, achieving metal-free catalyzed C-H bond activation poses a significant challenge for practitioners in pharmaceutical and agrochemical industries. Nevertheless, the most robust approach for C-H bond activations involves the development of metal-free, cost-effective photocatalysts. [143]

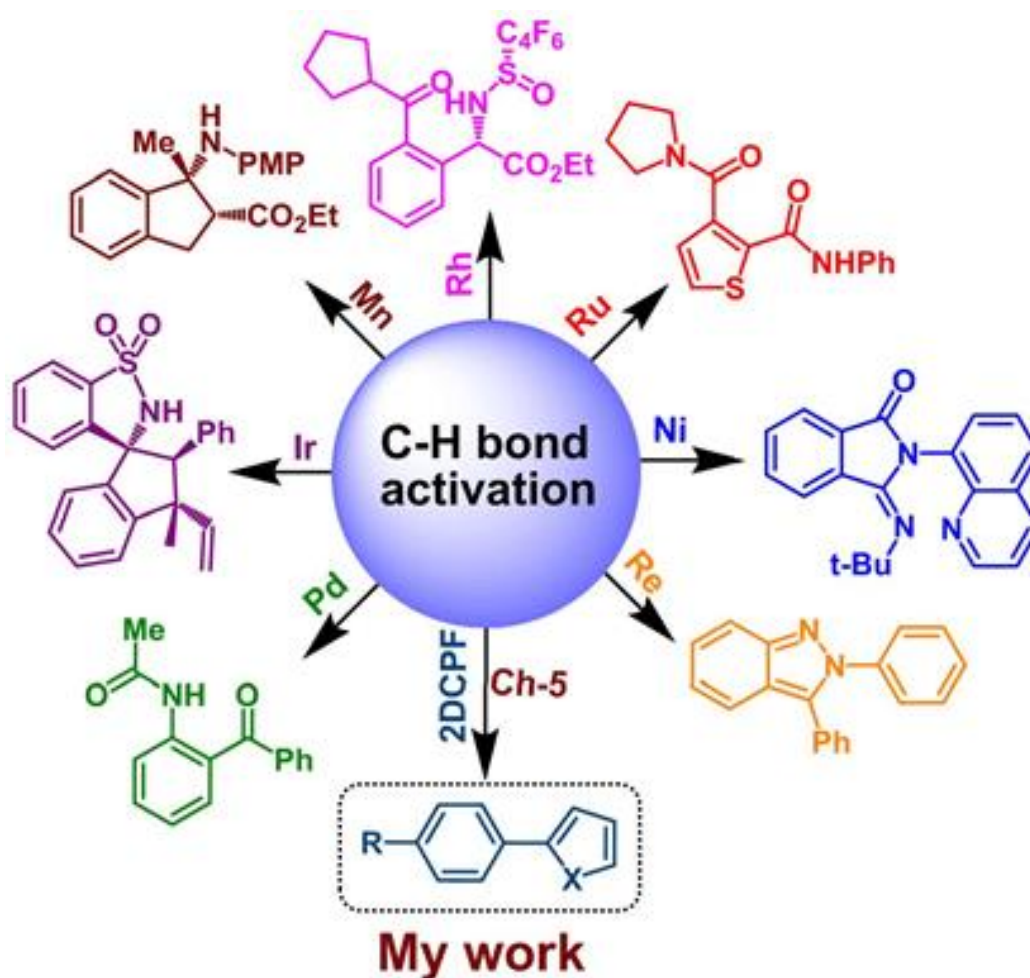


Figure 2. 11 Various metal catalysed and photocatalyzed protocols for C-H bond formation.

2.6.2 1, 3-oxathiolane-2-thiones

A variety of natural products and biologically active compounds contain the 1,3-oxathiolane moiety, exhibiting tuberculostatic, antibacterial, antifungal, and neuroprotective activities [97], [98]. Furthermore, 1,3-oxathiolane-2-thiones serve as valuable intermediates for synthesizing thiols, alkanes, and alkenes, with established applications in material science [99]. While the most efficient synthesis methods of 1,3-oxathiolane-2-thiones involve the opening of oxiranes, catalyzed by alkali metals, these methods suffer from drawbacks such as low yields, efficiency, high loading catalyst, high pressure requirements, and the formation of regioisomeric products. Therefore, a highly efficient, convenient, and regioselective method has been developed to synthesize 1,3-oxathiolane-2-thiones, playing a crucial role in this field. This involves preparing 1,3-

oxathiolane-2-thiones by attaching two functional groups to the styrene substrate under photoredox catalysis

2.6.3 β -keto Sulfoxidation

β -Keto sulfoxides play a significant role in a wide range of pharmaceuticals and natural products, showcasing diverse synthetic applications [102]. The synthesis of β -Keto sulfoxides aligns with the principles of green chemistry by employing eco-sustainable and non-toxic atmospheric oxygen as an oxidant. Many drug molecules feature sulfoxide, sulfonamide, or sulfone groups [100], [101], [102], enhancing the biological activity and solubility of the drug, as exemplified by penilumamide [103]. Furthermore, sulfoxides exhibit antioxidant properties in conjunction with amino acids, potentially contributing to preventing liver damage and activating detoxifying enzymes [104], [105]. Certain sulfoxides also demonstrate anti-tuberculosis activity with notable biological effects [106].

CHAPTER-3

An Efficient Polydopamine Modified
sulphur doped GCN photocatalyst for
Generation of HCOOH from CO₂ under
Sun ray Irradiation

An efficient polydopamine modified sulphur doped GCN photocatalyst for generation of HCOOH from CO₂ under sun ray irradiation

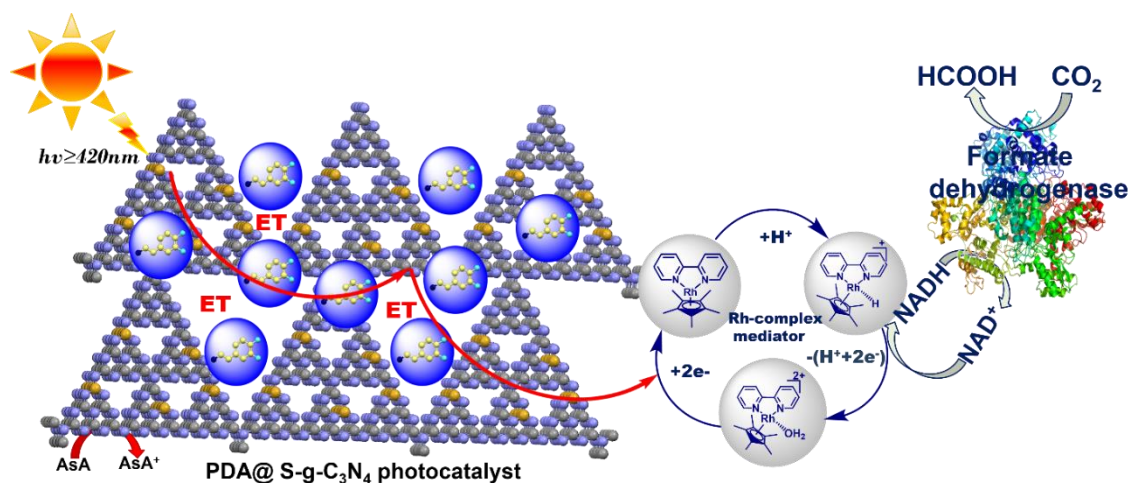
The photocatalytic conversion of CO₂ into solar chemicals presents a promising avenue for green energy and environmental sustainability. However, overcoming the low catalytic performance and poor selectivity of photocatalysts remains a significant challenge in this field. To address these issues, we devised a strategy inspired by natural photosynthesis, harnessing the high specificity and efficiency of enzymes. In this study, we developed a metal-free photocatalyst, polydopamine (P) modified sulfur-doped graphitic carbon nitride (P@SGCN), aimed at synergistically addressing the aforementioned challenges. Our work focuses on the regeneration of NADH and the highly selective production of formic acid, HCOOH, from CO₂. This research introduces a novel approach utilizing polydopamine-modified photocatalysts for the production of solar chemicals/fuels from CO₂.

3.1 Introduction

In greenhouse gases, carbon dioxide, CO₂, is one of the important factors which causes crucial environmental problems, such as global warming, sea levels rising, and glacier melting [107]. Reducing CO₂ in an efficient manner is a complicated issue and a big challenge [108]. Following this, extensive investigations have been carried out on the multi-electron reduction of CO₂ to formic acid, HCOOH. Drawing inspiration from the natural photosynthesis process, numerous scientists have explored methods for transforming CO₂ into solar chemicals or high-value-added products, employing techniques such as electrocatalysis [108], photocatalysis [109], thermal catalysis [110], and others. Among these experimental approaches, photocatalytic conversion of CO₂ utilizing light-harvesting materials offers several advantages, including energy savings and environmentally friendly conditions [1]. Currently, various semiconductor materials such as cadmium sulfide (CdS) [111], TiO₂ [112], ZnO [113], zero-valent copper [114], heteroatom-doped catalysts [115], and graphene carbon nitride (g-C₃N₄ or GCN) [116] have been employed in this field. Among these photocatalysts, the GCN complex stands out as an inexpensive and metal-free option that has garnered significant attention due to its outstanding physical and chemical properties, including a suitable bandgap (~2.7 eV), excellent responsiveness to solar light, non-toxicity, and stable thermal stability [117]. Nevertheless, the utilization of GCN as a photocatalytic material for CO₂ reduction still presents several limitations, including poor photocatalytic activity, rapid charge recombination, and low specific surface area [118]. In response, numerous studies have been conducted to enhance its photocatalytic performance, employing strategies such as

surface functionalization [119], metal-nonmetal doping [120], noble metal deposition [121], and integration with carbonaceous materials [122]. Among these approaches, non-metal chemical doping, particularly sulfur atom incorporation, has emerged as a promising avenue. Sulfur doping has been found to enhance visible light absorption and promote the separation rate of charge carriers in GCN [123]. Through a self-doping technique, Wang et al. demonstrated that sulfur-doped GCN (SGCN) exhibited favorable photocatalytic properties for CO₂ reduction [66]. Among the various surface modifications explored, the coupling of electron acceptors along with the attachment of organic groups to SGCN appears particularly promising. This approach is anticipated to augment the solar light absorption capacity, facilitate efficient electron-hole separation, and enhance photocatalytic efficiency.

Therefore, exploring stable immobilized modifiers for graphitic carbon nitride photocatalysts is imperative to effectively enhance light-harvesting and photocatalytic efficiency. Dopamine, a biopolymer utilized across various fields including biomedicine, environmental science, and energy, holds significant importance due to its excellent biocompatibility, hydrophilicity, and diverse adhesion capabilities, making it a valuable organic material for surface functionalization [124]. Its polymeric form, known as polydopamine (P), possesses high UV and visible-light absorption properties, making it readily applicable for surface modification [125]. Moreover, polydopamine (P) contains numerous catechol groups, enabling the formation of semiquinone/quinone groups under neutral and basic conditions, facilitating electron and proton transfer from an electron donor. In this study, we developed a metal-free photocatalyst, polydopamine (P) modified sulfur-doped graphitic carbon nitride (P@SGCN), through direct chemical doping of polydopamine into SGCN. In the resulting photocatalyst, polydopamine (P) efficiently facilitates the transfer of photoinduced electrons for the artificial photocatalytic process, thereby reducing rapid electron-hole recombination. Notably, polydopamine (P) exhibits exceptional adhesion capabilities, allowing straightforward modification onto the surface of SGCN. The P@SGCN photocatalyst demonstrated remarkable photocatalytic efficiency in regenerating NADH and selectively producing formic acid, HCOOH, from CO₂, as depicted in Scheme 3.1.



Scheme 3. 1 Artificial photosynthesis process based on P@SGCN photocatalyst/biocatalyst coupled process for the generation of HCOOH from CO₂ under the irradiation of solar light.

3.2 Experimental Section

3.2.1 Materials Used

Thiourea, dopamine hydrochloride (purity $\geq 98\%$), formate dehydrogenase (FDH), NaH₂PO₄·2H₂O, Na₂HPO₄·2H₂O, and NAD⁺ (purity $\geq 98\%$) were purchased from Sigma-Aldrich. The electron mediator organometallic Rh-complex ([Cp*⁺Rh(bpy)Cl]Cl), (Cp* = η^5 -C₅M_e₅, bpy = 2,2-bipyridyl) was prepared by reported protocol.

3.2.2 Instruments and measurements

The linear absorption spectra were recorded by the Shimadzu spectrophotometer. Fourier transform infrared (FT-IR) spectrum was recorded on a Bruker ALPHA-T FT-IR spectrometer. Zeta-potential and particle size were measured by a nano-zeta sizer (NYS90). A powder X-ray diffractometer (Bruker, D8 Advance Eco) was used for investigations of crystallinity. A scanning electron microscope (JSM 6490 LV, JEOL) was used to investigate the morphologies of the as-synthesized chemical composites. Transmission electron microscopic (TEM) images were collected by TECNAI G2 F30 microscope operated at 300 kV.

3.2.3 Preparation of SGCN

The SGCN was synthesized by heating the 5g thiourea in the muffle furnace at 520°C for 5 hours shown in Figure 3.1.

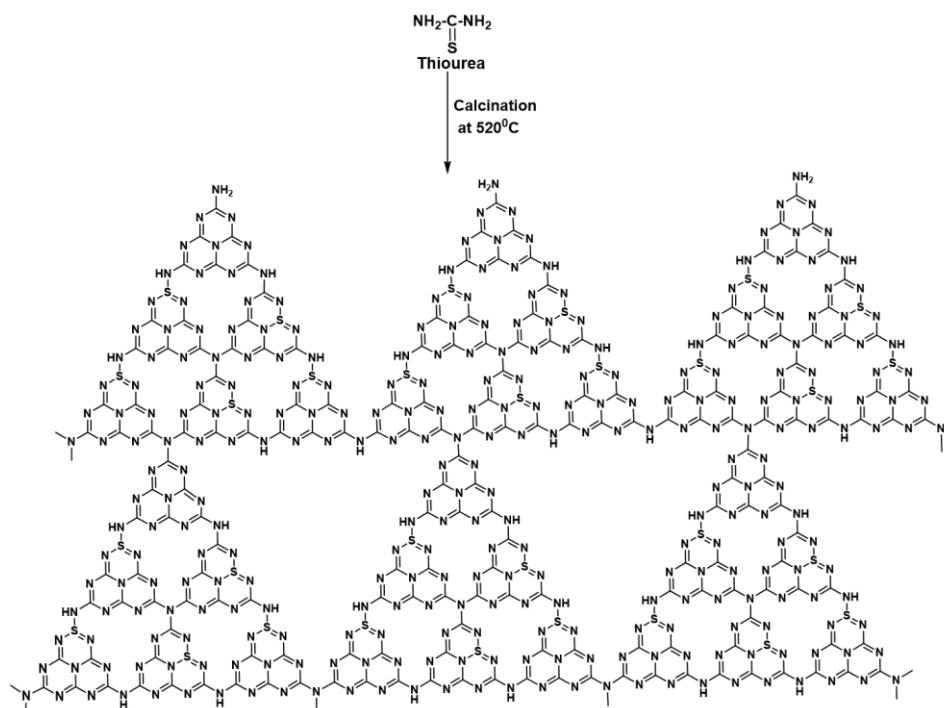
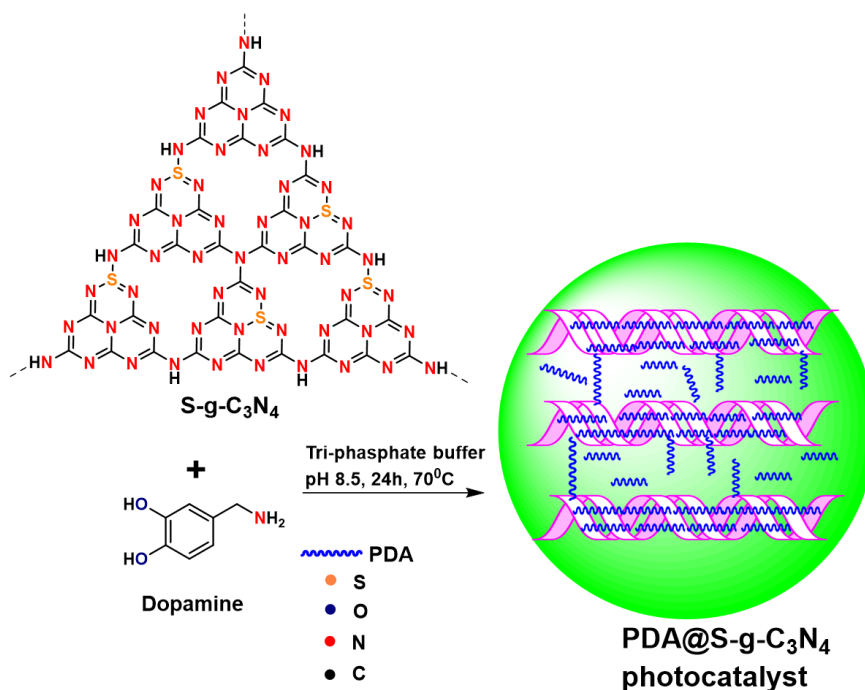


Figure 3. 1 Synthesis of S-g-C₃N₄ photocatalyst.

3.2.4 Preparation of the P@SGCN

The P@SGCN was synthesized according to the reported protocol Scheme 3.2 [109]. Initially, 700 mg of SGCN was mixed in 100 mL of buffer solution followed by the addition of 140 mg of dopamine. The suspension was stirred at 1200 rpm at 70 °C for 24 h. Afterward, the obtained product was cooled at ambient temperature and washed thoroughly with distilled water 3 times to remove unreacted reagents. Lastly, the resultant product was dried at 60 °C. The details about the photocatalytic experiments were described in Supporting Information.



Scheme 3. 2 Schematic diagram of the preparation of the PDA@S-g-C₃N₄ photocatalyst.

3.2.5 Photoregeneration of NADH

The NADH regeneration was carried out in a quartz reactor at room temperature in an inert atmosphere, using a 450 W xenon lamp (Newport 66921) with a 420 nm cutoff filter as a light source. The photocatalytic reaction was taken place in a quartz reactor. The reaction was composed with NAD⁺(248 μL), Rh (124 μL), AsA (310 μL), and photocatalyst (31 μL) in 3.1mL of buffer solution (0.1M, pH 7.0).

3.3 Result and Discussion

3.3.1 UV-Visible spectroscopy

The UV–visible absorption spectra of SGCN and P@SGCN were measured with the samples dispersed in DMF solvent. The UV–visible absorption spectrum of SGCN clearly shows that the pristine SGCN shows a higher absorption near UV range and a low absorption spectrum near visible range, with an optical bandgap of 2.74 eV, which is an important characteristic property of SGCN [110]. The incorporation of P on the SGCN medium significantly enhanced the optical absorption of the P@SGCN photocatalyst compared to the SGCN in the entire spectral range (Figure 3.2). By the incorporation of P onto SGCN, the optical bandgap of P@SGCN gradually decreases. This optical property is likely to enhance the intense light absorption capability as well as the efficient charge generation in the P@SGCN photocatalyst [111].

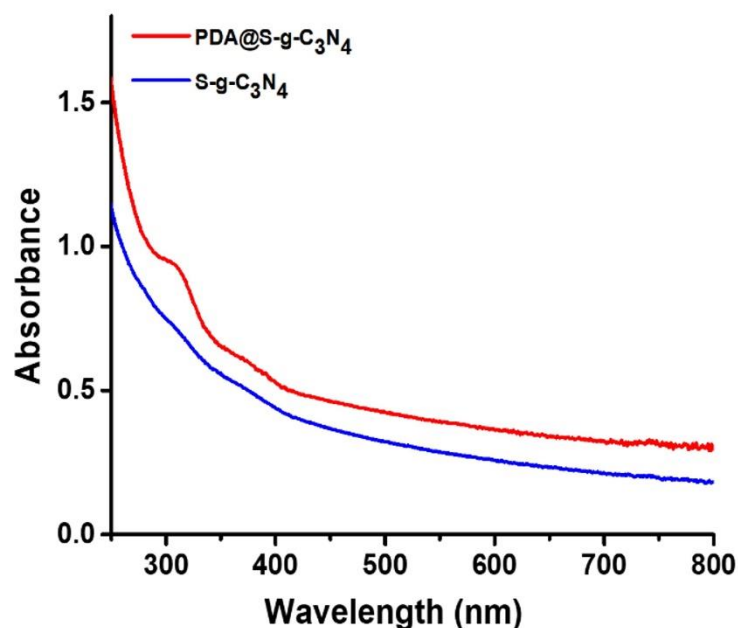


Figure 3. 2 UV-visible absorption spectra of PDA@S-g-C₃N₄ (red) and S-g-C₃N₄(blue) photocatalysts

3.3.2 FTIR spectroscopy

The chemical structures of pristine SGCN and P@SGCN were examined by FT-IR spectroscopy. As shown in Figure 3.3, the FTIR spectrum of the P@SGCN photocatalyst is similar to that of the pristine SGCN with the minor changes, implying that the original structure of SGCN was well kept in the P@SGCN photocatalyst. The mode at 800 cm^{-1} was attributed to the characteristics breathing vibration in the triazine unit. The broad peak around $1200\text{--}1700\text{ cm}^{-1}$, with the typical peaks at 1327 , 1473 , and 1616 cm^{-1} corresponds to the stretching vibrations of C–N, and C–N in SGCN[112]. The peak exhibited at 3113 cm^{-1} is mainly due to the stretching vibration of the O–H and N–H bonds, which demonstrated that the P was well incorporated onto the surface of the SGCN medium [113].

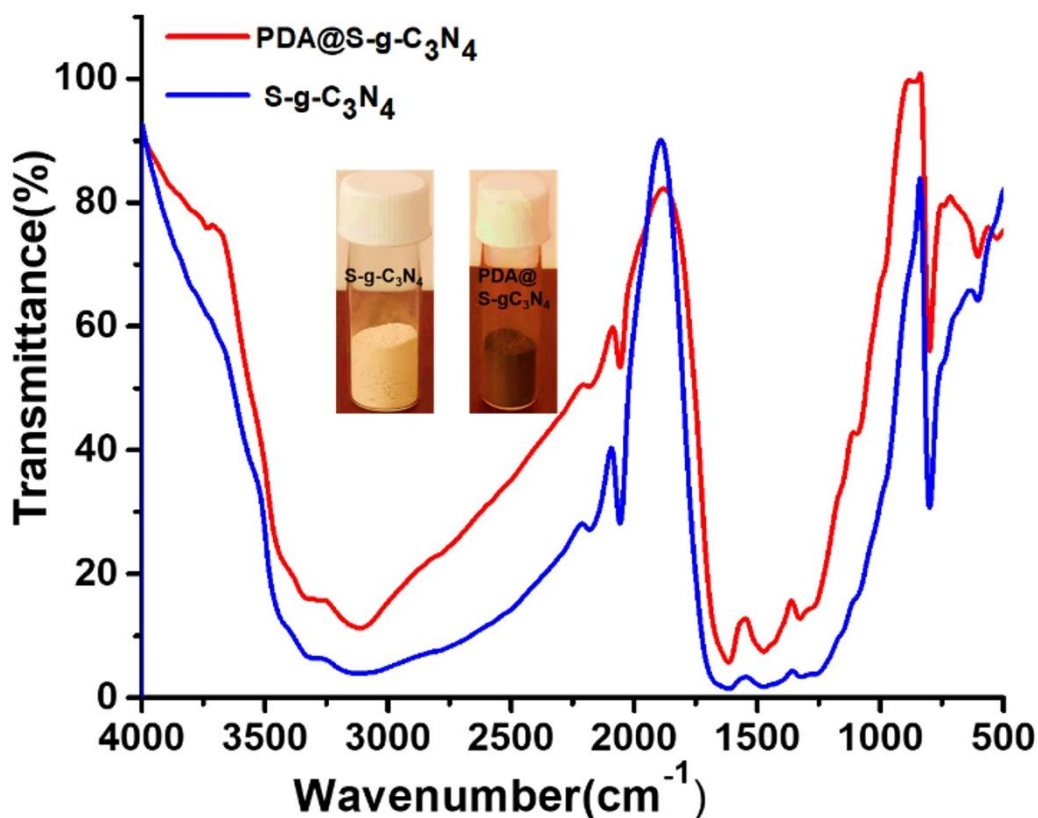


Figure 3. 3 FTIR spectra of PDA@S-g-C₃N₄(red) and S-g-C₃N₄(blue) photocatalysts.

3.3.3 X-ray diffraction Analysis

To investigate the morphologies of SGCN and P@SGCN photocatalysts, scanning electronic microscopy (SEM) technique was used as shown in Figure 3.4. The SEM images of SGCN exhibited an agglomerated morphology with the sheet and some short rods stuck on the sheet, whereas the morphology of P@SGCN shows the sub-micrometer crystallite with the shape of short rods [114]. To further study the crystalline structure of P@SGCN photocatalyst, we implemented the powder X-ray diffraction (PXRD) analysis. In the as-synthesized P@SGCN photocatalyst, the two prominent peaks at 12.38° and 27.81° were observed as shown in Figure 3.4. According to the previous study [51], the two prominent peaks of SGCN around 13.35° and 27.69° were reported and were attributed to the inter-planar structural packing and stacking of the conjugated aromatic system, respectively. We expected that even though the polydopamine moieties were incorporated onto the SGCN medium, the structure of SGCN was well kept [115].

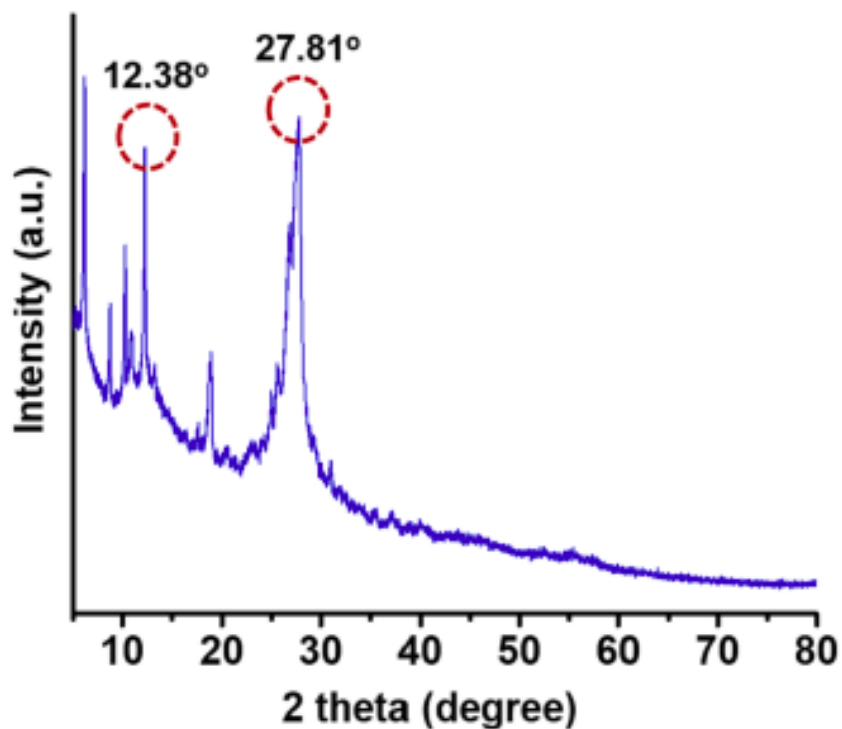


Figure 3. 4 Powder X-ray diffraction (PXRD) analysis of as-synthesized P@SGCN photocatalyst.

3.3.4 HR-TEM Analysis

To examine the high-resolution topography of the P@SGCN photocatalyst, we also performed the measurement using transmission electron microscopy (TEM). The selected area electron diffraction (SAED) pattern, measured with the same instrument, was azimuthally averaged by using the established protocol in order to determine the d-spacing value between the diffraction peaks [116]. As shown in Figure 3.5, the lattice spacing (d-spacing) of 0.333 nm ($=1/3.002$ nm) was observed in the SAED pattern. The observed lattice spacing was well matched to the (002) planes observed in the Bragg's peak at 27.81° in the PXRD. To confirm the existence of atomic elements in the P@SGCN photocatalyst, we performed the energy dispersive spectroscopy (EDS) installed in the TEM instrument. As shown in Figure 3.5, the element-specific mapping images clearly show the co-existence of C, N, and O elements with the different relative fractions. The relative amounts of atoms (C, N, O, S) were listed in the Figure 3.5. We also performed the X-ray photoelectron spectroscopic (XPS) measurement for the as-synthesized P@SGCN photocatalyst. Based on the measured XPS spectra shown in Figure 3.5, the O1s spectrum shows the clear two peaks around 530.8 eV and 532.4 eV. According to

the previous study for polydopamine nanoparticle [117], those peaks can be attributed to the components of C–O–H and C=O, respectively. It is noted that the positions for the doping sites of polydopamine moieties on the ay-synthesized catalyst can be checked from the EDS mapping image for oxygen atom. The S2p spectrum shows the clearly separated two peaks at 163.5 eV and 167.9 eV. Among those peaks, the peak around 164 eV can be assigned to the element of C–S bond which is formed by the replacement of nitrogen in pristine g-C₃N₄ to sulfur atom [66]. On the other hand, the N1s spectrum exhibits the broad-shaped feature around 398 eV including the several peaks. The most intense peak at 398.6 eV corresponds to the sp² hybridized aromatic nitrogen atom connected to carbon atoms of C–N–C in the sulfurdoped g-C₃N₄. The results from the SEM, PXRD, TEM, and XPS measurements support that the polydopamine moieties are well doped onto the surface of SGCN surface [37,51].

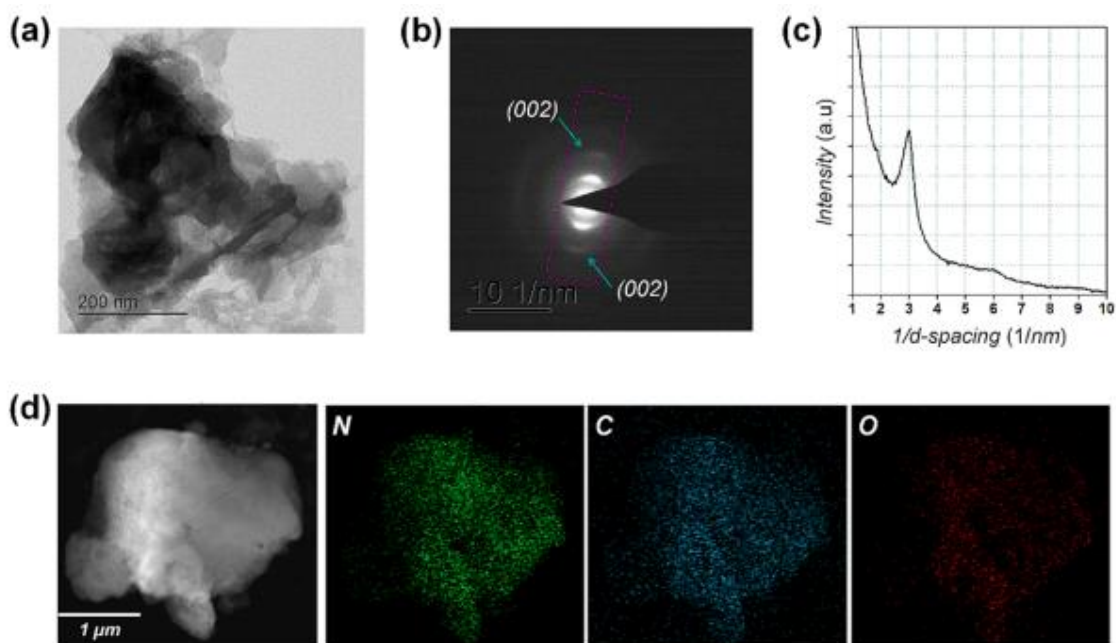


Figure 3. 5 Transmission electron microscopy (TEM) measurement of P@SGCN photocatalyst. (a) TEM image of P@SGCN photocatalyst. (b) Selected area electron diffraction (SAED) image. (c) The one-dimensional profile of the area indicated by the magenta rectangle in the SAED image. The lattice spacing (d-spacing) of 0.333 nm (=1/3.002 nm) corresponds to the (002) planes in the SGCN medium. (d) Elemental mapping measured by the energy dispersive spectroscopy (EDS) for P@SGCN photocatalyst. Left figure shows the target range for the EDS mapping and right figures

show the element-specific mapping images. The existence of oxygen element (red color) in the measured range implies that the polydopamine moieties are well doped onto the SGCN medium.

The average particle sizes of SGCN and P@SGCN photocatalysts were investigated by using the dynamic light scattering (DLS) technique. As shown in Figure 3.6, the average particle size of the pristine SGCN and P@SGCN photocatalysts were to be ~ 600 nm and ~ 250 nm, respectively. The smaller particle size of the P@SGCN is likely to improve the photocatalytic properties due to the efficient charge migration with the large surface area.[118]

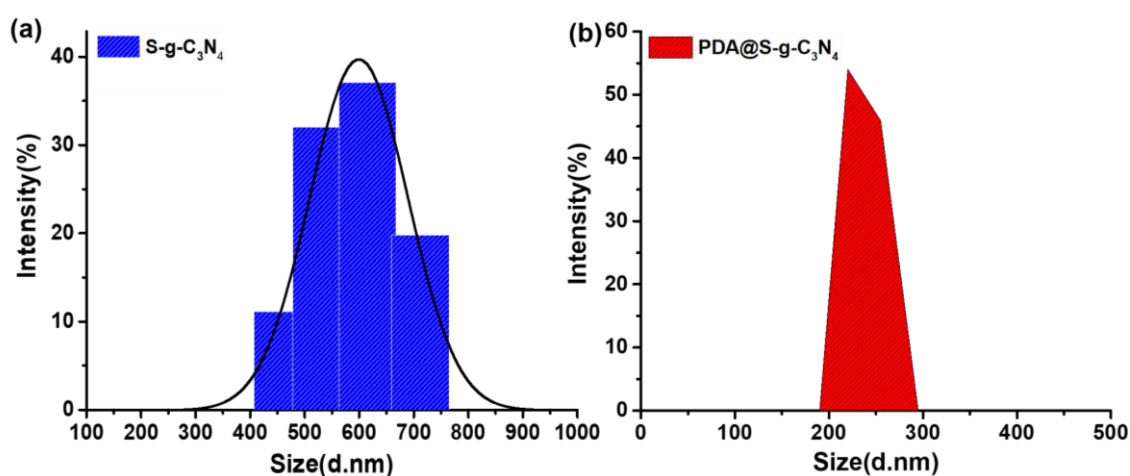


Figure 3.6 Particle size analysis of (a) S-g-C₃N₄ and, (b)PDA@S-g-C₃N₄ photocatalysts.

3.3.6 Zeta potential

Furthermore, the modification of P on the SGCN surface was also confirmed by the zeta potential. As depicted in Figure 3.7, the P-modified SGCN shows more negative zeta potential with - 13.4 mV as compared to SGCN with - 3.39 mV which indicates the surface modification of P into SGCN surface [119].

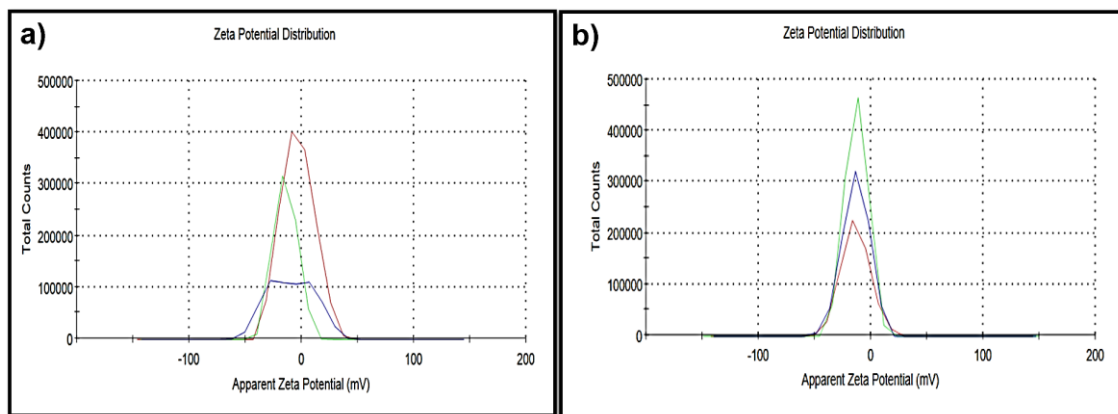


Figure 3. 7 Zeta potential analysis of (a) S-g-C₃N₄ (-3.39 mV), and (b) PDA @S-g-C₃N₄ (-13.4 mV) photocatalysts.

3.4 A Photoinduced regeneration of NADH and production of HCOOH from CO₂

We performed the catalytic tests for the photoinduced regeneration of NADH using the polydopamine units (P), pristine SGCN, and P@SGCN photocatalysts. As shown in Scheme 3.1, we employed the artificial photosynthetic scheme including the photocatalyst/biocatalyst coupled process for the generation of HCOOH from CO₂ under the irradiation of solar light. In all cases, the production yield of NADH was checked by UV–visible spectroscopic measurement. As depicted in Figure 3.8a, the P@SGCN photocatalyst showed the maximum yield of 80.38 % within 150 min. In contrast, the P and pristine P@SGCN showed 0 % and 20.14 % for the NADH regeneration, respectively. Using the same samples, we examined the photocatalytic efficiencies of the P, pristine SGCN, and P@SGCN photocatalyst for the production of HCOOH from CO₂. As depicted in Figure 3.8b, the P@SGCN photocatalyst showed that the catalytic yield of HCOOH linearly increased as a function of reaction time. The P@SGCN photocatalyst produced the amount of HCOOH with 310.16 μM from CO₂ under the irradiation of solar light. The highly selective generation of HCOOH in a more amount clearly indicates the outstanding photocatalytic efficiency of P@SGCN compared to the other photocatalysts of P and SGCN. The trends in the NADH regeneration and the production of HCOOH as a function of reaction time were deviated from the linear relationship in terms of production yield versus reaction time.

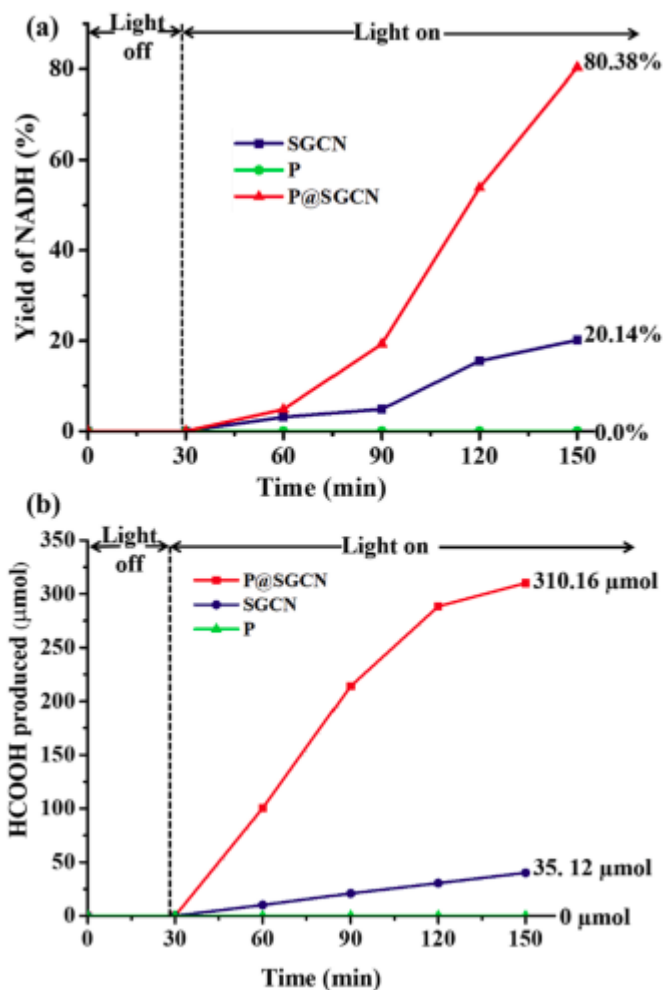


Figure 3. 8 Photocatalytic activities using polydopamine (P), pristine SGCN, and P@SGCN photocatalysts. Catalytic tests for (a) NADH regeneration and (b) production of HCOOH from CO₂.

3.4.1 Reusability and Chemical Stability

Such a trend can originate from the instability of the P@SGCN photocatalysts used in the catalytic tests. To check this possibility, we investigated the stability and reusability of the P@SGCN photocatalyst under the same experimental conditions. In the first cycle (fresh condition), the P@SGCN photocatalyst showed the regeneration yield for NADH with 80.38 % and the production yield for HCOOH with 310.16 μM. At the fifth cycle, we found that the regeneration yield of NADH was slightly decreased to 76.38 % and the production yield of HCOOH was also slightly decreased to 290.78 μM. This result implies that the P@SGCN photocatalyst has the excellent chemical stability in view of the long-term performance. Nevertheless, to verify the non-linearity of catalytic

performance in terms of production yield versus reaction time, it is required to understand the detailed reaction mechanism during the photocatalyst/biocatalyst coupled process. To do so, the additional studies based on time-resolved and operando spectroscopies [57–58] should be performed in near future.

3.5 Photocatalyst/biocatalyst coupled process for the generation of HCOOH from CO₂

Scheme 3.1 shows a pictorial illustration of the photocatalytic-biocatalytic coupled process for the generation of HCOOH from CO₂. The polydopamine-modified SGCN photocatalyst (P@SGCN) is a primary light-harvesting material in which P acting as an electron acceptor is incorporated to the SGCN medium acting as an electron donor. First, the P@SGCN can absorb the sunlight and transfer the photo-excited electrons to the organometallic Rh-complex (Rh), acting as an electron mediator. The Rh-complex will effectively accept the photo-generated electron and subsequently be reduced .[120] Afterward, Rh can abstract an H⁺ from an aqueous solution, and transfer the electron and a hydride to a nicotinamide cofactor (NAD), which is transformed to NADH . As a consequence, the Rh acts as an electron mediator between the P@SGCN and nicotinamide cofactor (NAD⁺), showing to be a significant factor in NADH regeneration. Ultimately, the form of NADH can be utilized for the generation of HCOOH from CO₂ via the enzymatic conversion in the formate dehydrogenase.

In summary, a newly synthesized P@SGCN photocatalyst for the artificial photosynthesis. The properties of as-synthesized P@SGCN photocatalyst were systematically characterized by employing the optical spectroscopies, SEM, XRD, TEM, XPS, and EDS analyses. Due to the strong interfacial adhesion of P, the polydopamine moieties were readily incorporated onto the SGCN. The chemical modifications facilitate the enhanced electron transfer between P moieties and SGCN medium. The P@SGCN photocatalyst showed the excellent photocatalytic performance for the NADH regeneration and the direction conversion of CO₂ to HCOOH. Our study demonstrates that for the generation of solar chemicals from CO₂, the P@SGCN is an excellent light-harvesting module in the photocatalytic/biocatalytic integrated system.

CHAPTER-4

A Spherical Photocatalyst to Emulate Natural Photosynthesis for the Production of Formic Acid from CO₂

A spherical photocatalyst to emulate natural photosynthesis for the production of formic acid from CO₂

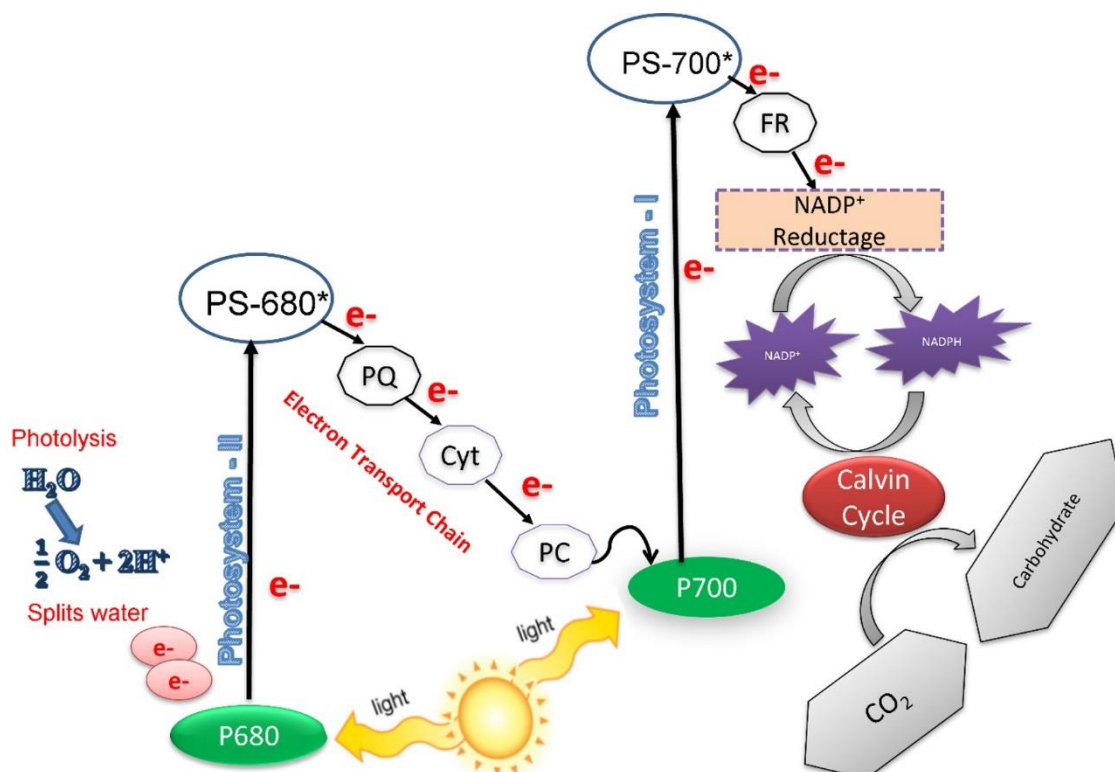
The conversion of carbon dioxide (CO₂) into fuels is an attractive solution to many energy and environmental challenges. However, the chemical inertness of CO₂ renders many photochemical conversion processes inefficient. In this work, efficient photocatalytic formic acid production from CO₂ has been carried out by a novel Bromophenol-Bakelite (BPB) composite that is made of bromophenol blue dye-doped inside the Bakelite matrix. The BPB-composite act as a visible light-harvesting photocatalyst in a photocatalyst–enzyme coupled artificial photosynthetic system. Seven-fold increase in the yields of NADH and formic acid has been obtained with the BPB-composite photocatalyst than bromophenol along with photocatalyst being thermally very stable. Hence, an effective photocatalyst has been synthesised for the selective production of solar chemicals directly from CO₂ via artificial photosynthesis.

4.1 Introduction

Global warming is one of the greatest threats to human survival. The upsurge in global carbon emission is the major factor causing global warming. Excessive dependence on fossil fuels to meet the ever-increasing energy demand is one of the main sources of carbon emission [121]. Hence there are efforts made throughout the world to develop strategies that are scientifically sound and economically viable to moderate the trends in global warming and to reverse the adverse climate changes [122][123]. Many effective strategies for reducing carbon emissions have been developed [124]. An especially fascinating and attractive approach is direct energy conversion from solar to chemical to produce fuels that are non-polluting and renewable [125]. Observing nature could offer a key method for the realisation of efficient solar energy conversion [126]. During photosynthesis, green plants convert light into chemical energy [127]. Solar energy is absorbed by chlorophyll present in the leaves of plants and generates high energy electrons [128]. These photoinduced electrons are transferred to enzyme ferredoxin through the electron transport chain causing NAD⁺ (nicotinamide adenine dinucleotide to be converted to NADH (reduced form of the nicotinamide cofactors) [129][130]. Solar energy is thus stored as the energy currency of cells (Scheme 4.1). In Calvin Cycle, NADPH with high reducing power serves as a hydrogen source for the synthesis of carbohydrates from carbon dioxide [131]. Motivated by the photocatalyst/biocatalyst system in natural photosynthesis, scientists are working to develop its artificial analogue [128][132]. For solar energy conversion, artificial photosynthesis has been recently

recognised as an eco-friendly and highly useful method [133]. The most suitable system for artificial photosynthesis is a photocatalyst–enzyme coupled system [134]. In this system, fuels and chemical synthesis take place by utilisation of solar energy. The most daunting task for the practical applicability of the photocatalyst–enzyme coupled artificial photosynthesis process is finding materials that are visible light active and highly efficient so can be used as photocatalysts [135]. Such photocatalyst should actively participate in the regeneration of NADH and henceforth initiate the formation of solar chemicals from CO₂ [131][136][137][138]. A chemical that has gained extensive attention is formic acid which is a two-electron reduction product of CO₂ [134]. Formic acid is a versatile acid and has several uses such as it can be used as insecticide, preservative, reducing agent and in industries of synthetic chemicals; it can be employed as a source of carbon [125]. Sustainable efforts are required for the search of photocatalyst that would produce formic acid from carbon dioxide, as for till now only a few have been reported [134][131][139][107]. We sought to use a unique architecture consisting of a bakelite matrix with bromophenol blue dye trapped in its structure for the selective production of formic acid from CO₂. To the best of the author's knowledge, such a structure as a photocatalyst has not been studied yet. Bakelite with its remarkable properties has proved to be a mounting superstar with its wide variety of uses in the electrical insulator, kitchenware, jewelry children's toys, pipe stems, molding compounds, and also as thermal insulating materials for many industrial applications [139]. Roza et.al [140] has reported that the strategic addition of a small number of particles in the polymer matrix that forms composite material opens a whole new avenue to not only enhance the electrical and mechanical properties of composite in the desired manner but also improves its optical and thermal properties.

In this work, we have synthesized a novel Bromophenol-Bakelite (BPB) composite with bromophenol blue dye-doped inside the Bakelite matrix that is visible light active photocatalyst in an artificial photocatalyst-enzyme couple set up for the production of formic acid from carbon dioxide. The results show enhancement in photocatalytic properties of BPB- composite in comparison to pure bromophenol blue dye.



Scheme 4. 1 Schematic illustrations of Z-scheme in natural photosynthesis. The absorption of solar light energy by chlorophyll in the leaves of plants causes electrons to excite. NAD⁺ is reduced to NADH as a result of a sequential multi-electron transfer. The cofactor thus formed is used to produce carbohydrates in the Calvin cycle (PC = plastocyanin, PQ = plastoquinone, FR = ferredoxin and Cyt = cytochrome complex) [126][128]

4.2 General remarks

Bromophenol blue [C₁₉H₁₀Br₄O₅S], formaldehyde, acetic acid (CH₃COOH), phenol, hydrochloric acid (HCl), NAD⁺ and ascorbic acid have been used in the present study. All the chemicals were utilized as purchased from TCI and Sigma-Aldrich. Rhodium complex [Cp*Rh(bpy)Cl]⁺ was prepared using the approach described in the literature

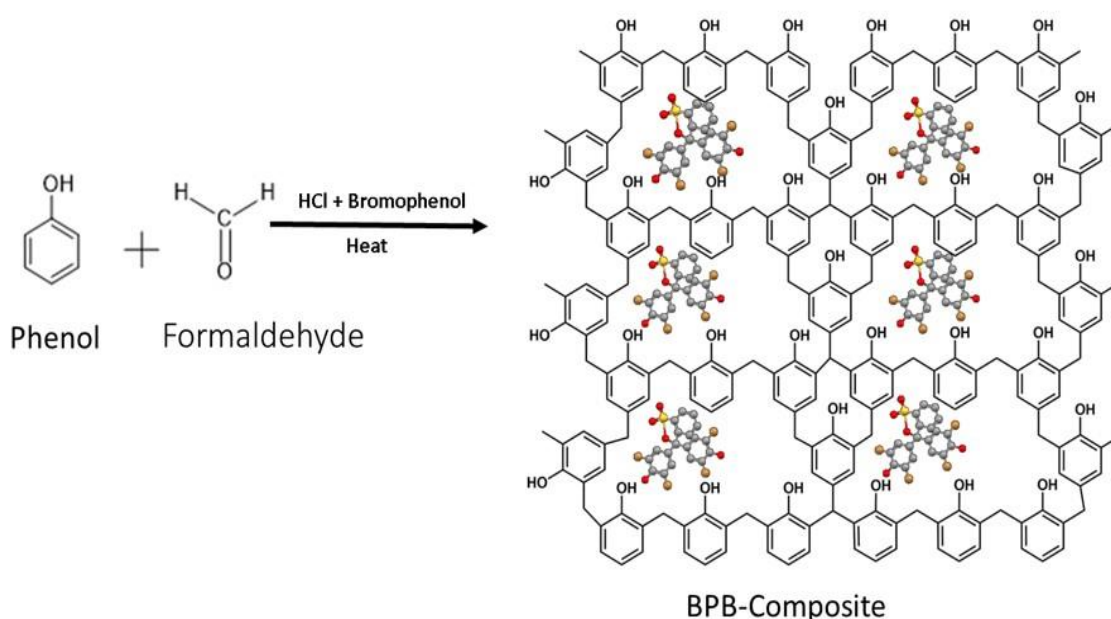
4.3 Instruments and Measurement

The LI-2700 UV-VIS double beam spectrophotometer was used for the analysis of Ultraviolet-Visible (UV-Vis) absorption spectra of bromophenol, bakelite and BPB-composite. The spectrometer (ALPHA-T FT-IR) was used to record Fourier transform infrared spectroscopy (FTIR) spectra of bromophenol and BPB-composite. At 15kV accelerating voltage, instrument FET Phillips (Model No. 200k VLAB6, (FEL TECNAI G2 -20S-Twin)) was used for obtaining field emission scanning electron microscopes

(FE-SEM) images. The thermal stability of bromophenol and BPB-composite was investigated using differential scanning calorimetry (DSC) on a DSC Q-1000 in a nitrogen atmosphere. Dynamic light scattering (DLS) measurements were done on the Zetasizer Nano ZS (NZS90) to estimate the particle size of the synthesized photocatalyst. At $T = 25\text{ }^{\circ}\text{C}$ zeta potential analysis was done of photocatalyst on the instrument Zetasizer Nano ZS. HPLC (high-performance liquid chromatography, Model: LC-20AP) was used to determine the quantity of formic acid produced.

4.4 Synthesis of BPB-composite photocatalyst

To synthesise BPB-composite (Scheme 4.2), initially 2g of phenol and 4 mL of formaldehyde were mixed along with the con. CH_3COOH and HCl in a pre-dried beaker. Thereafter 40 wt% of bromophenol was incorporated into the reaction mixture and heated to $60\text{ }^{\circ}\text{C}$ with continuous stirring [141]. White precipitate starts appearing and with constant and vigorous stirring pink colour plastic forms. Thereafter, the obtained solid powder of BPB-composite was washed with water multiple times and kept for drying at $70\text{ }^{\circ}\text{C}$ under a vacuum [141]



Scheme 4. 2 Synthesis of BPB-Composite.

4.5 Process of photocatalytic NADH regeneration

The NAD⁺ to NADH photochemical reduction was accomplished by employing a 450W Xenon lamp as a light source in a quartz reactor at ambient temperature [142]. The reaction was done under an inert atmosphere. A 420 nm cut-off filter was used to trim the spectrum generated by the lamp, allowing UV radiation to be irradiated selectively into the sample. 1.24 mmol ascorbic acid AsA (sacrificial agent) and 0.62 μmol Rh complex mixed in sodium phosphate buffer (3.1 mL) were used in the reaction sample. The photocatalyst bromophenol or BPB-composite (concentration 0.031X10⁻⁶ mol) was also added to the solution, along with NAD⁺ (1.24X10⁻⁶ mol). The regeneration progression of NADH was followed spectroscopically [142].

4.6 Procedure to produce Formic Acid from CO₂

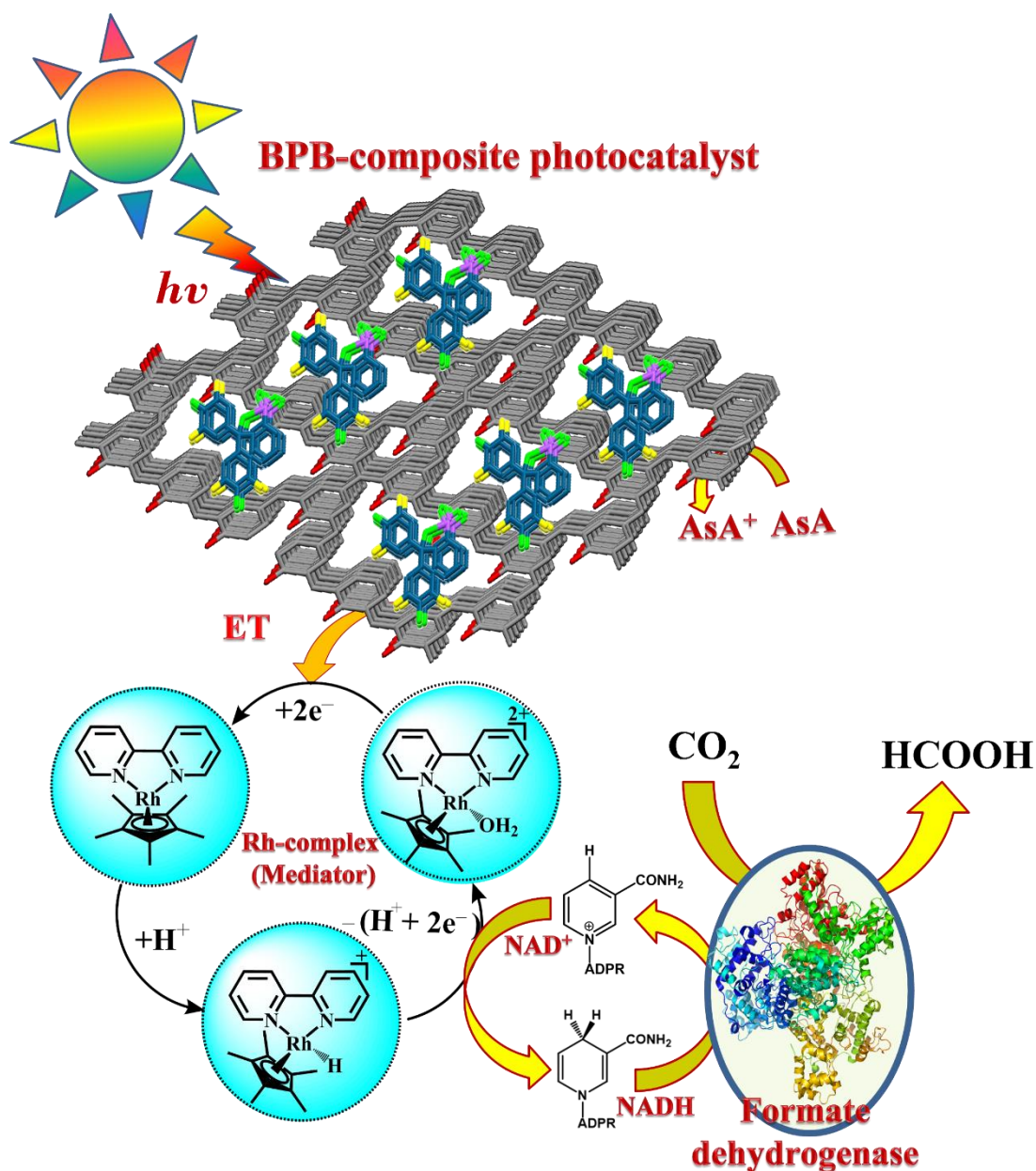
Formic acid production from carbon dioxide in artificial photosynthesis was carried out in a quartz reactor employing a 450W Xenon lamp as a source of light at ambient temperature. The reaction was performed under an inert atmosphere. A cut-off filter of 420 nm was used to trim the spectrum generated by the lamp, allowing UV radiation to be irradiated selectively into the solution. The sample consisted of sacrificial agent ascorbic acid 1.24 mmol (AsA), formate dehydrogenase (3 units) and 0.62 μmol Rh complex, mixed in sodium phosphate buffer (3.1 mL) solution in the presence of CO₂ (flow rate: 0.5 mL/min). The photocatalyst bromophenol or BPB-composite (0.5 mg) was also added to the solution, along with β-NAD⁺ (1.24 10⁻⁶ mol). For one hour the reactor was bubbled with CO₂ with lights off and then exposed to visible light (lights on). HPLC (high-performance liquid chromatography, Model: LC-20AP) was used to determine the quantity of formic acid produced.

4.7 Results and Discussion

4.7.1 Design an artificial enzyme-coupled photocatalytic system

Many experimental attempts in artificial photosynthesis are being made to replicate the principle of natural photosynthesis in facilitating the required reaction sequence (8). Scheme 4.3 shows a pictorial representation of the photocatalyst/enzyme coupled system using synchronised photocatalysis and bio-catalysis working mechanisms for formic acid formation from CO₂ [143]. The absorption of visible light by BPB-composite that plays the role of primary photosensitiser causes electrons to excite that are transferred to rhodium complex Rh [Cp*Rh(bpy)H₂O]₂⁺ which here is the reaction mediator. Upon

reduction, a proton is extracted by the Rh complex and a hydride ion is provided to NAD^+ , causing the NADH cofactor to regenerate [129]. Hence the rhodium complex act as a reaction centre and efficient mediator of electron between the photocatalyst and NAD^+ . Finally, the CO_2 conversion to formic acid takes place with the consumption of the NADH cofactor by the formate dehydrogenase enzyme. The released NAD^+ from the enzyme then again functions as a precursor for the photocatalytic cycle resulting in the regeneration of NADH. Formic acid is thus produced directly from CO_2 by this integrated working of photocatalytic and enzymatic cycles [134]. The suggested mechanism has also been reported earlier by many studies [134][143][139].



Scheme 4. 3 Schematic illustration of a BPB-composite photocatalyst-enzyme coupled system for formic acid production from CO₂.

4.7.2 Characterisation of N-EGQD photocatalyst

4.7.2.1 UV-Visible studies

UV-Vis's absorption spectra were used to investigate the visible light-harvesting efficiency of bromophenol, bakelite, and BPB-composite photocatalysts, as shown in Figure 4.1. UV study of bromophenol, bakelite and BPB-composite was performed in dimethylformamide. The ability to absorption of visible light by BPB-composite is indicated by a broad band of 520 nm to 650 nm whereas bakelite does not show such characteristic. Solutions of bromophenol, which is a well-known indicator [144] when irradiated by UV light show an absorption peak at $\lambda = 602$ nm and an optical bandgap of 2.05 eV. There is an increase in absorbance of BPB-composite than that of pure bromophenol. The regeneration of NADH requires organometallic rhodium complex reduction and the obtained optical band gap of BPB-composite is sufficient for reducing the Rh complex. Hence the efficiency of BPB-composite photocatalyst for solar energy harvesting is indicated by its absorbance characteristics.

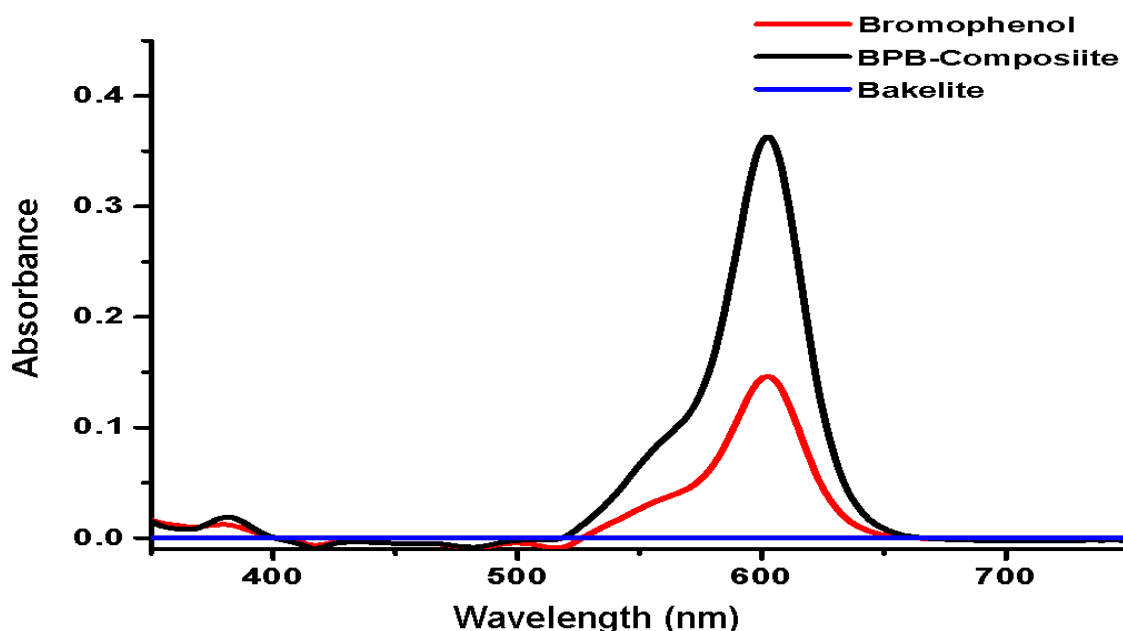


Figure 4. 1 UV-visible absorption spectra of bromophenol (red colour), bakelite (blue colour) and BPB-composite photocatalyst (black colour)

4.7.2.2 FTIR studies

FTIR (Fourier-transform infrared) spectra of bakelite have been reported [26] in-band region of 3000-3620 cm^{-1} corresponds to OH stretch; 1500 cm^{-1} (phenolic ring); 820 cm^{-1} (aromatic ethylene bonds (C=C) of the phenolic ring). From the spectra of BPB-composite (Figure 4.2), the absorption peak appearing at 3555.6 cm^{-1} and 1396 cm^{-1} is of OH stretching and OH bending of phenol group respectively. The 1470 cm^{-1} peak can be ascribed to the phenolic ring [145] and the presence of peaks at 747 cm^{-1} and 1661 cm^{-1} corresponds to C=C bending and stretching respectively of aromatic ethylene bonds (C=C) of the phenolic ring [145]. Hence, the FTIR spectra of BPB-composite show distinct differences in the frequency of functional groups as compared to bakelite. In addition, C-Br and S=O strong stretching is obtained at 631 cm^{-1} and at 1339 cm^{-1} that confirms the formation of bakelite and bromophenol composite. This indicates that the bromophenol has been captured in the voids of bakelite resulting in the formation of BPB-composite.

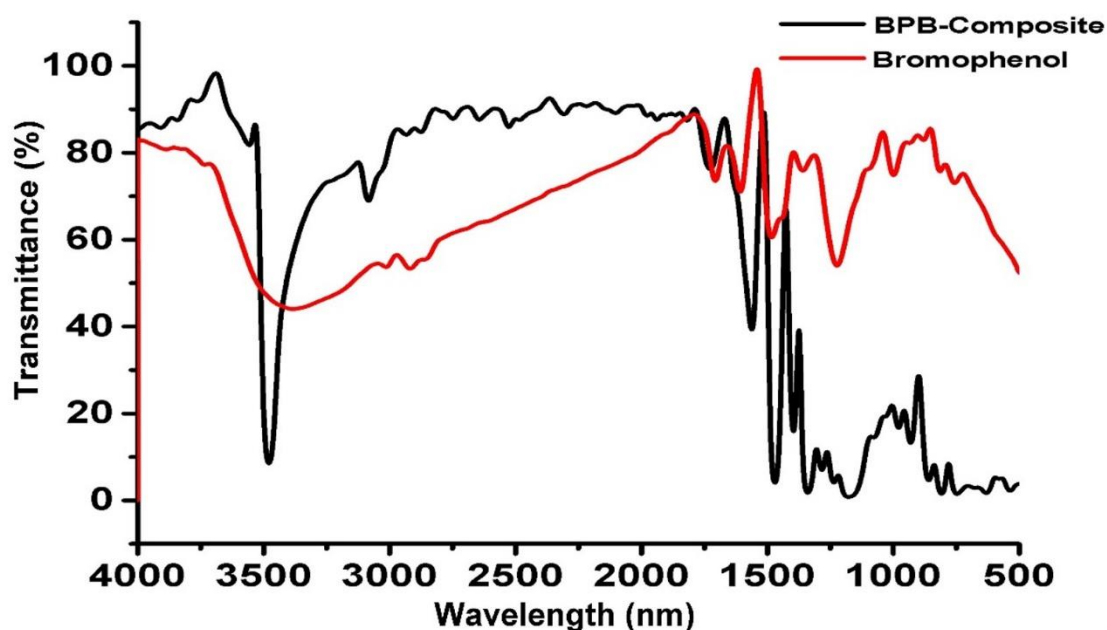


Figure 4. 2 Fourier-transform infrared (FTIR) spectra of bromophenol and BPB-composite (black colour) photocatalyst.

4.7.2.3 SEM Analysis

The morphology of bromophenol and BPB-composite photocatalyst were analysed from FE-SEM (field emission scanning electron microscopic) [142] studies, shown in Figure 4.3. The SEM image of BPB-composite photocatalyst displays a spherical shape (Figure

2b), which is completely different from bromophenol (Figure 2a). Also, the size of BPB-composite is smaller than bromophenol as depicted in SEM images and particle size measurement confirms this observation.

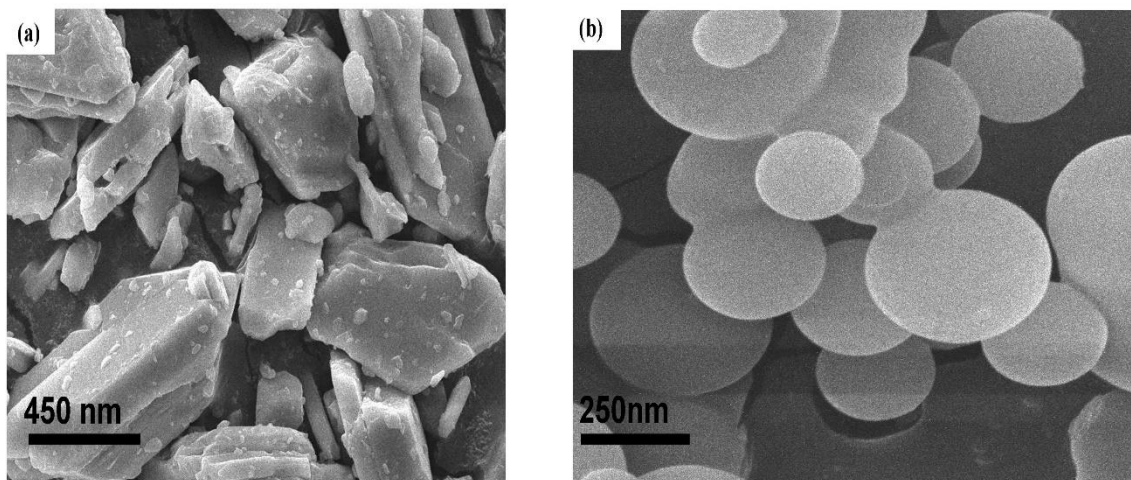


Figure 4. 3 Field emission scanning electron microscopy (FESEM) images of a) bromophenol and b) BPB-composite photocatalyst.

4.7.2.4 Particle size

The average particle size of bromophenol and the BPB-composite photocatalyst was determined using the dynamic light scattering (DLS) method (refer to Figure 4.4). The synthesized BPB-composite exhibited an average particle size of 252.50 nm (as shown in Figure 3), which is considerably smaller than that of bromophenol blue, with varying particle sizes of 458.84 nm and 1478.56 nm (as depicted in Figure 4.4). The reduced size of the BPB-composite photocatalyst suggests its enhanced photocatalytic activity.

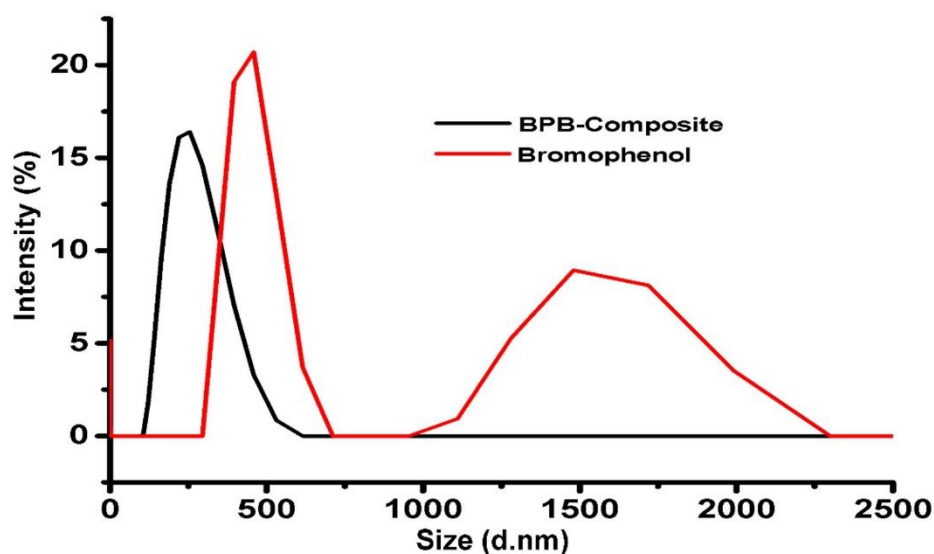


Figure 4. 4 Particle size of bromophenol and BPB-composite photocatalyst.

4.7.2.6 Zeta Potential Studies

As shown Figures 4.5(a) and 4.5(b), the zeta-potentials of the bromophenol and BPB-composite photocatalysts were -5.28 mV and -8.6 mV, respectively. As compared to bromophenol, the BPB-composite photocatalyst has a more negative value of zeta potential. This implies relatively better stability of BPB-composite than bromophenol blue.

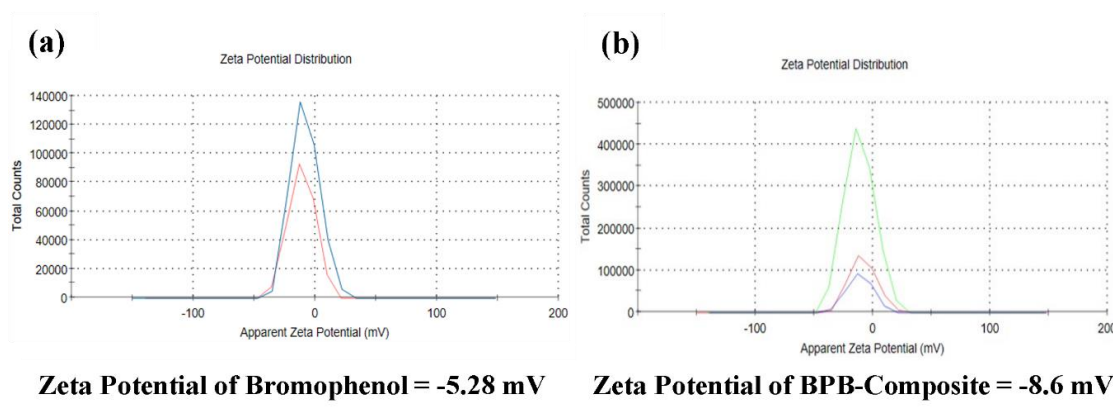


Figure 4. 5 Zeta potential plots of a) bromophenol and b) BPB-composite photocatalyst.

4.7.2.5 EDS Studies

EDS (energy-dispersive X-ray spectroscopy) is a useful technique for determining the percentage of different elements in materials [144]. EDS spectra of bromophenol [Figure 4.6a] and BPB-composite [Figure 4.6(b)] show the percentage of different elements present in the photocatalyst. In bromophenol, the major element is seen to be bromine while the content of carbon and oxygen is very less. The height of the peak of carbon is increased in the BPB-composite. BPB-composite is composed of oxygen (19.51 atom %), carbon (79.97 atom %), and bromophenol sample with oxygen (14.17 atom %) and carbon (74.56 atom %), respectively, according to EDS analysis. It is apparent that BPB-composite is formed, and the ratio of the bromine content is somewhat lower in the composite

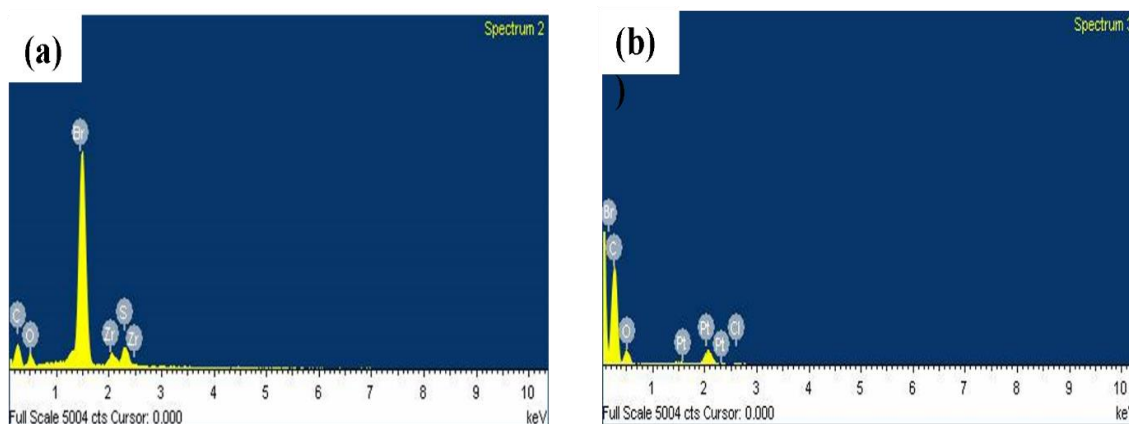


Figure 4. 6 EDS of (a) Bromophenol and (b) BPB-composite photocatalyst.

4.7.2.7 DSC Analysis

Using Differential scanning calorimetry (DSC) thermal behaviour of bromophenol and BPB-composite (Figure 4.7) was studied. A sharp melting peak of bromophenol is observed at 274.78°C in its DSC curve. So, bromophenol decomposes completely below 300°C whereas BPB-composite starts decomposing at a temperature near about 350°C that exhibits better stability than bromophenol blue. In the artificial photosynthetic system, the use of a photocatalyst with such remarkable thermal stability would open the possibility of executing the reduction of NAD^+ repetitively enhancing nucleotide co-factors' total yield [146].

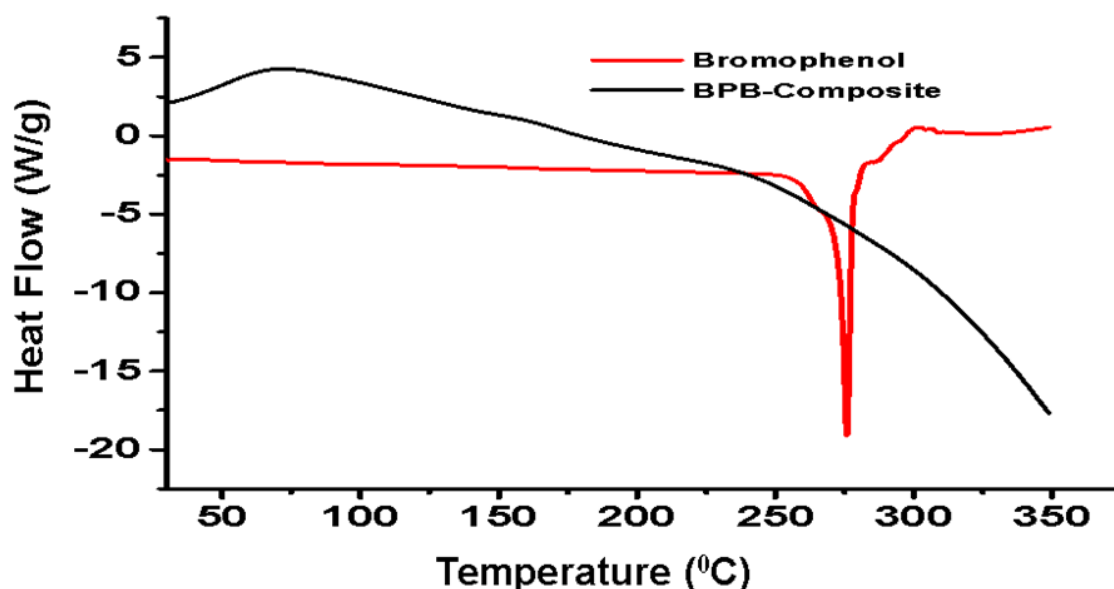


Figure 4. 7 DSC of bromophenol and BPB-composite photocatalyst.

4.8 Photocatalytic studies of NADH and formic acid yield

The presence of an optical absorbance band at 340 nm is commonly utilized to assess NADH regeneration yield [167]. When the BPB-composite photocatalyst is present, the notable absorption peak at 340 nm indicates the formation of NADH. The molar absorption coefficient of NADH at 340 nm is reported as $\epsilon = 6300 \text{ mol}^{-1} \text{ cm}^{-1}$ in the literature [167]. Figure 5a illustrates the percentage yield of NADH production versus reaction time. Conversely, when the reaction was conducted in darkness, no reduction of the oxidized form of NAD^+ occurred, as depicted in Figure 4.8a. Upon continuous irradiation of solar rays, the yield % of NADH regeneration was found to increase [147]. The accumulation of the product in the experiment was observed to happen at a fast rate and within a short time of 150 min, the total conversion of oxidised NAD^+ co-factor was accomplished. In this regard, a comparison of the photocatalytic performance of bromophenol and BPB-composite photocatalyst is interesting. The conversion efficiency of bromophenol and BPB-composite photocatalyst is shown in Figure 4.8a. As observed BPB-composite photocatalyst is extensively effective for photo-regeneration of NADH cofactor at constant accumulation up to 82.52% while the NADH photo regeneration efficiency of bromophenol was obtained to be 12.16% under the same condition. The above observation undoubtedly demonstrates the solar rays harvesting BPB-composite photocatalyst is suitable for conversion of NAD^+ to NADH cofactor with better yield in comparison to bromophenol.

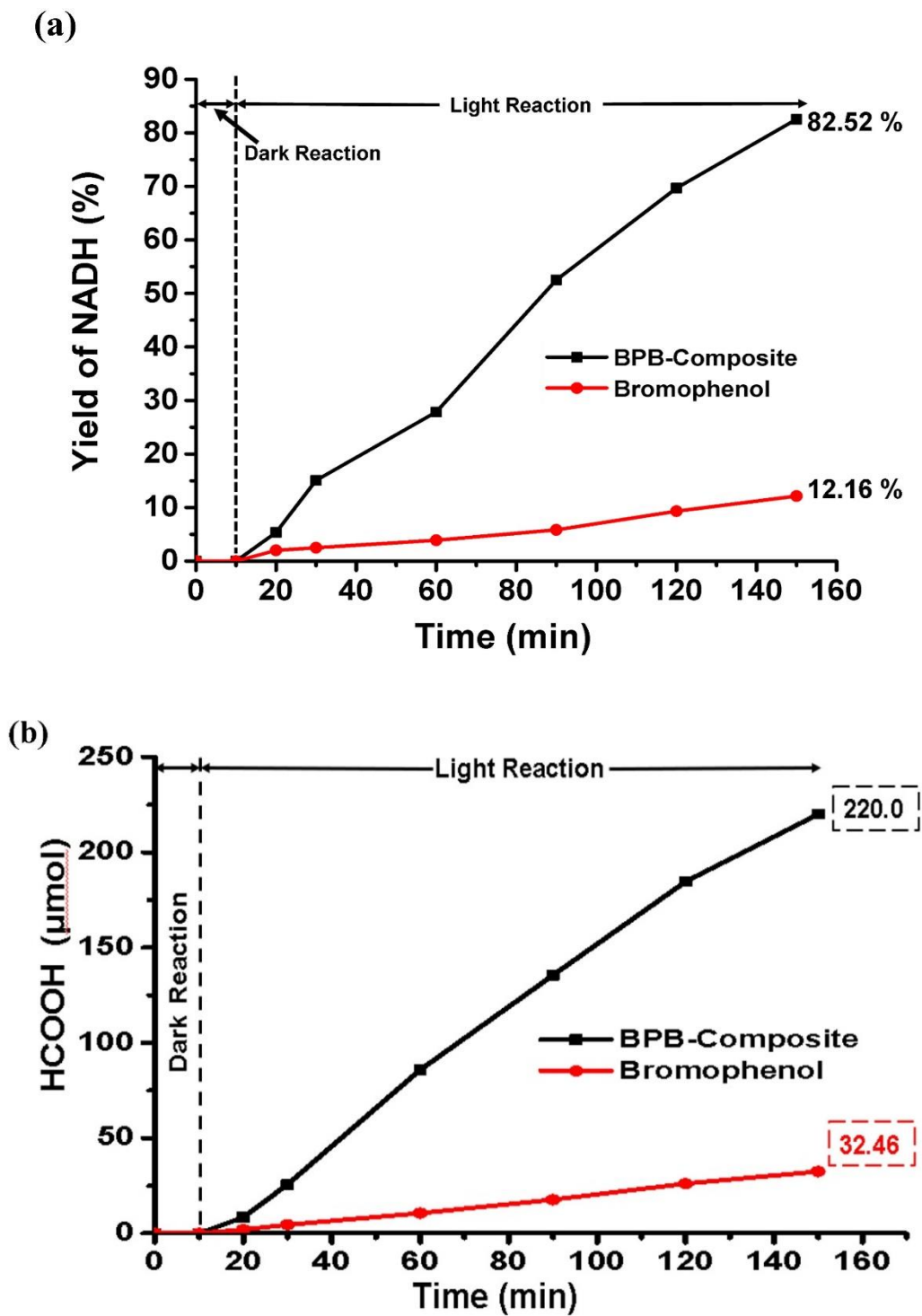


Figure 4. 8 Photocatalytic activity of bromophenol and BPB-composite photocatalyst for (a) NADH regeneration and (b) artificial photosynthetic production of formic acid from CO_2

4.8.1 Reusability and Chemical Stability

The stability and reusability of the BPB-composite photocatalyst was also investigated under the same experimental conditions (see in Figure 4.9).

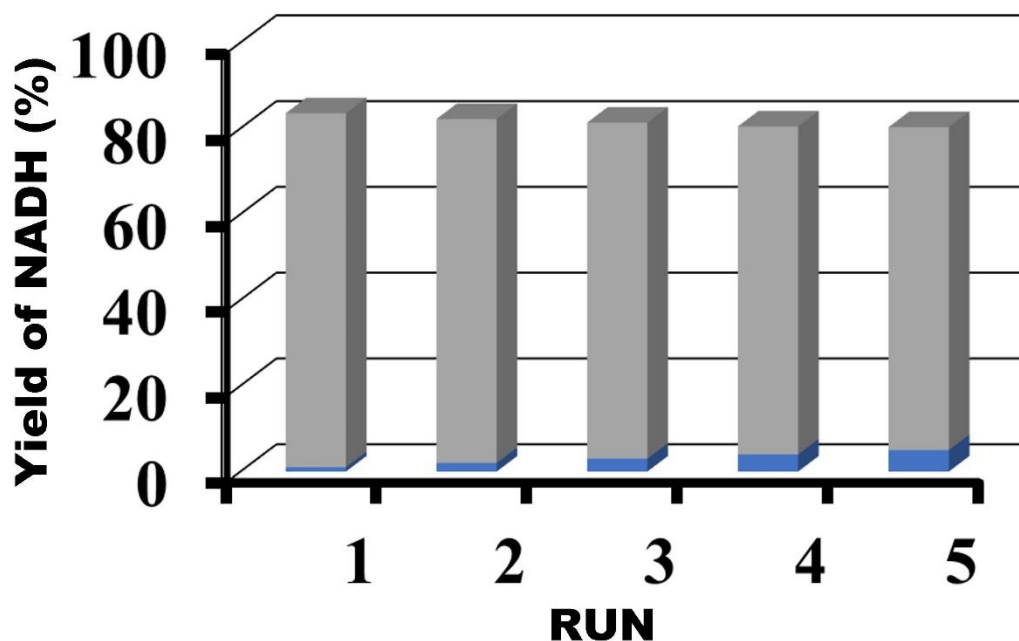


Figure 4. 9 Reusability and stability test of BPB-composite photocatalyst for 1,4-NADH regeneration.

4.8.2 HPLC chromatogram for Formic acid

The production of formic acid was confirmed using HPLC (high-performance liquid chromatography). The appearance of the absorption spectrum at 256 nm confirms the production of formic acid as shown in supplementary information Figure 4.10 (b). The peak observed for produced formic acid is like that of pure formic acid that confirms the formic acid production from carbon dioxide using the photocatalytic solution. The yield of formic acid increased linearly as a function of the reaction rate for BPB-composite photocatalyst as shown in Figure 4.10b. The efficiency of BPB-composite for the formic acid production was 220 μmol , while that of bromophenol was 32.46 μmol . The photocatalytic quantum efficiency (QE) of CO_2 reduction was calculated to be 2.74 %. These outcomes revealed the outstanding performance of BPB-composite photocatalyst in comparison to bromophenol.

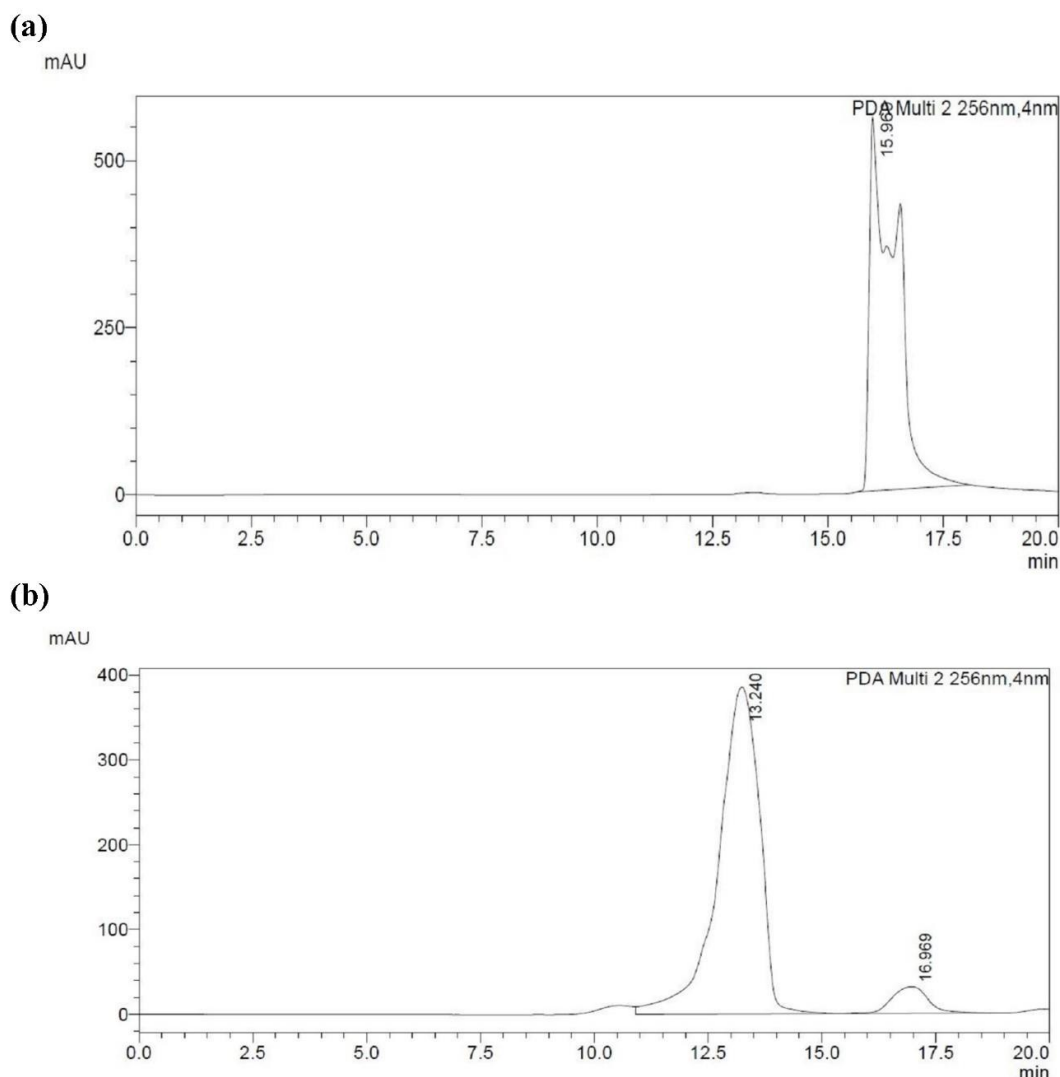
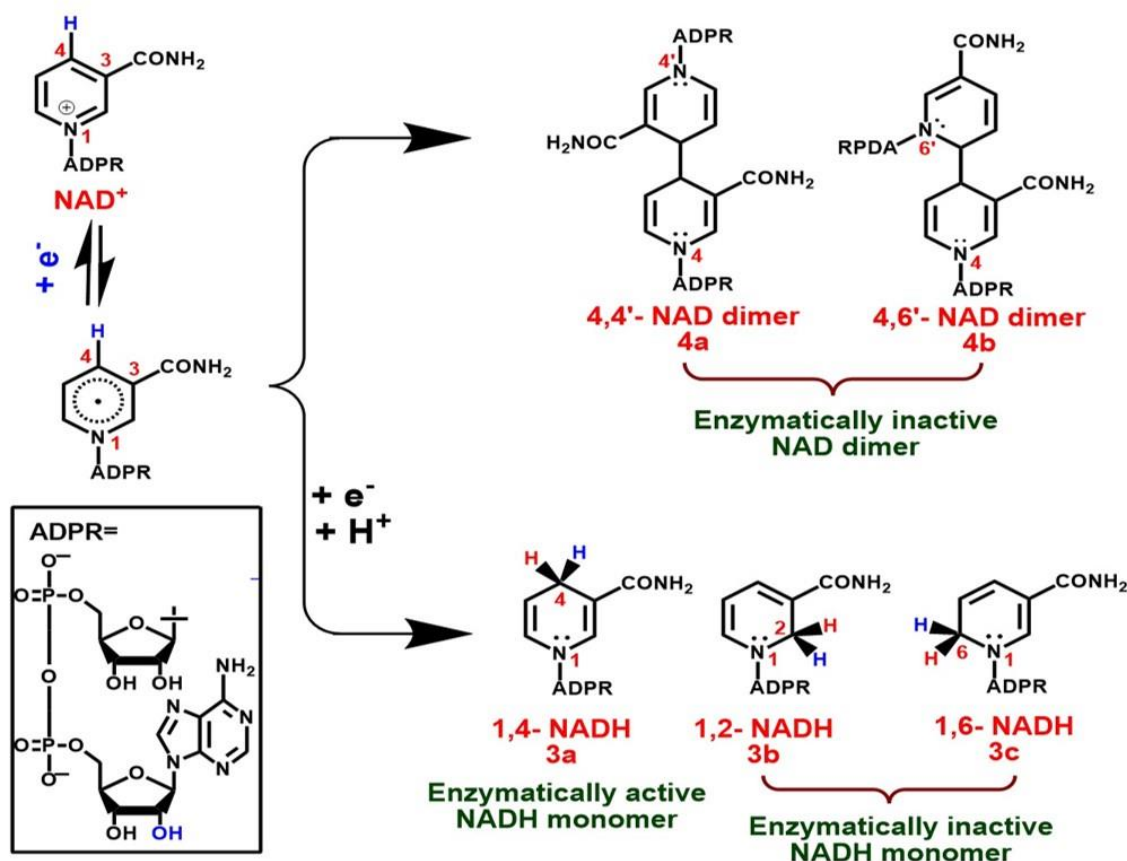


Figure 4. 10 Chromatogram of HPLC

4.9 During the reduction of NAD^+ , the possibility of producing different NADH isomers

The electrochemical reduction of NAD^+ to NADH involves a series of reactions facilitated by free radical intermediates, as depicted in Scheme 4.4. There are two possible routes for reducing the radical form of NAD^+ . The first pathway entails the protonation of a free radical intermediate to yield a monomer, while the second pathway involves radical-radical coupling to form a dimer. Monomers and dimers of NADH can exist in various forms of isomers, such as 3/3' and 4/4', as illustrated in Scheme 4.4. Monomers can take the form of 3/3' (3a/3a', 3b/3b', and 3c/3c'), including 1,6-, 1,4-, and 1,2-NADH, while dimers can exist as 4,4' and 4,6'-NADH. However, the 3a/3a' monomer (1, 4-

dihydro derivative) of NADH is the only isomer enzymatically active, making it valuable in artificial photosynthetic systems. [142].



Scheme 4. 4 Plausible NAD⁺ reduction for the production of ‘enzymatically active/inactive’ isomers of NADH via free radical intermediates.

In summary, an efficient visible light harvesting photocatalyst as BPB-composite has been synthesised successfully to emulate natural photosynthesis for the production of formic acid from CO₂. The photocatalyst-enzyme coupled system has been described in detail with the synthesised photocatalyst. The artificial photosynthetic system involves a sequence of the process that starts with electron excitation with the absorption of visible light by a photocatalyst. These electrons transfer to the Rh complex and lead to the formation of NADH which is utilised by the enzyme formate dehydrogenase to convert CO₂ to formic acid. More remarkably, BPB-composite unprecedentedly gave an excellent NADH yield of 82.52%. BPB-composite demonstrated good photo and thermal stability in addition to being an effective light-harvesting photocatalyst. Therefore, this study

opens the opportunity for further studies on bakelite-like polymer-based visible light harvesting photocatalysts. Furthermore, the approach proposed for producing formic acid from CO₂ utilising solar energy marks a new era in artificial photosynthesis.

CHAPTER-5

**Fully π -conjugated Yne-linked Eosin-Y Based
Photocatalyst for the Photoreduction of CO₂ to
HCOOH**

Fully π -conjugated Yne-linked Eosin-Y Based Photocatalyst for the Photoreduction of CO₂ to HCOOH

Utilizing visible light to drive CO₂ conversion for the production of solar chemicals/fuels is increasingly crucial due to global warming and the growing scarcity of fossil fuels worldwide. In this study, we present the successful integration of a novel yne-linked Eosin-Y functionalized (EY@DEHB) photocatalyst via a Pd-catalyzed Sonogashira–Hagihara cross-coupling polycondensation reaction. The EY@DEHB photocatalyst demonstrates higher activity in the reduction of environmental CO₂ to formic acid (HCOOH) under visible-light irradiation. Specifically, the EY@DEHB photocatalyst, synthesized by coupling Eosin Y (EY) with 3,5-diethynyl-4-hydroxybenzaldehyde (DEHB), exhibits excellent performance in NADH regeneration and the photoreduction of CO₂ into HCOOH, achieving 77.16% and 205.99 μ mole, respectively. This research provides valuable insights into the design and construction of highly efficient photocatalysts for converting solar energy into chemical energy.

5.1 Introduction

The concomitant rising level of atmospheric CO₂ and increasingly fossil fuel demands concerted carbon management. The fixation of ever-increasing CO₂ emission into value-added chemicals/fuels have been reported by using different methods such as electrochemical reduction, photocatalytic reduction, photoelectrochemical reduction, photothermal reduction and thermal chemical reduction. The conversion of CO₂ into value added chemicals/fuels such as CH₃OH, CH₄, CO, HCOOH and so on, involves single carbon compound and multi-electron processes. In addition, multi-carbon compounds product has also been reported by C-C coupling reaction. As a result, it appears that the fixation of CO₂ into value-added chemicals/fuels is a key strategy for reducing environmental pollution issues and global energy shortages. Therefore, the research is regularly increasing to convert CO₂ in to sustainable, non-polluting, clean, and abundant energy source.[169-172] In this regard, the development of a system for the fixation of CO₂ into solar chemicals and fuels is particularly fascinating. Consequently, many studies on the fixation of CO₂ to HCOOH have been executed so far. For instance, the fixation of CO₂ has been reported by using inorganic and organometallic catalysts,[173-175] which afford the product in poor yield and selectivity.[176-180]

Solar light is the most environmentally friendly energy source. Therefore, the efforts toward the selective reduction of CO₂ into solar chemicals and fuels led to the development of solar light harvesting semiconductors photocatalysts.[181-184] Hence, a variety of organic/inorganic semiconductors and transition-metal complexes have been

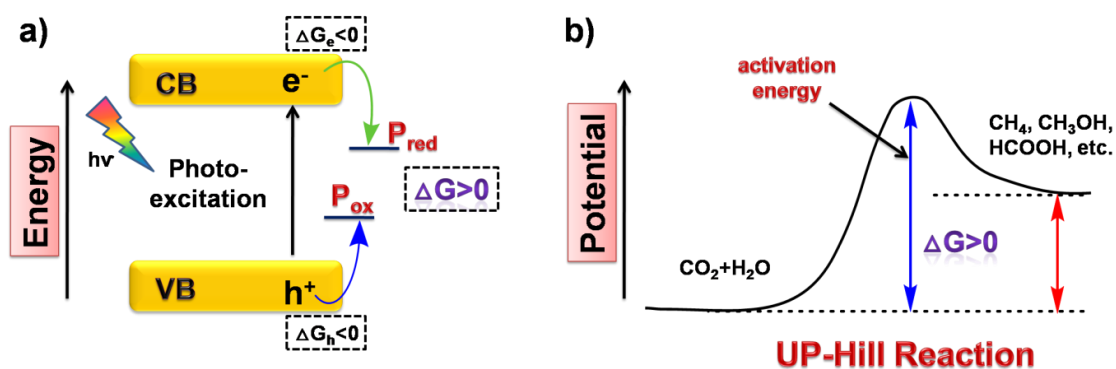
widely estimated for the direct conversion of solar to chemical energy via an artificial photosynthetic system. Nonetheless, most of them suffer from limited solar light harvesting ability, poor photo-stability, low conversion efficiency, and fast charge recombination.[185-187]

The literature demonstrates that the selective transformation of CO₂ to chemicals/fuels in high yield remains a major challenge. Therefore, it is necessary to build uv-visible light active photocatalyst to improve the photocatalytic efficiency for driving the photoreduction of CO₂ under visible light irradiation. Also, for the selective transformations, the enzymes or biocatalysts are carried out under ambient conditions. Hence, the production of HCOOH from CO₂ has been explored by using an enzyme. Although, the enzyme necessitates the NADH cofactor in a stoichiometric amount to carry out biocatalysis, therefore, the development of economic methods for the regeneration of NADH is essential. [188-189]Over the last few decades, electrochemical NADH regeneration has been developed to accomplish this target. Despite much investigation, it still has significant flaws like poor electron-transfer ability, low yields, and selectivity. To overcome these obstacles, a solar light driven photo&biocatalyst integrated system is used for the incessant regeneration of NADH, which is further consumed by the enzyme for solar chemicals/fuels production. .[188-189]

Surprisingly, the possibility of such an environmentally friendly method of obtaining HCOOH solely from CO₂ has yet to be explored. This research requires an efficient photocatalyst with the absorption of a broad spectrum for concurrent electron transfer and efficient light capturing. To accomplish this aim, we describe the creation of a photo&biocatalyst integrated system. In this context, the newly bottom-up construction of novel yne-linked Eosin-Y functionalized (EY@DEHB) photocatalyst coupled with a formate dehydrogenase enzyme to establish this system, which is illustrated in Scheme 5.1. To the best of our knowledge, the yne-linked Eosin-Y functionalized photocatalyst for the production of highly selective HCOOH from CO₂ under the irradiation of visible light using a photo&biocatalyst integrated system has not been constructed earlier to this research. Eosin-Y is a well-known organic dye of the fluorescein family which got more attention due to its eco-friendly, easy handling, and also have great potential for visible-light mediated applications. Eosin-Y is a promising photosensitizer that reveals better yield for solar chemicals/fuels.[189] Here, Eosin-Y coupled with DEHB as a

photosensitizer to enhance the visible light absorption ability of EY@DEHB photocatalyst and also for highly selective photocatalytic HCOOH production.

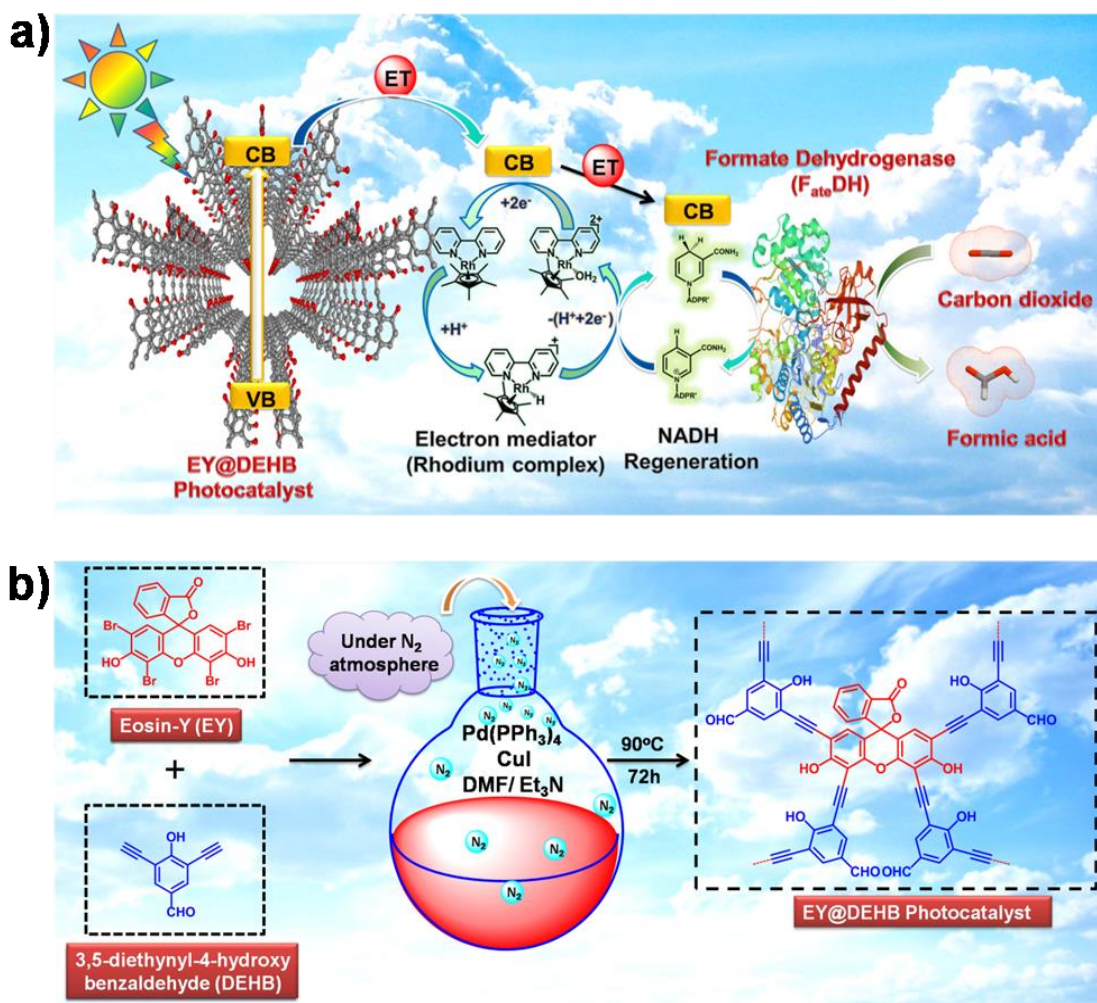
The photo&biocatalyst integrated system for HCOOH formation from CO₂ is depicted in Scheme 5.2a. In a photocatalytic reaction, the difference between reduction potential (P_{red}) and oxidation potential (P_{ox}) is changing the Gibbs free energy (ΔG) (Scheme 1a). The positive and negative value of ΔG exhibits uphill and downhill reactions respectively. The CO₂ reduction is a thermodynamic uphill reaction with a more positive change in ΔG (Scheme 5.1b).[190]



Scheme 5. 1 Diagrammatic illustration of: (a) Photocatalytic electronic structure and Gibbs free energy change in photocatalytic process. (b) UP-hill of photocatalytic reactions.

The visible light-capturing EY@DEHB photocatalyst absorbs incident photons and becomes excited for the transition of electrons from the valence band (VB) to the conduction band (CB) and left holes, which is reduced by ascorbic acid (AsA). Subsequently, the photoexcited electrons transfer to reduce the rhodium (Rh) complex ($[Cp^*Rh(bpy)H_2O]^{2+}$). The synthesis and 1H-NMR spectrum of the Rh-complex are detailed in the supporting information. Following reduction, the Rh-complex transfers hydride ions to convert NAD⁺ into NADH cofactor after removing a proton from an aqueous solution. In this capacity, the Rh-complex serves as an electron mediator between the EY@DEHB photocatalyst and NAD⁺ for NADH regeneration.[191,192] Furthermore, the formate dehydrogenase (FDH) enzyme is used to consume the NADH cofactor for the HCOOH production from CO₂. The NAD⁺ is again released to recycle this photocatalytic process, leading to NADH regeneration. Thus, the photocatalyst

couple enzyme integrated system leads to the production of HCOOH from CO₂ (Scheme 5.2).[188]



Scheme 5. 2 (a) Schematic illustration of HCOOH production from CO₂ via the route of photo&biocatalyst integrated system. (b) Synthesis of EY@DEHB photocatalyst via Pd-catalyzed.

Formic acid (HCOOH) revealed many industrial and pharmaceutical. It is used as an antibacterial agent in livestock feed and preservatives. It also plays a vital role in tanning, rubber production, leather production, textiles, and the dyeing industry. Also, it can be used as a fuel cell.[194,195]

5.2 Experimental Section

5.2.1 General remarks

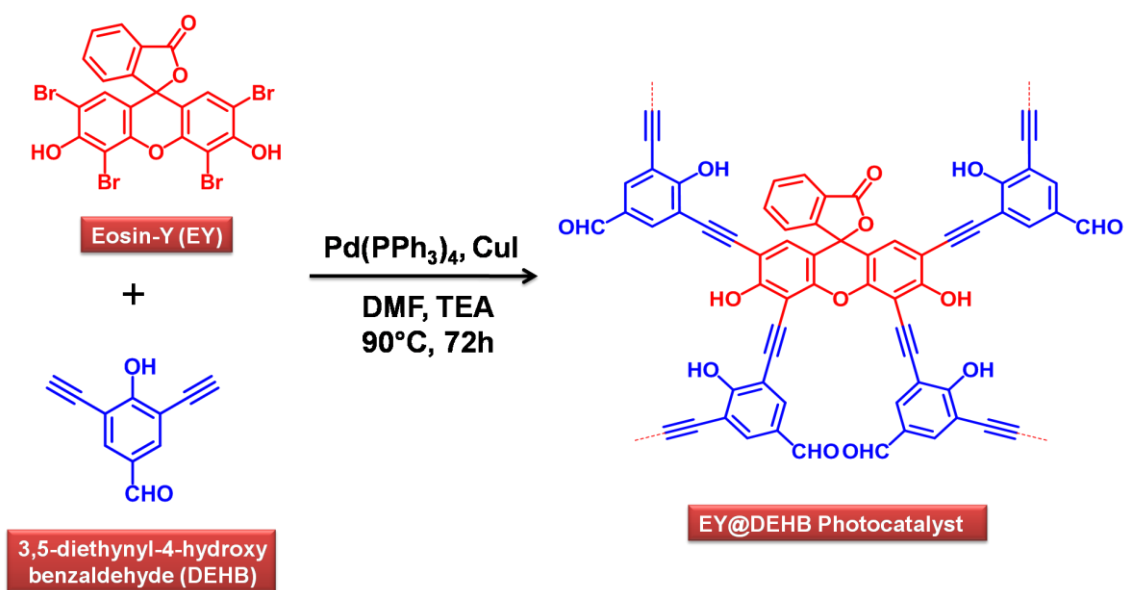
Eosin-Y, 3, 5-diethynyl-4-hydroxybenzaldehyde copper (I) iodide (CuI), tetrakis-(triphenylphosphine) palladium (0) [Pd (PPh₃)₄], N, N-dimethyl formamide (DMF) and 4.0 mL triethyl amine (Et₃N), ethanol (EtOH), tetrahydrofuran (THF), pentamethyl cyclopentadienyl rhodium (III) chloride dimer, [Rh(C₅Me₅) Cl₂]₂, β-NAD⁺, ammonium sulfate [(NH₄)₂SO₄], formate dehydrogenase enzyme and ascorbic acid were purchased from TCI and sigma-aldrich.

5.2.2 Instruments and measurements

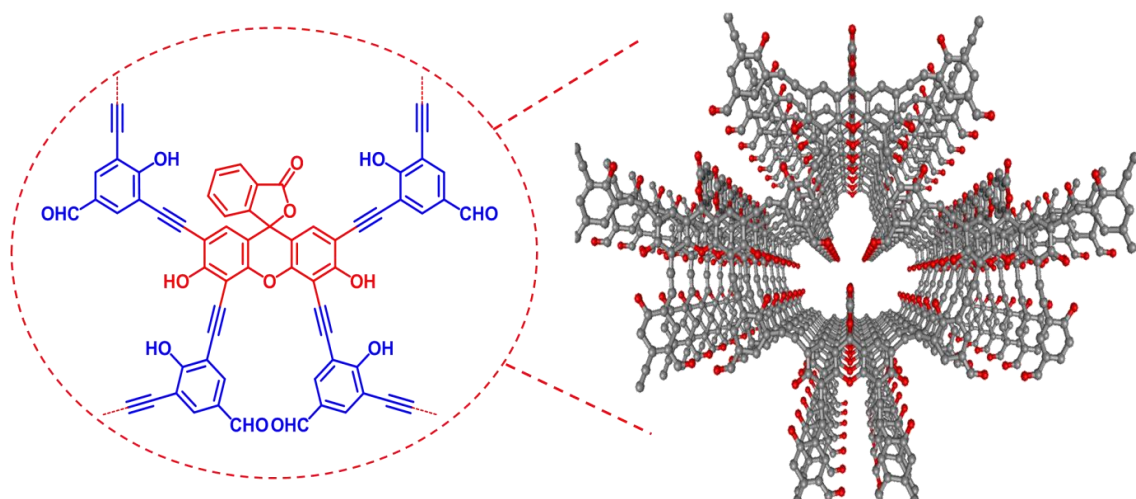
UV-visible spectra of materials were recorded by using a UV-VIS spectrophotometer (LI-2700: Lasany Inc.). Thermo-scientific, USA (Model: Nicole 6700) was used to record Fourier transform infrared spectrometer. Scanning electron microscope (SEM) images were collected to examine the morphology of materials by using JEOL, Japan (Model: JSM 6490 LV). The particle size of materials was measured by using a nano zeta sizer (NZS90).

5.2.3 Synthesis of EY@DEHB photocatalyst

To synthesize the EY@DEHB photocatalyst, initially all compounds such as 170 mg 3, 5-diethynyl-4-hydroxybenzaldehyde (DEHB, 1mmol), 346 mg eosin-Y (0.5 mmol), 10 mg copper (I) iodide (CuI), and 20 mg Pd(PPh₃)₄ were dissolved in a mixture of 4.0 mL DMF and 4.0 mL triethyl amine (Et₃N). After that, the reaction mixture was refluxed at 90 °C with a stirrer under an inert atmosphere for 72 h (Scheme 5.3). Subsequently, the reaction mixture was precipitated after cooling at room temperature. Furthermore, the obtained precipitate was filtered and washed with distilled water, EtOH, and THF to remove photocatalyst residues or any unreacted monomer. Then, followed by the purification of the product by soxhlet extraction using chloroform solvent. The product was dried by using a rotary evaporator.[196] Three-dimensional structure of EY@DEHB photocatalyst shown in Figure 5.4. The synthesized EY@DEHB photocatalyst was confirmed by proton nuclear magnetic resonance (¹H-NMR) (Figure 5.9).



Scheme 5. 3 Synthetic scheme of EY@DEHB photocatalyst via coupling of EY and DEHB at 90oC temperature for 72h.



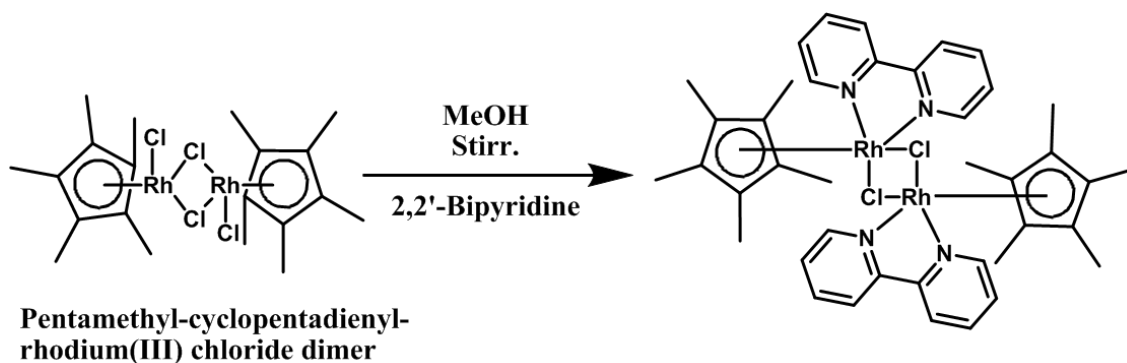
Scheme 5. 4 Three-dimensional structure of EY@DEHB photocatalyst.

5.2.4 CpM synthesis

[Cp*Rh(bpy)Cl] Cl, 25 mg pentamethyl cyclopentadienyl rhodium (III) chloride dimer [Rh(C₅Me₅) Cl₂]₂ was taken in pre-dried 25 ml round bottom flask and added 5 ml distilled methanol. The reaction mixture was stirred for 30 minutes at room temperature under an N₂ atmosphere. Subsequently, 2 eq. of 2,2'-bipyridyl (13 mg) was introduced into the reaction mixture, followed by the addition of diethyl ether to yield the yellow

precipitate (Scheme 5.5). The resulting precipitate was then dried at room temperature. 1, 2

The synthesized Rh-complex was confirmed by proton nuclear magnetic resonance (^1H -NMR) spectra in Figure 5.1.



Scheme 5. 5 Synthesis of organometallic rhodium complex.

2.5.5 Proton nuclear magnetic resonance (^1H -NMR) spectra of rhodium complex

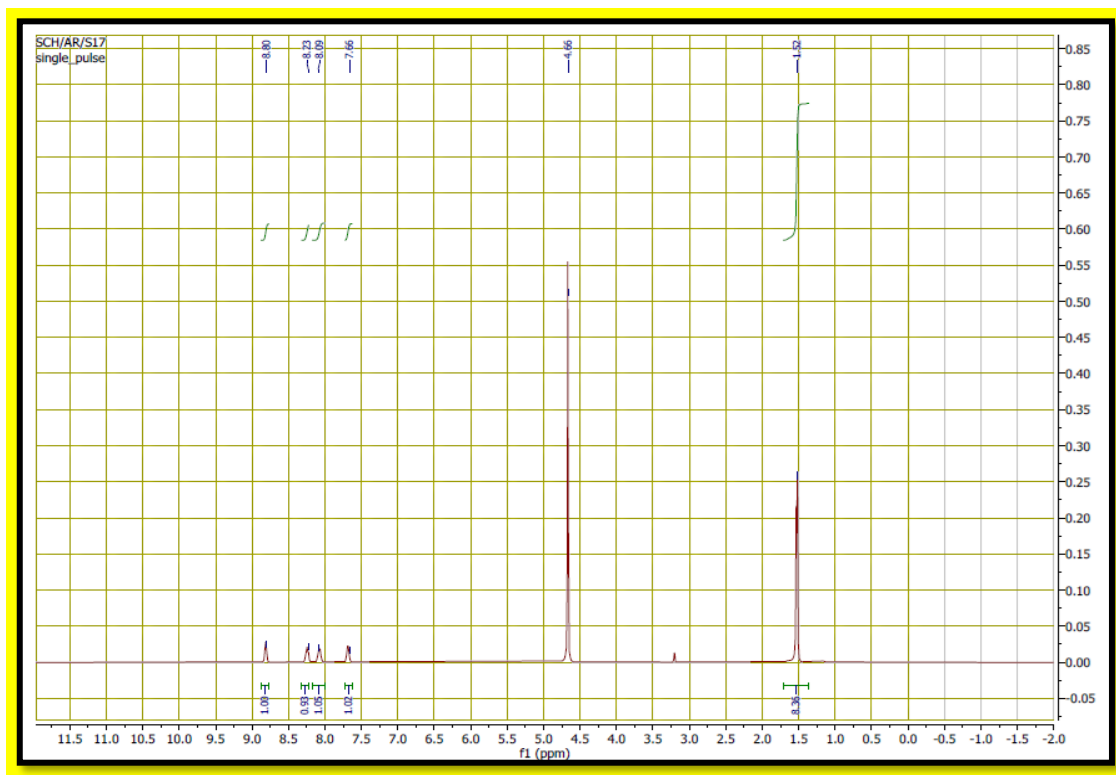


Figure 5. 1 Proton nuclear magnetic resonance (NMR) spectroscopic study of the electron mediator rhodium complex. ¹H-NMR (500 MHz, D₂O) δ 1.52 (s, 30H), 8.80 (d, 4H), 8.23 (d, 4H), 8.09 (t, 4H), 7.66 (t, 4H).

The production of HCOOH from CO₂ was also executed within a quartz reactor after the irradiation of a 450W xenon lamp with a cut-off filter of 420nm under an inert atmosphere at room temperature. The performed reaction mixture was composed of 1.24 mmol AsA, 0.5 mg EY@DEHB photocatalyst, 0.62 μmol Rh-complex, 1.24 μmol β-NAD⁺, and 3 units of FDH enzyme in 3.1mL of buffer (sodium phosphate buffer) to maintain pH up to 7.0 in the presence of CO₂. After 1h bubbling of CO₂ in absence of light, the reactor was irradiated in visible light. The produced HCOOH amount was detected by HPLC (high performance liquid chromatography, Model: 51-ADD0012).

5.3 Results and Discussion

5.3.1 Artificial AQBCN photocatalyst-biocatalyst coupled system

The robust EY@DEHB photocatalyst was created by covalently yne-linked EY dye with DEHB substrate . The as-prepared EY@DEHB photocatalyst was characterized by UV-visible spectroscopy, Fourier transform infrared spectroscopy (FTIR), Field emission scanning electron microscope (FESEM), powder X-ray diffraction (PXRD), and Dynamic light scattering (DLS) technique.

5.3.1.1 Uv-Visible spectroscopy

UV-vis spectroscopy was used to confirm the existence of EY in the EY@DEHB photocatalyst. The EY@DEHB photocatalyst exhibits a strong absorption spectrum at 536 nm (Figure 5.2). The EY dye also reveals a similar wavelength absorption spectrum albeit with low absorption. This blue shift maximum absorption spectrum of EY@DEHB photocatalyst attributed to the presence of DEHB with EY, which indirectly recommended the covalent attachment between them. This examination indicates the efficient visible light capturing ability of EY@DEHB photocatalyst, which provides photogenerated energy for enzymatically-active NADH regeneration and HCOOH production from CO₂ with good efficiency.

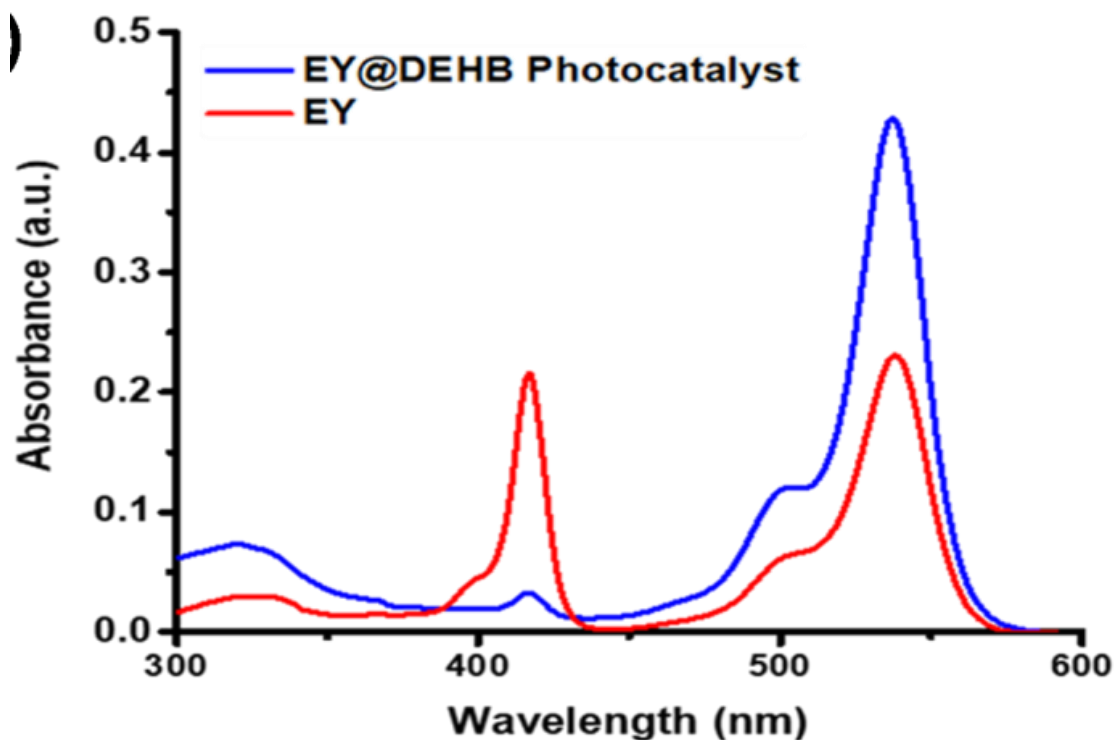


Figure 5. 2 UV-Visible absorption spectra of EY and (d) EY@DEHB photocatalyst

5.3.1.2 FTIR studies

To estimate the evidence regarding coupling between EY dye and DEHB, FTIR studies were conducted. The characteristic peaks of EY dye were exhibited at 1751 cm^{-1} and 3253 cm^{-1} , which were allocated to the vibration stretching of C=O and O-H respectively. The new characteristic peak of $\text{-C}\equiv\text{C-}$ stretching in EY@DEHB photocatalyst appeared at 2117 cm^{-1} (Figure 5.3a,b) along with $700\text{-}1600\text{ cm}^{-1}$ absorption bands of the aromatic ring.[197]

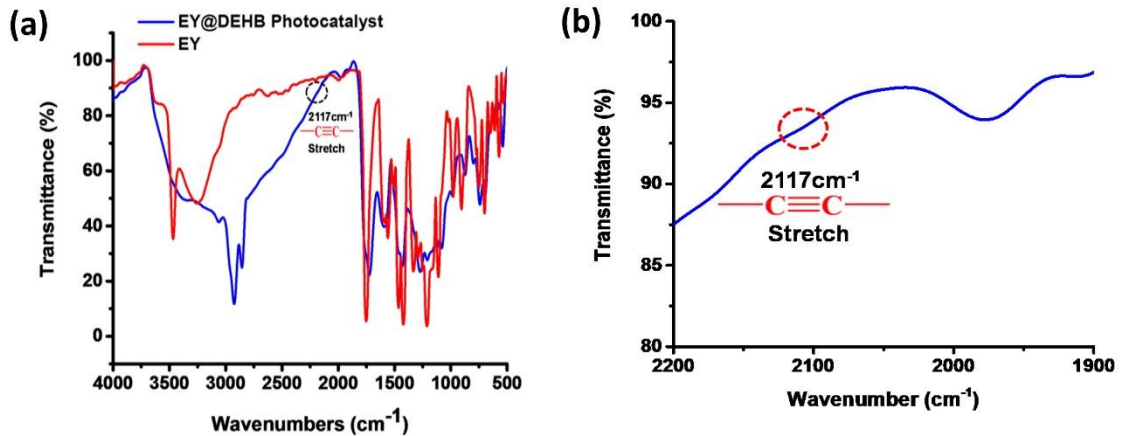


Figure 5. 3 FTIR spectrum of EY and EY@DEHB photocatalyst.and, FTIR spectrum of EY@DEHB photocatalyst

5.3.1.3 SEM analysis

The morphology of EY dye and EY@DEHB photocatalyst were investigated by FESEM analysis, which is shown in Figure 5.4 (a and b). The EY dye shows the agglomerated morphology[198] whereas the morphology of the as-synthesized EY@DEHB photocatalyst changed (Figure 5.4b). As a result, it indicates that the coupling of EY dye with DEHB changed the surface morphology of the synthesized EY@DEHB photocatalyst.

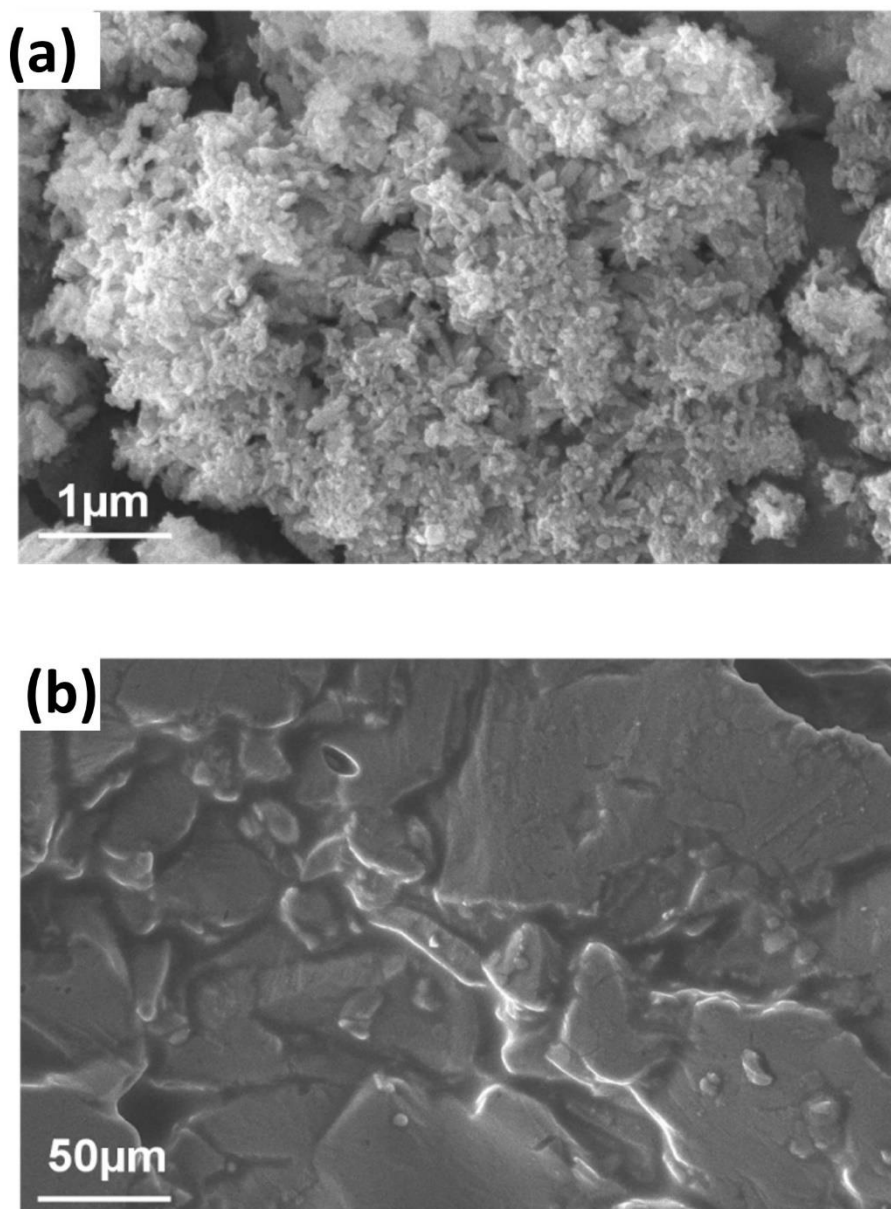


Figure 5. 4 FESEM morphology of (a) EY and (b) EY@DEHB photocatalyst.

5.3.1.4 X-ray diffraction studies

The PXRD measurements indicated the crystalline and amorphous nature of EY and EY@DEHB photocatalysts, respectively, which is demonstrated in Figure 5.5. The diffraction peak of the EY@DEHB photocatalyst exhibits a strong characteristic peak at 30.05° of 2θ value. The characteristic peak at 30.05° corresponds to an interlayer d-spacing about 0.0499 nm. The formation of a new $-C-C-$ bond in EY@DEHB

photocatalyst after the combination between EY and DEHB is recommended by the appearance of a new diffraction peak at 30.05°.[196]

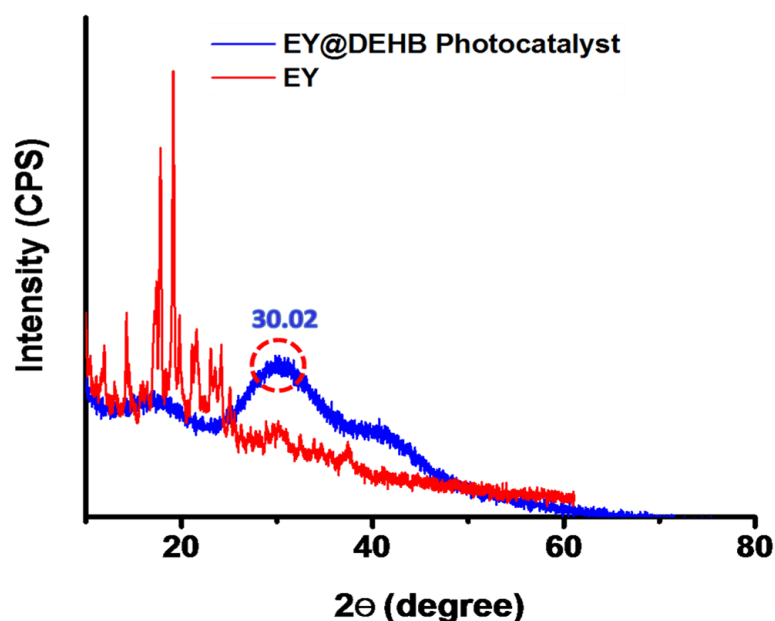


Figure 5. 5 PXRD measurements of EY and EY@DEHB photocatalyst.

5.3.1.5 Photocatalytic Reaction for NADH regeneration and production of HCOOH

The photocatalytic activity of EY and EY@DEHB photocatalyst for NADH regeneration and production of HCOOH were examined via an artificial photosynthetic system (Figure 5.6). The concentration of photo-regenerated NADH was determined using a UV-Visible spectrophotometer. As shown in Figure 5.6a, the EY@DEHB photocatalyst achieved the highest yield of NADH regeneration at 77.16% compared to EY (18.22%) over a period of 120 minutes.

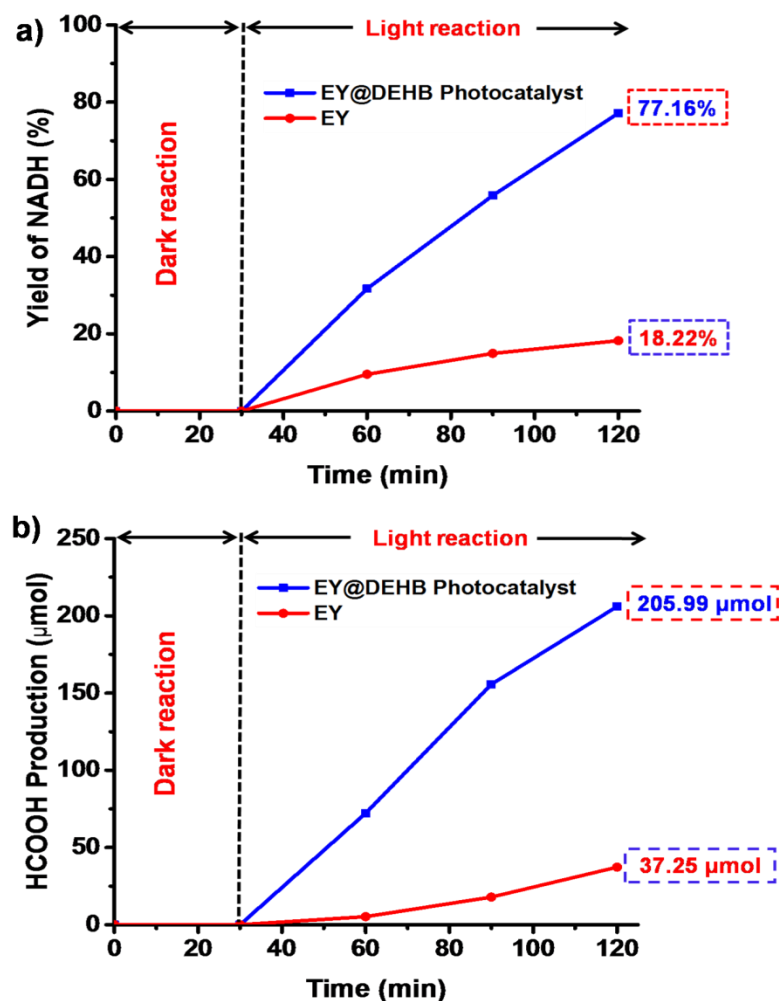


Figure 5. 6 The photocatalytic performance of EY and EY@DEHB photocatalyst for (a) regeneration of NADH and (b) production of HCOOH from CO₂ via artificial photosynthetic route.

5.3.1.6 Particle size analysis

In addition, the size of the particle also shows more significance in photocatalytic properties. The particle size distribution was investigated by using the DLS technique, which is demonstrated in Figure 5.7. The particle size of the EY@DEHB photocatalyst after the linkage of $-C\equiv C-$ was reduced (8.91nm) relative to that of EY dye (164.95nm). The smaller size of the EY@DEHB photocatalyst enhances the rate of charge transfer, which is responsible for higher photocatalytic activity.[199,200]

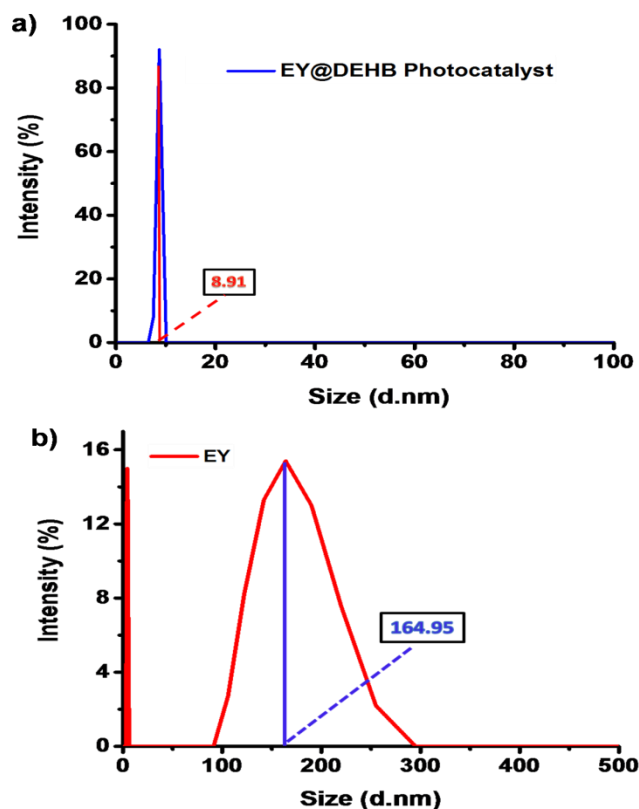


Figure 5. 7 Particle size analysis of (a) EY and (b) EY@DEHB photocatalyst.

5.3.1.7 High-performance liquid chromatography (HPLC) analysis for the determination of formic acid

Additionally, the production of HCOOH was detected by using HPLC (Figure 5.8). As shown in Figure 5.6, the production of HCOOH linearly increased up to 205.99 μmol along with reaction time in the presence of highly efficient EY@DEHB photocatalyst. While, EY was afforded up to 37.25 μmol . The production of HCOOH was detected by using high-performance liquid chromatography (HPLC). The absorption spectrum of produced formic acid appears at 254nm, which is shown in Figure 5.8. The analyzed peak of produced formic acid is similar to pure formic acid peak,[172] which confirmed the formation of formic acid from CO₂ using the photocatalytic solution.[173]- [201-205]

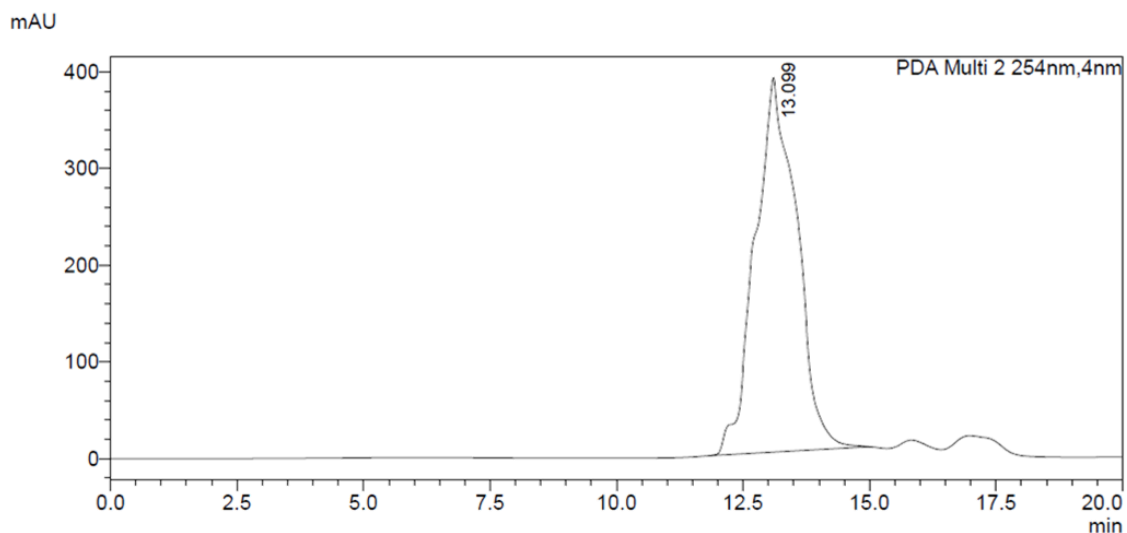
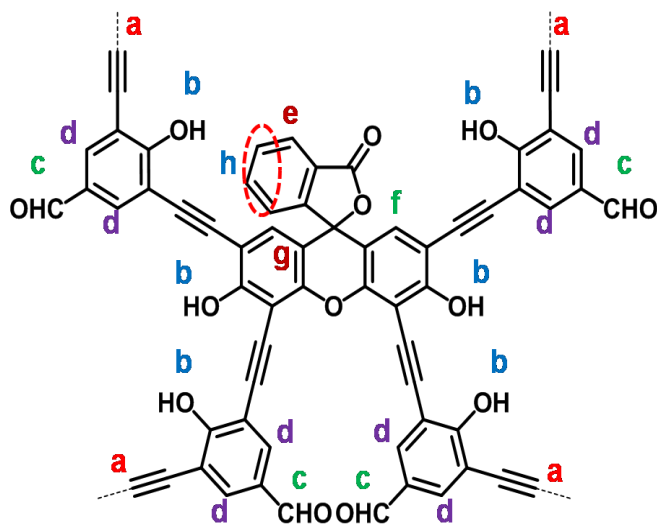


Figure 5. 8 Chromatogram of HPLC for HCOOH.

5.3.1.8 Proton nuclear magnetic resonance ($^1\text{H-NMR}$) spectra of EY@DEHB photocatalyst



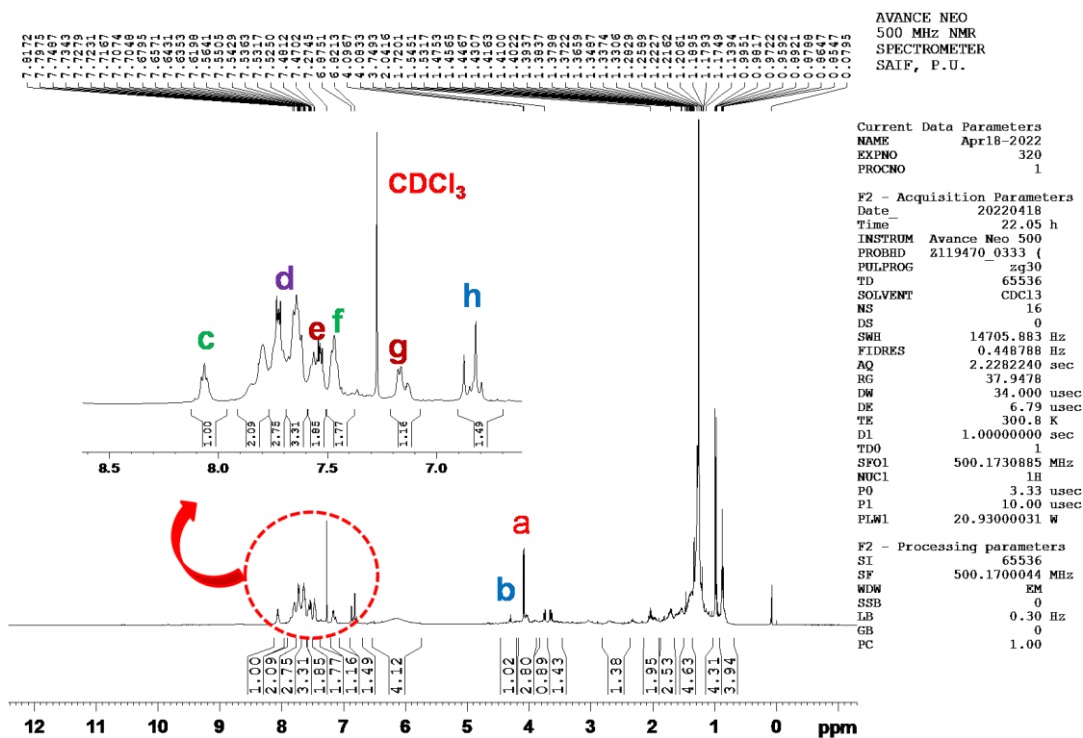


Figure 5. 9 ^1H NMR spectra of the EY@DEHB photocatalyst. The sp^2 hybridized aromatic proton is located in the range of 6.5~8 ppm. The chemical shifts of acetylene protons were located at 4 ppm and benzaldehyde protons shows in the range of 8-9 ppm. The chemical shift of phenolic proton shows in the range of 4-4.5 ppm.

5.3.1.9 Reusability test of EY@DEHB photocatalyst

The reusability test (5 runs) of fully π -conjugated Yne-linked Eosin-Y based photocatalyst (EY@DEHB) for the NADH regeneration and HCOOH production under the same reaction conditions has been examined. In view of the yield of NADH and HCOOH, EY@DEHB photocatalyst showed good photocatalytic efficiency during the recycling tests shown in Figure 5.10.

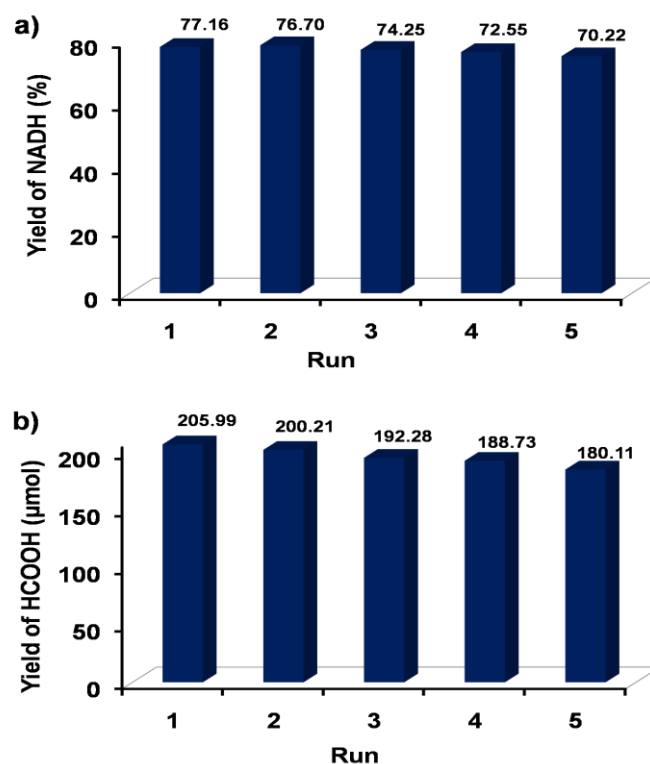
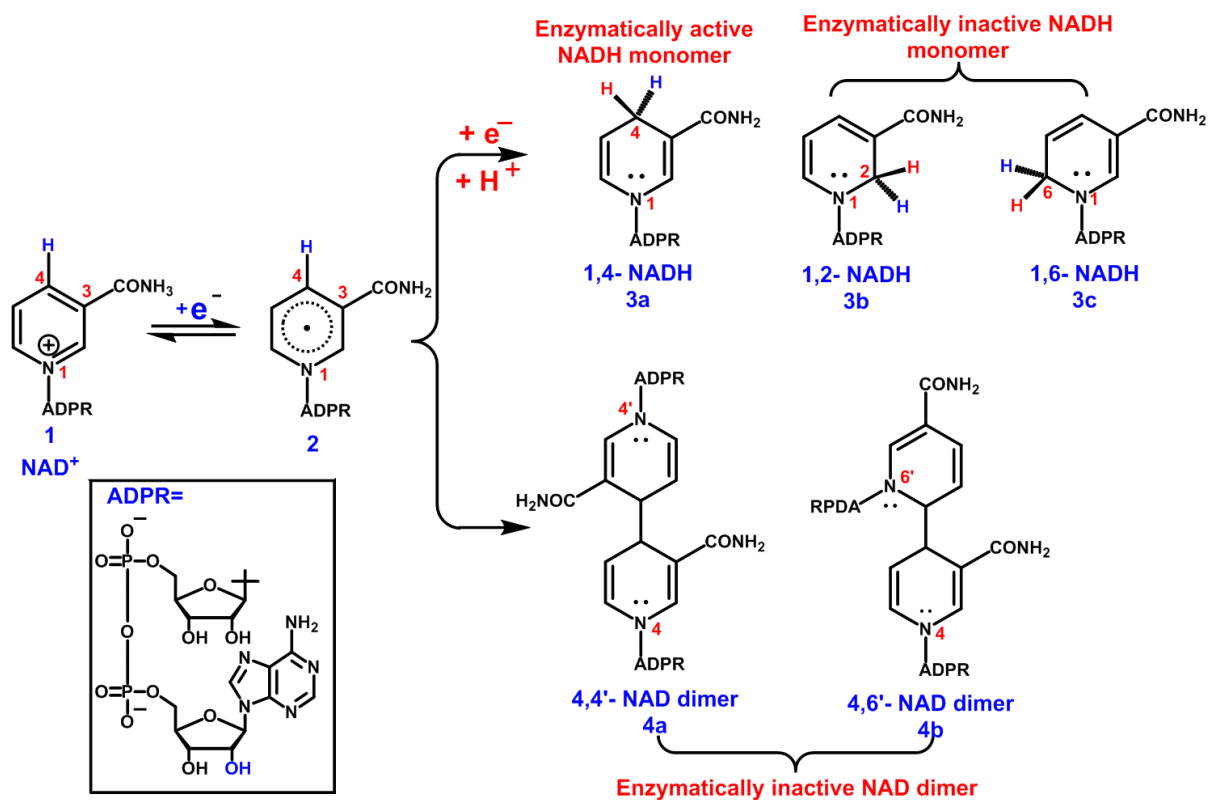


Figure 5. 10 Reusability test of EY@DEHB photocatalyst under visible-light irradiation for the NADH regeneration and HCOOH production.

5.4 Mechanism of NADH regeneration



Scheme 5. 6 Plausible electrochemical reduction of NAD^+ via free radical intermediates to be formed ‘enzymatically active/inactive’ NADH isomers.

In summary, here we presented a new solar light active fully π -conjugated yne-linked eosin-y based photocatalyst for the transformation of CO_2 to HCOOH via artificial photosynthesis. The EY@DEHB photocatalyst has been fully characterized by spectroscopy, microscopy, XRD, and particle size analyzer techniques. The EY@DEHB photocatalyst of the photocatalyst–enzyme coupled system is highly visible light active for efficient production of HCOOH from CO_2 . The artificial photosynthesis field opens many possibilities of applications for fully π -conjugated yne-linked eosin-y based materials. The presence of EY in photocatalyst makes it responsible for excellent photocatalytic activity with 77.16 % yield of NADH regeneration and 205.99 μmol production of HCOOH from CO_2 . The above result reveals the superiority of yne-linked eosin-y based photocatalyst. To the best of our knowledge, an yne-linked eosin-y based photocatalyst sets a new benchmark in the artificial photosynthesis area for the ultimate goal of solar fuel production from environmental CO_2 .

CHAPTER- 6

Nature-Inspired CO₂ Fixation Through Photopolymer Modified Sulphur Doped Graphitic Carbon Nitride Photocatalyst

Nature-Inspired CO₂ Fixation Through Photopolymer Modified Sulphur Doped Graphitic Carbon Nitride Photocatalyst

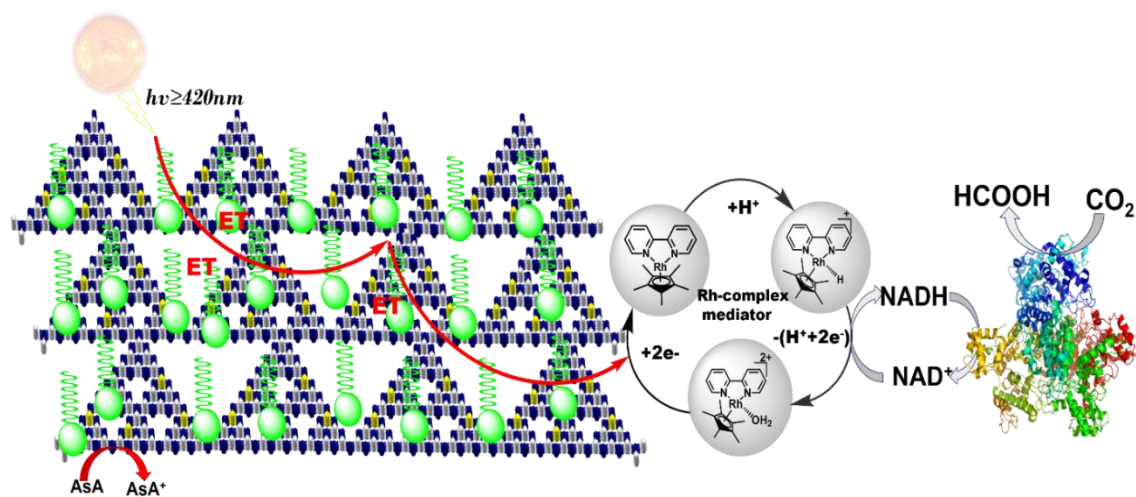
Creating effective and cost-efficient photocatalysts for CO₂ fixation, inspired by nature, poses a significant challenge in material chemistry. The photoinduced polymer grafting of metal-free sulfur-doped graphitic carbon nitride (SGCN) has recently gained substantial attention due to its diverse applications spanning photocatalysis, energy conversion and storage, and biomaterials. In this research study, we delve into the development of a light-harvesting photocatalyst synthesized through the grafting of Poly (vinylidene fluoride-co-hexafluoropropylene) polymer brush onto sulfur-doped graphitic carbon nitride (PVDHFP@SGCN) using visible light irradiation. Subsequently, PVDHFP@SGCN films can be produced through spin coating on glass substrates. The investigation highlights the exceptional properties of the newly formulated photocatalysts, including outstanding solar light-harvesting capability, optimal optical band-gap suitability, and highly structured π -electron pathways facilitating efficient charge migration. These attributes position the photocatalyst as a highly promising candidate for various photocatalytic applications, particularly in utilizing solar energy for diverse chemical reactions. Moreover, the current PVDHFP@SGCN photocatalyst demonstrates remarkable efficiency as a catalyst in CO₂ fixation, resulting in the production of formic acid as a green solar chemical.

6.1 Introduction

The greenhouse effect and global warming are the most serious issues for modern society in the twenty-first decade, providing key challenges to the scientific community [211]. The emissions of greenhouse gases increase daily with rapid consumption of energy sources such as coal, oil, and natural gas, which leads to environmental problems [212-214]. It is important to note that an over-reliance on fossil fuels has led to an energy crisis and that the environment has suffered greatly as a result of the released greenhouse gases [215,216]. CO₂ stands out as the most prevalent greenhouse gas among these emissions, driving significant global climate shifts and adverse environmental impacts. With CO₂ emissions continually rising due to human activities, the conversion of CO₂ into valuable fuels like HCOOH, CH₃OH, and CH₄ emerges as a crucial objective. Such transformations hold the potential to enhance the global carbon balance and facilitate

energy storage in a positive manner. [217,218]. As CO₂ is chemically the most stable and linear greenhouse gas having low electron affinity, the reaction of CO₂ is defined by the nucleophilic assault at the carbon atom [217]. As a result, the conversion of CO₂ to fuels is a scientifically challenging problem that requires suitable catalysts and considerable energy input [219]. Therefore, many researchers employ various strategies such as photoelectrochemical [220], biochemical [221] electrochemical [222], and thermochemical processes [223] to reduction of CO₂. As commonly known that the CO₂ molecule requires eight electrons to complete the 21 conversion to hydrocarbon molecules [220-224]. As a result, the reported methods for reduction often result in low yields and limited specificity towards the desired hydrocarbon products [10-14]. To overcome these drawbacks, the development of highly efficient process/technologies/methods are required for the conversion of CO₂. The natural photosynthesis process plays a crucial role in maintaining the carbon/oxygen cycle which is essential for sustaining life on Earth [225]. Therefore, inspired by natural photosynthesis, we have designed artificial photosynthetic systems that are reasonable and effective technologies for the conversion of CO₂ into value-added solar chemicals. Accordingly, many scientists have developed various types of artificial photosynthetic materials, such as TiO₂/CdS photocatalysts [226,227], pigment sensitizers [228], semiconductors [229], metal-based covalent frameworks [230], transition-metal based complexes so on [231]. Still, the use of these photocatalytic materials has various limitations such as poor conversion efficiency, photostability, and high cost [232-234]. To enhance the photocatalytic efficacy of photocatalysts, novel semiconducting materials have been introduced to actively harness visible light in solar energy applications. Notably, the utilization of two-dimensional layered materials like graphitic carbon nitride (GCN) has been prominent in augmenting the photocatalytic activity of metal-free photocatalysts, owing to their exceptional optical properties and thermal stability. With an optical band gap of approximately 2.7 eV, GCN is adept at absorbing solar light within the spectral range below 500 nm, making it suitable for various applications. GCN catalysts have found widespread use in processes such as water splitting and carbon dioxide photo-reduction, leveraging their optical characteristics. Despite its widespread application, pristine GCN encounters limitations in efficiently covering the broad spectral window of solar light below ~500 nm due to its wide optical band gap. One strategy to overcome this hurdle involves the incorporation of a sulfur heteroatom, leading to the development of heteroatom-doped GCN, commonly referred to as SGCN. In this research

endeavor, we introduce a novel SGCN photocatalyst by grafting a Poly (vinylidene fluoride-co-hexafluoropropylene) polymer brush onto sulfur-doped graphitic carbon nitride (PVDHFP@SGCN), as illustrated in Scheme 6.1. In this process, SGCN facilitated radical formation under visible light exposure, which was utilized to initiate polymerizations. Among the various modifications of g-CN, polymers have garnered increasing interest due to their versatile properties, such as flexibility, ease of functionalization, and cost-effectiveness. Notably, the PVDF-HFP polymer's high electron-absorbing C–F bonds have attracted significant attention from scientists and researchers owing to its exceptional thermal endurance and chemical stability. The copolymer PVDF-HFP, created by introducing amorphous HFP into PVDF, can disrupt the symmetric and regular chain structure of pure PVDF, thereby reducing its crystallinity and enhancing polymer membrane adsorption. To our knowledge, no prior studies have explored the grafting of polymer brushes onto SGCN, which could potentially enhance the interface properties of SGCN. Polymer brushes, surface coatings comprising polymers tethered to a substrate, can be achieved through covalent attachment. In this study, the grafting technique is employed to attach a Poly (vinylidene fluoride-co-hexafluoropropylene) polymer brush onto sulfur-doped graphitic carbon nitride (PVDHFP@SGCN) for CO₂ reduction. The PVDHFP@SGCN was analyzed using UV spectroscopy, TGA, and FT-IR.



Scheme 6. 1 Polydopamine modified photocatalyst catalyzed the artificial photosynthesis process for the generation of HCOOH from CO₂ under sun ray irradiation

6.2 Experimental Section

6.2.1 General remarks

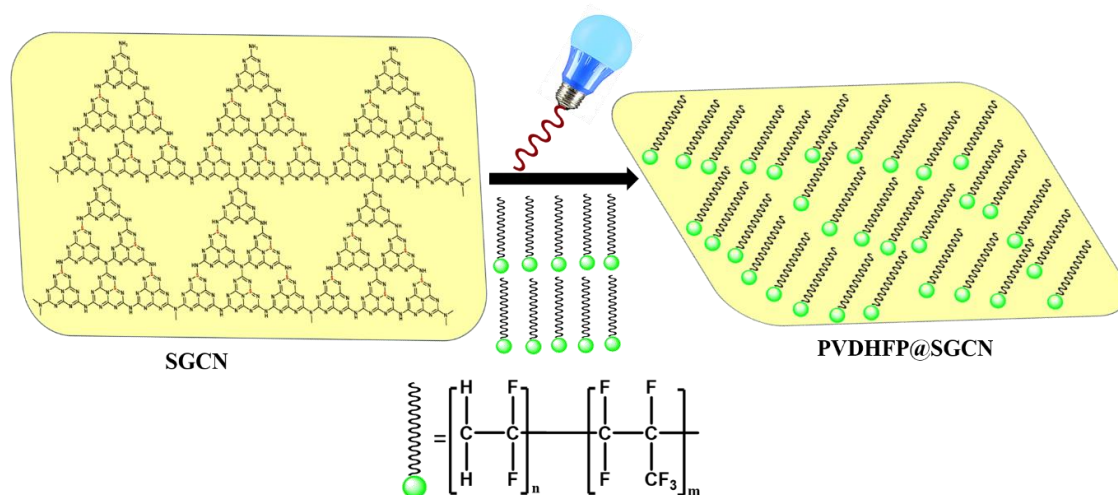
Poly (vinylidene fluoride-co-hexafluoropropylene-) polymer (PVDHFP), Thiourea (T), chloroform, imidazole, ammonia solution, ethanol, methanol and dimethyl sulfoxide (DMSO), N, N-dimethylformamide (DMF), Acetonitrile (ACN), NAD⁺ (Nicotinamide adenine dinucleotide oxidized), Ascobic Acid (AsA), were purchased from sigma aldrich.

6.2.3 Preparation of the SGCN

The SGCN photocatalyst was synthesized through the thermal copolymerization method as per the reported procedure [246]. Initially, 20 g of thiourea was placed in a crucible and covered with foil paper after that heated at 520 °C in a muffle furnace for 3 hrs with a ramping rate of 5 °C/min. Afterward the 3 h calcination process, the resulting samples were cooled to ambient temperature. Lastly, the obtained product was employed for the synthesis of the PVDHFP@SGCN photocatalyst.

6.2.4 Preparation of the PVDHFP@SGCN

The PVDHFP@SGCN photocatalyst was synthesized as per the reported method [245]. Firstly, 66 mg of SGCN photocatalyst and 20 mL of THF were mixed in a glass vial and sonicated for 1 h. After that, 660 mg of PVDHFP polymer was added to the SGCN photocatalyst, and the glass vial was sealed with a rubber septum and passed with argon for 30 min. After that glass vial was irradiated under a visible light source at a distance of 5 cm to initiate the grafting process. After 48 hrs, the entire solution was washed with THF and dried under vacuum and we found the desired photocatalyst (Scheme 6.2).



Scheme 6. 2 Grafting of Polymer Brushes onto SGCN under Visible- Light Irradiation

6.2.5 Photochemical Cofactor Regeneration of NADH

NADH was photochemically regenerated in a quartz reactor at room temperature with an inert environment using sunlight. The following procedure was used to regenerate NADH by photocatalysis. A quartz reactor was used to carry out the reaction. The reaction contained 2.48 mol of NAD^+ , 1.24 mol of Rc complex, 1.24 mmol of AsA, and 0.4 mg of photocatalyst in 3.1 ml of buffer (100 mM, pH 7.0). Using a spectrophotometer, the NADH cofactor renewal was observed.

6.3 Results and discussion

6.3.1 Photo regeneration of NADH and generation of HCOOH from CO_2

Several experiments were conducted to assess the photo-regeneration of NADH using P, SGCN, and PVDHFP@SGCN photocatalysts. In each case, the concentration of NADH was monitored using UV-visible spectroscopy. As illustrated in Figure 6.1a, PVDHFP@SGCN exhibited significant efficacy in NADH photo-regeneration, steadily increasing to 88.42% over time. In contrast, SGCN and P photocatalysts yielded only 28.14% and 0% NADH regeneration, respectively. Additional experiments were performed to evaluate the photocatalytic efficiency of P, SGCN, and PVDHFP@SGCN photocatalysts for the production of HCOOH from CO_2 . As shown in Figure 6.2b, the yield of HCOOH increased linearly with reaction time when PVDHFP@SGCN was utilized as a photocatalyst. PVDHFP@SGCN produced a greater amount of HCOOH

(290.16 μmol) from CO_2 compared to all other photocatalysts under sunlight irradiation. This highly selective generation of HCOOH in larger quantities underscores the remarkable photocatalytic efficiency of PVDHFP@SGCN compared to the other photocatalysts (P, SGCN). Consequently, PVDHFP@SGCN emerges as an outstanding light-harvesting photocatalyst for HCOOH generation.

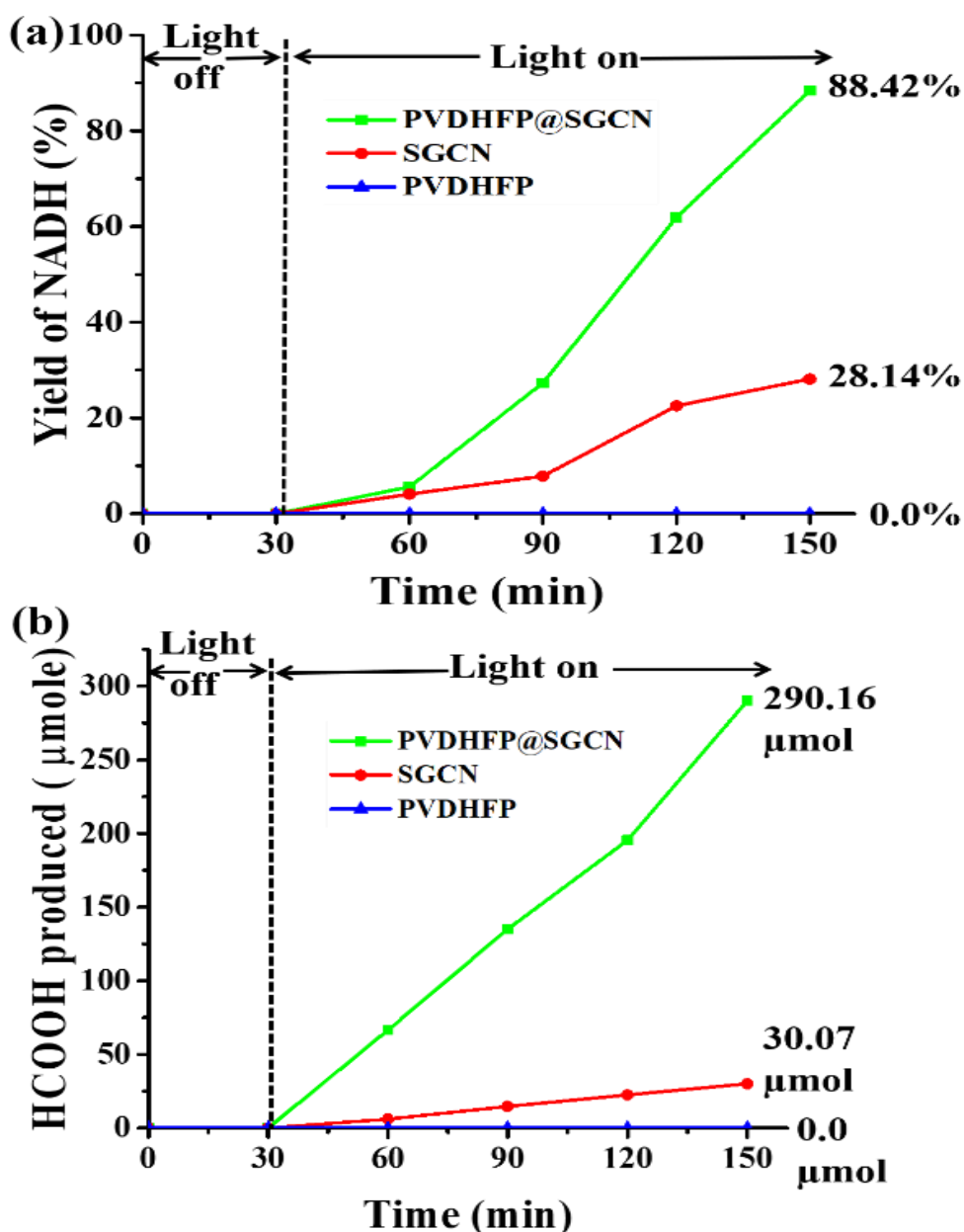


Figure 6. 1 Photocatalytic activities of P, SGCN, and PVDHFP@SGCN photocatalysts in (a) NADH photogeneration, and (b) Generation of HCOOH from CO_2 .

6.3.2 Optical Properties of Highly Efficient PVDHFP@SGCN Photocatalyst for CO₂ Fixation

The optical and electrochemical properties of PVDHFP@SGCN photocatalyst were examined by using UV-vis absorption spectroscopy and cyclic voltammetry (CV) analysis respectively.

As depicted in Figure 6.2, UV-visible spectroscopy results indicated that SGCN exhibited an absorption band position at approximately 455 nm [249,250]. Upon integration of PVDHFP onto SGCN, the UV-visible light absorption spectrum narrowed to approximately 420-700 nm (Figure 6.2). Notably, the narrowed UV-visible light absorption was primarily attributed to the SGCN molecule, which endowed available charge carrier properties despite its lower energy function [251]. Consequently, these enhanced photocatalytic properties of the PVDHFP@SGCN photocatalyst are more efficient compared to the starting material for NADH co-factor regeneration and the conversion of CO₂ to formic acid.

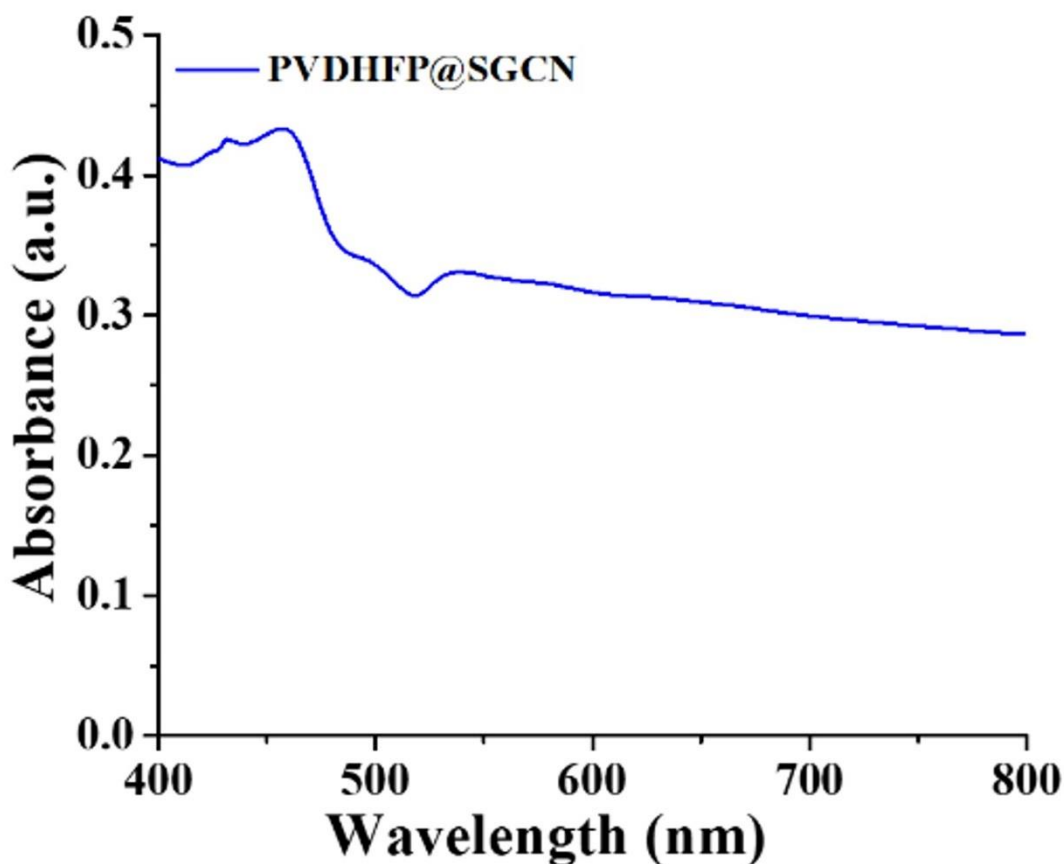


Figure 6. 2 The absorption spectrum of the PVDHFP@SGCN photocatalyst

6.3.3 Tauc plot of PVDHFP@SGCN photocatalyst

It should be noted that the grafting of PVDHFP polymer enhances the UV-visible absorption property. The optical band gap energy of the PVDHFP@SGCN photocatalyst was determined by the Kubelka-Munk (KM) method shown in Figure 6.3.

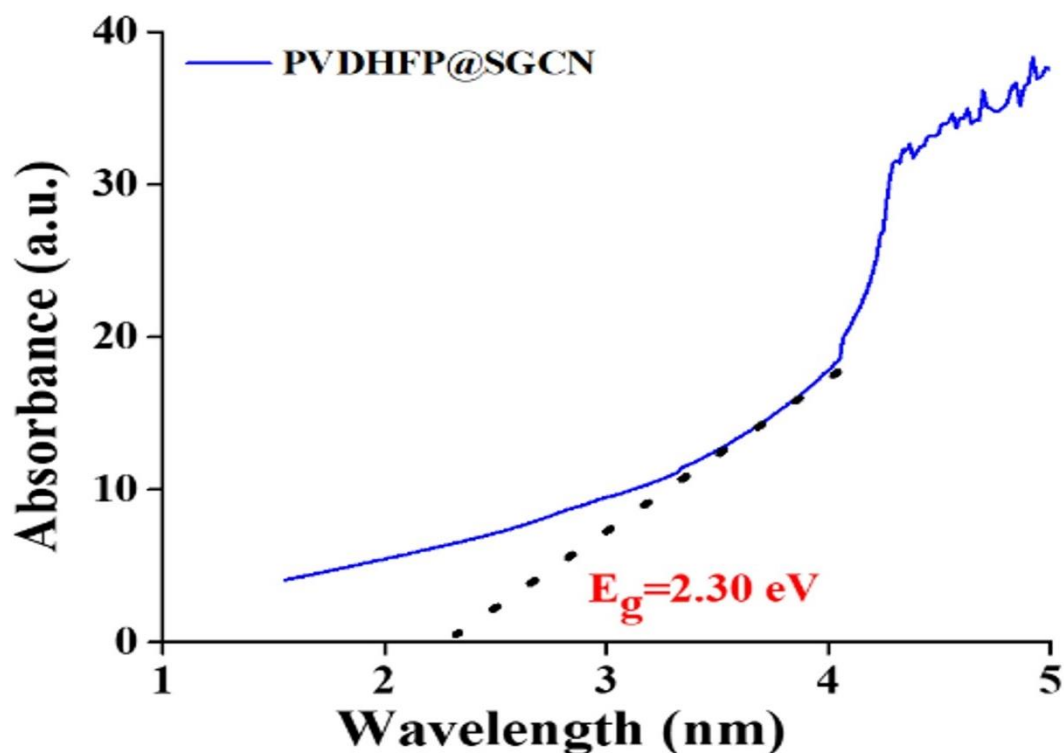


Figure 6. 3 The band gap calculated by the Kubelka-Munk (KM) method of the PVDHFP@SGCN photocatalyst

6.3.4 Cyclic voltammetry studies

By using a CV evaluation (Figure 6.4) with Pt as a counter electrode, glassy carbon as a working electrode, and Ag/AgCl as a reference electrode in anhydrous acetonitrile containing 0.1 M tetra-butyl-ammonium hexafluorophosphate with a scan charge of a 100 mV s⁻¹, the electrochemical band gap of PVDHFP@SGCN photocatalyst.

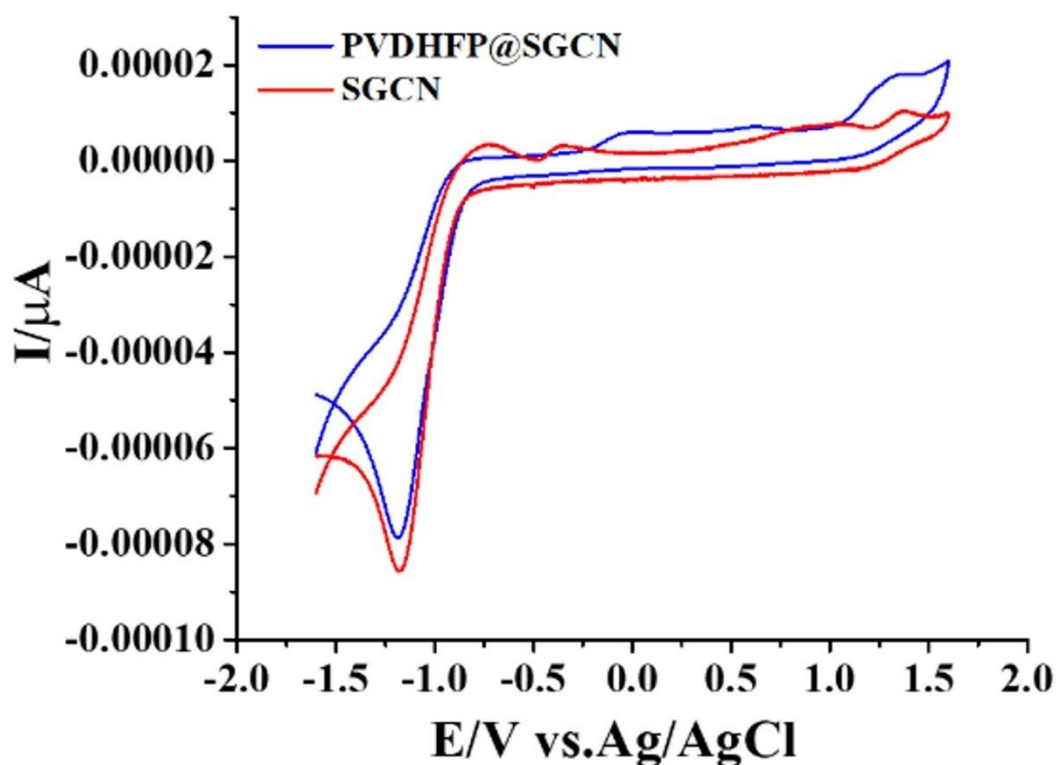


Figure 6. 4 Cyclic voltammetric analysis PVDHFP@SGCN photocatalyst and a mixture of three components in the presence Rh, NAD⁺ and PVDHFP@SGCN photocatalyst

6.3.5 EIS electrochemical studies

The separation and migration characteristics of charge carriers in a three-electrode system were assessed by analysing electrochemical impedance spectra (EIS). This investigation encompassed a frequency range from 100 kHz to 0.1 Hz, employing an AC amplitude of 5 mV. Throughout all electrochemical analyses, the distance between the working and reference electrodes was maintained at a constant 1 cm. Figure 6.5 shows the EIS data of SGCN and PVDHFP@SGCN photocatalyst. All samples exhibit Nyquist plots with a flattened semicircular shape. The PVDHFP@SGCN photocatalyst shows a smaller radius than the SGCN photocatalyst, indicative of a significantly their much more efficient migration and transfer ability of photo-generated charge carriers [252]. The structure of the PVDHFP@SGCN photocatalyst establishes a direct pathway for photo-induced electrons and holes to diffuse to the surface, resulting in a notable reduction in charge transfer resistance (R_{ct}). Furthermore, the diminished charge resistance signifies efficient electron transfer during the proton reduction process at the interface of the

photocatalyst and electrolyte, mostly indicate the grafting of PVDHF polymer on SGCN photocatalyst [253,254].

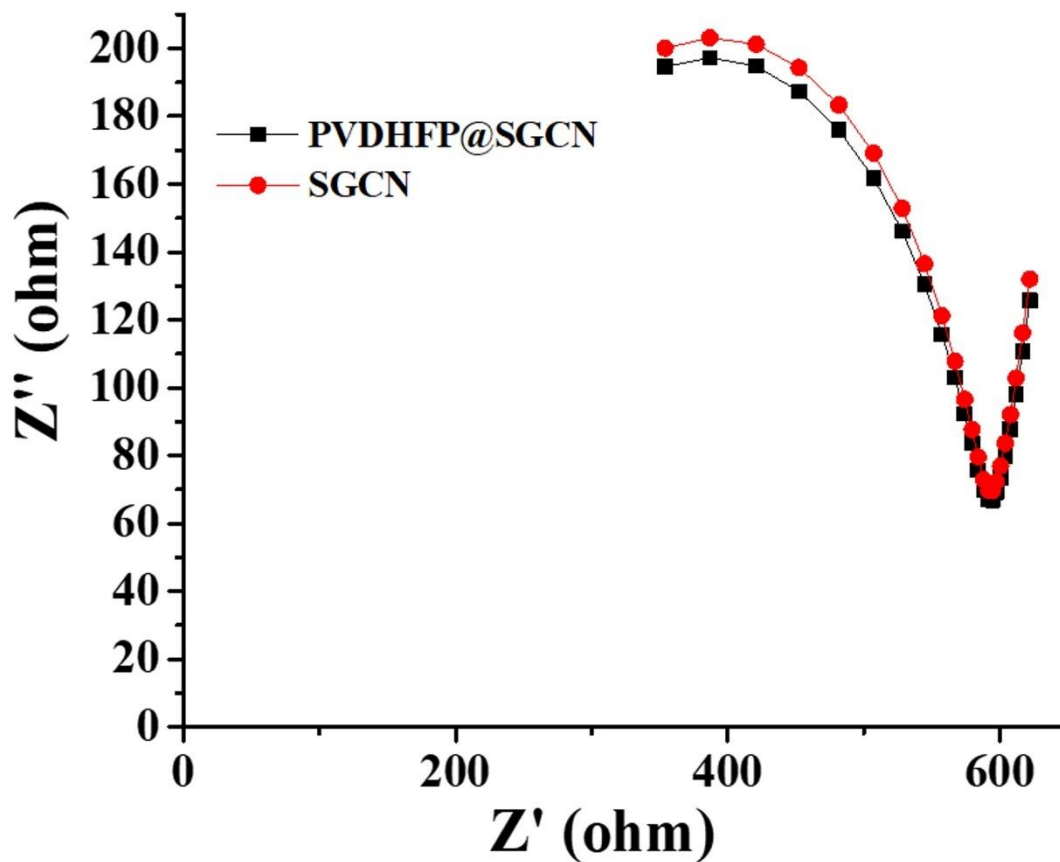


Figure 6. 5 EIS of PVDHFP@SGCN and SGCN photocatalysts.

6.3.6 Tafel plot studies

As depicted in Figure 6.6 the PVDHFP@SGCN photocatalyst shows more negative Tafel slope in comparison to starting material PVDHF which indicated PVDHFP@SGCN photocatalyst more efficient for the photocatalytic reaction [255].

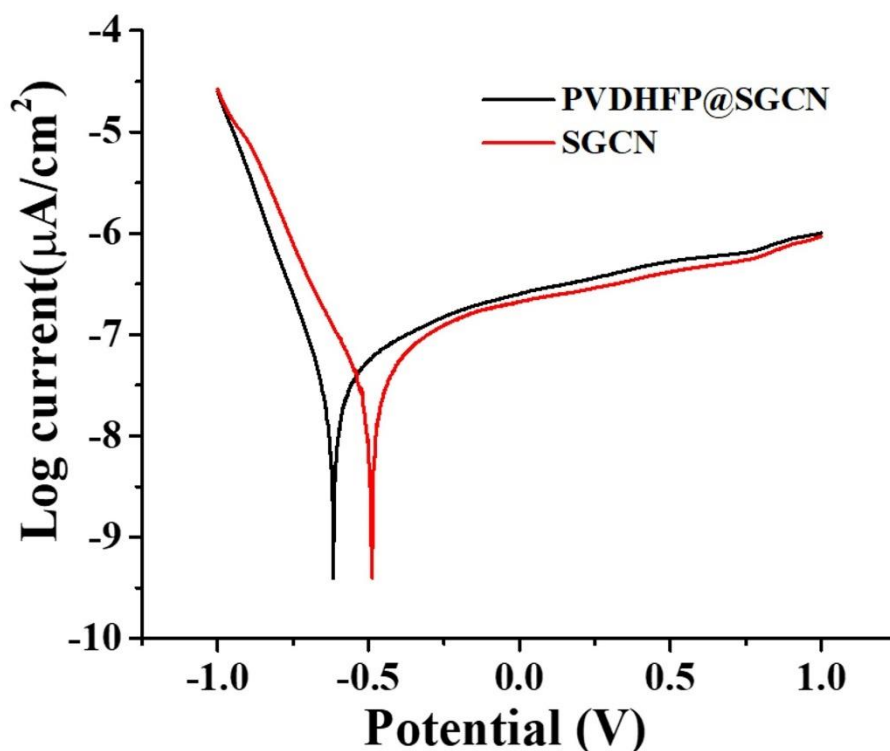


Figure 6. 6 Tafel plots of PVDHFP@SGCN and SGCN photocatalysts.

6.3.7 FTIR studies

FTIR analysis was utilized to examine the chemical bonding characteristics of the PVDHFP@SGCN photocatalyst, as illustrated in Figure 6.7. Within the FTIR spectrum of the PVDHFP@SGCN photocatalyst, a wide band spanning from 3100 cm^{-1} to 3500 cm^{-1} was observed, attributed to the stretching vibration modes of -NH and -OH groups, indicating the presence of -NH , -NH_2 , and -OH functional groups. Notably, distinctive peaks detected in the range of 1250 cm^{-1} to 1600 cm^{-1} (including 1250 , 1328 , 1429 , 1455 , and 1571 cm^{-1}) closely resemble the characteristic vibrational stretching modes of CN heterocycles. Additionally, the resonance around 800 cm^{-1} corresponds to the breathing mode of triazine components intricately linked with the modified CN heterocycles. The observed vibration peaks at 1395 , 867 , and 485 cm^{-1} are attributed to the C-F2 bending, wagging, and stretching vibrational modes, respectively. Moreover, the peak at 1185 cm^{-1} arises from the C-C bond of PVDF. In the spectrum of PVDF-HFP, peaks are observed at 611 , 872 , 1064 , 1180 , and 1400 cm^{-1} , corresponding to vinylidene, CH_2 wagging of the vinylidene band, -C-F- stretching, scissoring, and bending vibration of the vinyl group, respectively [256,257].

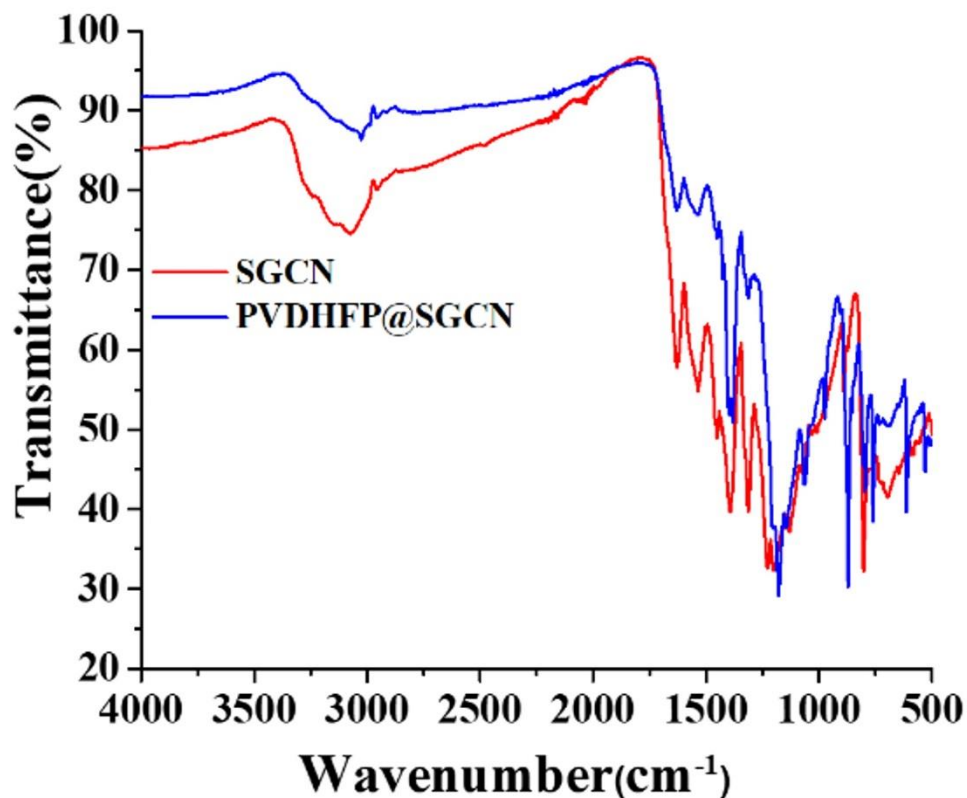


Figure 6. 7 FTIR spectra of SGCN and PVDHFP@SGCN photocatalysts. The potential was scanned at 100 mVs^{-1} .

6.3.8 XRD pattern studies

Powder X-ray crystallography is used for the investigation of the crystallinity nature of PVDHFP@SGCN, PVDHFP and SGCN photocatalysts in Figure 6.8. As per reported literature [49] the PVDHFP shows characteristic peaks at $2\theta = 20^\circ$ and 38° corresponding to the (020) and (021) [50]. These Characterstic peaks are shifted in case of PVDHFP@SGCN photocatalyst which indicate the grafting of PVDHFP on the SGCN photocatalyst.

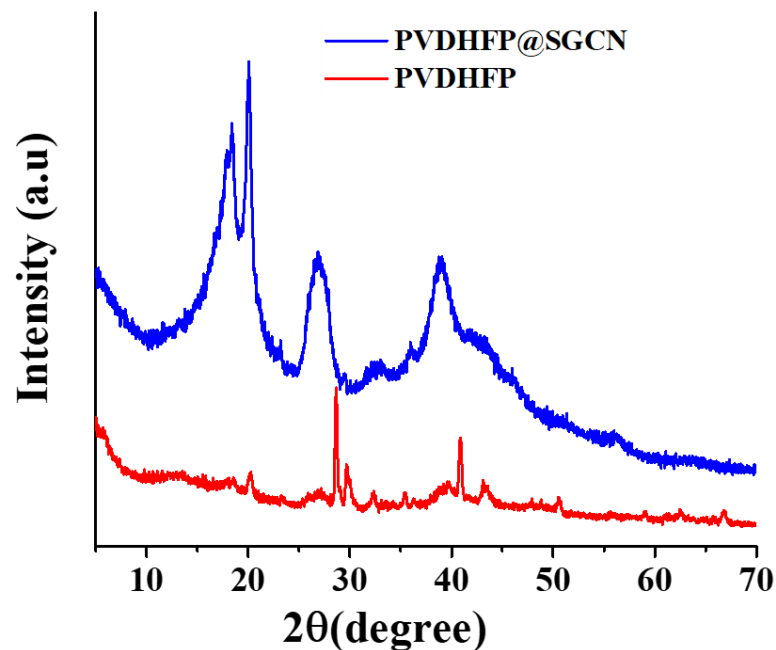


Figure 6. 8 XRD pattern of PVDF HFP and PVDHFP@SGCN photocatalysts.

6.3.9 EDS analysis and SEM analysis

To study the carbon (C), sulphur (S), nitrogen (N), and fluorine (F) element existence in the PVDHFP@SGCN photocatalyst, we carried out a detailed study on chemical compositions and element distribution by Energy-dispersive X-ray spectroscopy analysis. As shown in Figure 6.9a. C, S, N, and F elements were found and they were evenly incorporated into the PVDHFP@SGCN photocatalyst. These results confirmed that polymer grafting of PVDHFP along with elemental existence in the PVDHFP@SGCN photocatalyst [51].

To examine the morphologies of SGCN and PVDHFP@SGCN photocatalysts, we employed the scanning electronic microscopy (SEM) technique. In the SEM image of PVDHFP@SGCN the PVDHFP polymer shows a globular structure and porous regions between the globes as shown in Figure (6.9b,c). Further, the morphology of PVDHFP@SGCN changed from the morphology of SGCN which indicated the Grafting of PVDHFP on the SGCN surface [52,53].

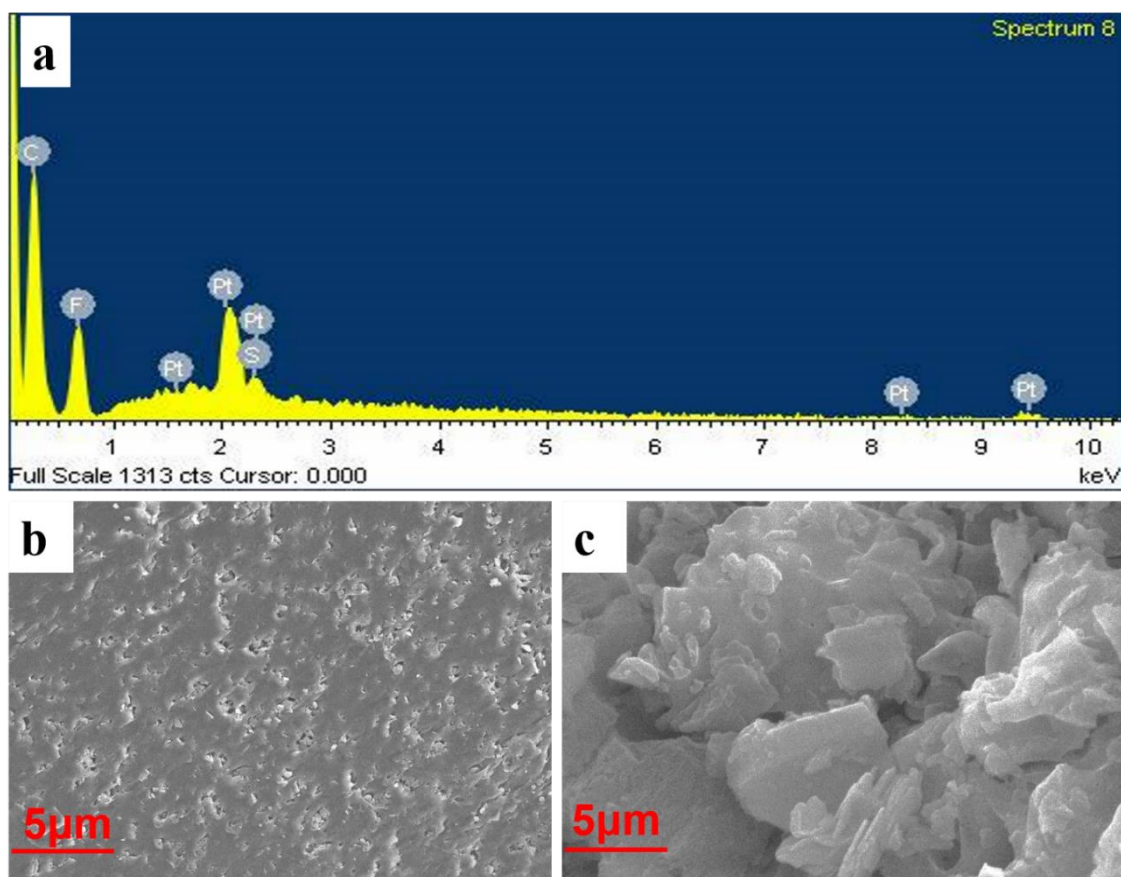


Figure 6. 9 Energy-dispersive X-ray spectroscopy (EDS) and morphology studies by field emission scanning electron microscopy (FE-SEM). The SEM images of (b) SGCN, and (c) PVDHFP@SGCN photocatalysts

6.3.10 The average particle Size

The particle size of SGCN and PVDHFP@SGCN photocatalysts was examined by using the dynamic light scattering method. Particle size plays a pivotal role in determining the photocatalytic activity of photocatalytic materials. As depicted in Figure 6.10, the particle size of the PVDHFP@SGCN photocatalyst (~15 nm) is smaller in comparison to the SGCN monomer (~90 nm). This reduction in particle size enhances the photocatalytic properties of the PVDHFP@SGCN photocatalyst, attributed to the covalent attachment of SGCN and PVDHFP. [263, 264].

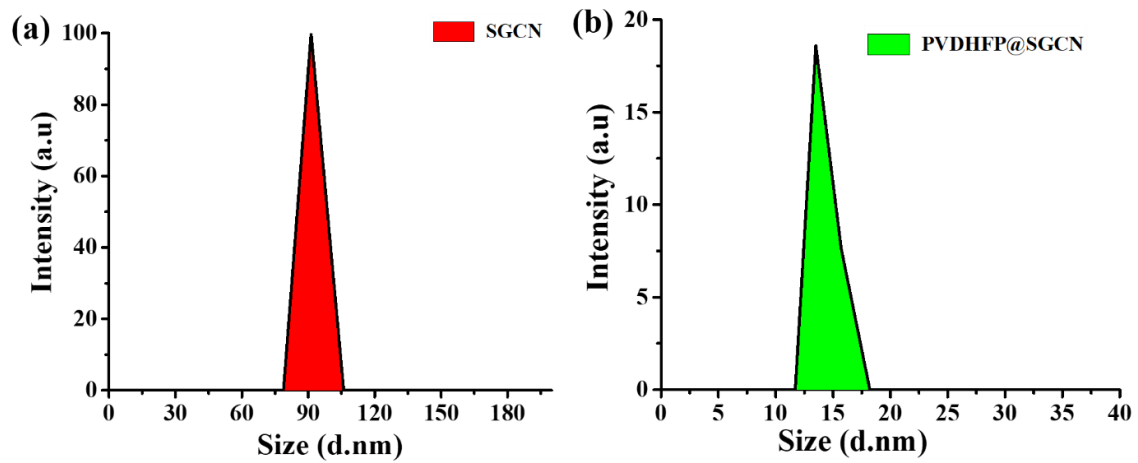


Figure 6. 10 Particle size analysis of (a) SGCN and (b) PVDHFP@SGCN photocatalysts.

CHAPTER-7

CONCLUSIONS OF RESEARCH WORK AND THEIR SCOPE IN FUTURE RESEASERCH

7.1 Conclusion

The immense potential of artificial photosynthetic systems lies in their ability to convert solar energy into valuable chemical energy through the use of photocatalysts that harness solar light. This thesis details the successful synthesis of various photocatalysts designed for solar chemical/fuel production and organic transformations. Multiple approaches were employed in this study to achieve highly active photocatalysts tailored for innovative applications. The photocatalytic activity and physiochemical properties of these custom-designed photocatalysts were assessed using various techniques, including UV-Vis, FESEM, FTIR, DLS, DFT, etc. The key findings and overall outcomes of the study are summarized below. This thesis is structured into seven chapters. The first chapter provides a concise introduction and outlines the objectives of the thesis. The second chapter delves into a comprehensive literature review on the escalating environmental issue of carbon dioxide and its fixation. Additionally, it discusses the design strategies for different types of photocatalysts intended for solar chemical and fuel production through artificial photosynthetic systems, as well as their applications in organic transformations like, C-keto sulfoxidation, and 1,3-oxathiolane-2-thiones.

Chapters three to six offer in-depth exploration of various photocatalysts and their applications in solar chemical and fuel production, along with their roles in organic transformations under solar light irradiation. In the seventh chapter, I not only summarize my work but also discuss the future scope and direction for the development of photocatalysts in solar chemical production.

Additionally, we successfully synthesized an efficient visible light-harvesting photocatalyst, the BPB-composite, to mimic natural photosynthesis for formic acid production from CO₂. The detailed description of the photocatalyst-enzyme coupled system using the synthesized photocatalyst is provided. The artificial photosynthetic process involves a series of steps initiated by electron excitation through the absorption of visible light by the photocatalyst. These electrons are then transferred to the Rh complex, resulting in the formation of NADH, which is utilized by the enzyme formate dehydrogenase to convert CO₂ to formic acid. Notably, the BPB-composite achieved an outstanding NADH yield of 82.52%. Furthermore, the BPB-composite exhibited

excellent photo and thermal stability, in addition to its effectiveness as a light-harvesting photocatalyst.

In chapter fifth we designed and synthesized new solar light active fully π -conjugated yne-linked eosin-y based photocatalyst for the transformation of CO₂ to HCOOH via artificial photosynthesis. The EY@DEHB photocatalyst has been fully characterized by spectroscopy, microscopy, XRD, and particle size analyzer techniques. The EY@DEHB photocatalyst of the photocatalyst–enzyme coupled system is highly visible light active for efficient production of HCOOH from CO₂. The artificial photosynthesis field opens many possibilities of applications for fully π -conjugated yne-linked eosin-y based materials. The presence of EY in photocatalyst makes it responsible for excellent photocatalytic activity with 77.16 % yield of NADH regeneration and 205.99 μ mol production of HCOOH from CO₂. The above result reveals the superiority of yne-linked eosin-y based photocatalyst.

In Chapter Six, we present a green and environmentally friendly approach for formic acid production. We systematically investigated the photocatalytic performance and key influencing factors for practical application of the PVDHFP@SGCN photocatalyst. The PVDHFP@SGCN photocatalyst exhibited enhanced photocatalysis for formic acid generation. This research offers a straightforward pathway for developing an environmentally benign photocatalyst with significantly improved photocatalytic activity for formic acid generation under solar light irradiation. Moreover, the PVDHFP@SGCN photocatalytic and photo-enzymatic system holds potential for a wide range of diversified applications.

Based on my comprehension, artificial photosynthesis appears to be the most favorable method for economically generating value-added chemicals and fuels through the use of affordable photocatalysts. The findings indicate that these photocatalysts exhibit considerable potential and are promising candidates deserving further investigation in both research and practical applications.

7.2 Future Scope

In this thesis, investigations delved into the realm of artificial photosynthetic systems, aiming to replicate natural photosynthesis for the synthesis of valuable chemicals and fuels.

With a significant role in pharmaceutical and medicinal chemistry, my research focuses on the synthesis of diverse solar light-harvesting photocatalysts, including graphene, carbon nitride-based materials, and covalent organic frameworks. These materials are obtained through processes like diazonium reaction, calcination, condensation reaction, and Friedel-Craft alkylation. The synthesized photocatalysts have been applied in various innovative applications such as NAD(P)H regeneration, L-glutamate production, formic acid synthesis, sulfoxidation, keto sulfoxidation, 1,3-oxathiolane-2-thiones, C-H and C-S bond activation. Their advantages in natural, biological, and pharmaceutical product contexts are evident.

In addition to these achievements, my interest extends to the design of other cost-effective and highly efficient photocatalytic materials. Future studies will explore methodologies such as cross-coupling, Diels-Alder reaction, Heck reaction, and other approaches. These efforts aim to open up new avenues for applications in value-added solar chemicals/fuels production (e.g., methanol, formaldehyde) and organic transformations like C-N and C-P bond formation, substituted benzothiazoles, aromatic benzylamine, etc. Such applications garner attention in pharmaceutical chemistry, offering societal benefits. The outlined research endeavors are presented below:

- Creating an eosin-based conjugated framework photocatalyst through cross-coupling to facilitate the synthesis of benzothiazoles from thiophenol and benzonitrile under visible light irradiation in aerobic conditions.
- Designing a porphyrin-based covalent organic framework through Friedel-Craft alkylation for the generation of formic acid from CO₂ and aromatic benzyl amine from the corresponding benzyl amine under visible light.
- Formulating a graphene-based photocatalyst through a condensation process to enable the production of methanol from CO₂.
- Developing a multicomponent polymerized photocatalyst through the linkage of alicyclic poly(oxaselenolane)s for epoxidation applications under visible light irradiation.

References

- [1] A. Reisinger and H. Clark, “How much do direct livestock emissions actually contribute to global warming?,” *Glob. Chang. Biol.*, vol. 24, no. 4, pp. 1749–1761, 2018.
- [2] S. C. Peter, “Reduction of CO₂ to chemicals and fuels: a solution to global warming and energy crisis,” *ACS Energy Lett.*, vol. 3, no. 7, pp. 1557–1561, 2018.
- [3] T. M. L. Wigley, “The Paris warming targets: emissions requirements and sea level consequences,” *Clim. Change*, vol. 147, pp. 31–45, 2018.
- [4] C.-H. Huang and C.-S. Tan, “A review: CO₂ utilization,” *Aerosol Air Qual. Res.*, vol. 14, no. 2, pp. 480–499, 2014.
- [5] F. Dong, Y. Wang, B. Su, Y. Hua, and Y. Zhang, “The process of peak CO₂ emissions in developed economies: A perspective of industrialization and urbanization,” *Resour. Conserv. Recycl.*, vol. 141, pp. 61–75, 2019.
- [6] A. Mardani, D. Streimikiene, F. Cavallaro, N. Loganathan, and M. Khoshnoudi, “Carbon dioxide (CO₂) emissions and economic growth: A systematic review of two decades of research from 1995 to 2017,” *Sci. Total Environ.*, vol. 649, pp. 31–49, 2019.
- [7] M. Khalil, J. Gunlazuardi, T. A. Ivandini, and A. Umar, “Photocatalytic conversion of CO₂ using earth-abundant catalysts: A review on mechanism and catalytic performance,” *Renew. Sustain. Energy Rev.*, vol. 113, p. 109246, 2019.
- [8] K. M. K. Yu, I. Curcic, J. Gabriel, and S. C. E. Tsang, “Recent advances in CO₂ capture and utilization,” *ChemSusChem Chem. Sustain. Energy Mater.*, vol. 1, no. 11, pp. 893–899, 2008.
- [9] L. Li, N. Zhao, W. Wei, and Y. Sun, “A review of research progress on CO₂ capture, storage, and utilization in Chinese Academy of Sciences,” *Fuel*, vol. 108, pp. 112–130, 2013.
- [10] C. Song, Q. Liu, S. Deng, H. Li, and Y. Kitamura, “Cryogenic-based CO₂ capture technologies: State-of-the-art developments and current challenges,” *Renew. Sustain. energy Rev.*, vol. 101, pp. 265–278, 2019.
- [11] Y. Duan *et al.*, “Amorphizing of Cu nanoparticles toward highly efficient and robust electrocatalyst for CO₂ reduction to liquid fuels with high faradaic

- efficiencies,” *Adv. Mater.*, vol. 30, no. 14, p. 1706194, 2018.
- [12] M. M. Zain and A. R. Mohamed, “An overview on conversion technologies to produce value added products from CH₄ and CO₂ as major biogas constituents,” *Renew. Sustain. Energy Rev.*, vol. 98, pp. 56–63, 2018.
- [13] S. Kar, A. Goeppert, V. Galvan, R. Chowdhury, J. Olah, and G. K. S. Prakash, “A carbon-neutral CO₂ capture, conversion, and utilization cycle with low-temperature regeneration of sodium hydroxide,” *J. Am. Chem. Soc.*, vol. 140, no. 49, pp. 16873–16876, 2018.
- [14] M. L. Heinnickel and A. R. Grossman, “The GreenCut: re-evaluation of physiological role of previously studied proteins and potential novel protein functions,” *Photosynth. Res.*, vol. 116, pp. 427–436, 2013.
- [15] M. F. Hohmann-Marriott and R. E. Blankenship, “Evolution of photosynthesis,” *Annu. Rev. Plant Biol.*, vol. 62, pp. 515–548, 2011, doi: 10.1146/annurev-arplant-042110-103811.
- [16] J. C. S. Costa, R. J. S. Taveira, C. F. R. A. C. Lima, A. Mendes, and L. M. N. B. F. Santos, “Optical band gaps of organic semiconductor materials,” *Opt. Mater. (Amst.)*, vol. 58, pp. 51–60, 2016, doi: 10.1016/j.optmat.2016.03.041.
- [17] F. Cui *et al.*, “Interaction of methyl viologen-induced chloroplast and mitochondrial signalling in Arabidopsis,” *Free Radic. Biol. Med.*, vol. 134, pp. 555–566, 2019.
- [18] A. Huang *et al.*, “A review of recent applications of porous metals and metal oxide in energy storage, sensing and catalysis,” *J. Mater. Sci.*, vol. 54, pp. 949–973, 2019.
- [19] R. K. Yadav *et al.*, “Highly improved solar energy harvesting for fuel production from CO₂ by a newly designed graphene film photocatalyst,” *Sci. Rep.*, vol. 8, no. 1, p. 16741, 2018.
- [20] X. Wang and C. Song, “Carbon capture from flue gas and the atmosphere: A perspective,” *Front. Energy Res.*, vol. 8, p. 560849, 2020.
- [21] B. Sertyesilisik, “Carbon Capturing Smart Construction Industry Model to Foster Green and Sustainable Total Factor Productivity Growth of Industries,” in *The Impact of Environmental Emissions and Aggregate Economic Activity on Industry: Theoretical and Empirical Perspectives*, Emerald Publishing Limited, 2023, pp. 11–23.
- [22] T. Tabanelli, D. Bonincontro, S. Albonetti, and F. Cavani, “Conversion of CO₂ to valuable chemicals: organic carbonate as green candidates for the replacement of noxious reactants,” in *Studies in Surface Science and Catalysis*, vol. 178, Elsevier, 2019, pp. 125–144.

- [23] I. Ganesh, "Electrochemical conversion of carbon dioxide into renewable fuel chemicals—The role of nanomaterials and the commercialization," *Renew. Sustain. Energy Rev.*, vol. 59, pp. 1269–1297, 2016.
- [24] Q. Liu, L. Wu, R. Jackstell, and M. Beller, "Using carbon dioxide as a building block in organic synthesis," *Nat. Commun.*, vol. 6, no. 1, pp. 1–15, 2015.
- [25] A. Modak, P. Bhanja, S. Dutta, B. Chowdhury, and A. Bhaumik, "Catalytic reduction of CO₂ into fuels and fine chemicals," *Green Chem.*, vol. 22, no. 13, pp. 4002–4033, 2020.
- [26] C.-X. Guo, R. Ma, and L.-N. He, "Metal-promoted synthesis of cyclic carbonates from 1, 2-diols and carbon dioxide," *Open Org. Chem. J.*, vol. 8, no. 1, 2014.
- [27] K. Agus Paul Setiawan *et al.*, "Unraveling the study of liquid smoke from rice husks as a green corrosion inhibitor in mild steel under 1 M HCl," *Eastern-European J. Enterp. Technol.*, vol. 5, no. 6, p. 119, 2022.
- [28] D. Yadav, R. K. Yadav, A. Kumar, N. Park, J. Y. Kim, and J. Baeg, "Fullerene polymer film as a highly efficient photocatalyst for selective solar fuel production from CO₂," *J. Appl. Polym. Sci.*, vol. 137, no. 14, p. 48536, 2020.
- [29] R. K. Yadav, A. Kumar, N. Park, D. Yadav, and J. Baeg, "New carbon nanodots-silica hybrid photocatalyst for highly selective solar fuel production from CO₂," *ChemCatChem*, vol. 9, no. 16, pp. 3153–3159, 2017.
- [30] M.-Q. Yang and Y.-J. Xu, "Photocatalytic conversion of CO₂ over graphene-based composites: current status and future perspective," *Nanoscale Horizons*, vol. 1, no. 3, pp. 185–200, 2016.
- [31] S. Liu, Z.-R. Tang, Y. Sun, J. C. Colmenares, and Y.-J. Xu, "One-dimension-based spatially ordered architectures for solar energy conversion," *Chem. Soc. Rev.*, vol. 44, no. 15, pp. 5053–5075, 2015.
- [32] M. Yang, M. Gao, M. Hong, and G. W. Ho, "Visible-to-NIR photon harvesting: progressive engineering of catalysts for solar-powered environmental purification and fuel production," *Adv. Mater.*, vol. 30, no. 47, p. 1802894, 2018.
- [33] C. Wang and D. Astruc, "Nanogold plasmonic photocatalysis for organic synthesis and clean energy conversion," *Chem. Soc. Rev.*, vol. 43, no. 20, pp. 7188–7216, 2014.
- [34] D. Ravelli, D. Dondi, M. Fagnoni, and A. Albini, "Photocatalysis. A multi-faceted concept for green chemistry," *Chem. Soc. Rev.*, vol. 38, no. 7, pp. 1999–2011, 2009.
- [35] M. R. Hoffmann, S. T. Martin, W. Choi, and D. W. Bahnemann, "Environmental applications of semiconductor photocatalysis," *Chem. Rev.*, vol. 95, no. 1, pp. 69–

96, 1995.

- [36] A. Fujishima and K. Honda, "Electrochemical photolysis of water at a semiconductor electrode," *Nature*, vol. 238, no. 5358, pp. 37–38, 1972.
- [37] M. Halmann, "Photoelectrochemical reduction of aqueous carbon dioxide on p-type gallium phosphide in liquid junction solar cells," *Nature*, vol. 275, no. 5676, pp. 115–116, 1978.
- [38] T. Inoue, A. Fujishima, S. Konishi, and K. Honda, "Photoelectrocatalytic reduction of carbon dioxide in aqueous suspensions of semiconductor powders," *Nature*, vol. 277, no. 5698, pp. 637–638, 1979.
- [39] S. Chen, T. Takata, and K. Domen, "Particulate photocatalysts for overall water splitting," *Nat. Rev. Mater.*, vol. 2, no. 10, pp. 1–17, 2017.
- [40] H. Pan and C. J. Barile, "Electrochemical CO₂ reduction to methane with remarkably high Faradaic efficiency in the presence of a proton permeable membrane," *Energy Environ. Sci.*, vol. 13, no. 10, pp. 3567–3578, 2020.
- [41] S. Yanagida, A. Kabumoto, K. Mizumoto, C. Pac, and K. Yoshino, "Poly (p-phenylene)-catalysed photoreduction of water to hydrogen," *J. Chem. Soc. Chem. Commun.*, no. 8, pp. 474–475, 1985.
- [42] S. Cao, J. Low, J. Yu, and M. Jaroniec, "Polymeric Photocatalysts Based on Graphitic Carbon Nitride," *Adv. Mater.*, vol. 27, no. 13, pp. 2150–2176, 2015, doi: 10.1002/adma.201500033.
- [43] X. Wang *et al.*, "A metal-free polymeric photocatalyst for hydrogen production from water under visible light," *Nat. Mater.*, vol. 8, no. 1, pp. 76–80, 2009.
- [44] J. Liu *et al.*, "Metal-free efficient photocatalyst for stable visible water splitting via a two-electron pathway," *Science (80-.)*, vol. 347, no. 6225, pp. 970–974, 2015.
- [45] R. K. Yadav, J.-O. Baeg, A. Kumar, K. Kong, G. H. Oh, and N.-J. Park, "Graphene–BODIPY as a photocatalyst in the photocatalytic–biocatalytic coupled system for solar fuel production from CO₂," *J. Mater. Chem. A*, vol. 2, no. 14, pp. 5068–5076, 2014.
- [46] S. Guo *et al.*, "Visible-light-driven photoreduction of CO₂ to CH₄ over N, O, P-containing covalent organic polymer submicrospheres," *ACS Catal.*, vol. 8, no. 5, pp. 4576–4581, 2018.
- [47] L. Guo and S. Jin, "Stable covalent organic frameworks for photochemical applications," *ChemPhotoChem*, vol. 3, no. 10, pp. 973–983, 2019.
- [48] R. K. Sharma *et al.*, "Recent development of covalent organic frameworks (COFs): synthesis and catalytic (organic-electro-photo) applications," *Mater. Horizons*, vol. 7, no. 2, pp. 411–454, 2020.

- [49] J. Bi *et al.*, “Covalent Triazine-Based Frameworks as Visible Light Photocatalysts for the Splitting of Water,” *Macromol. Rapid Commun.*, vol. 36, no. 20, pp. 1799–1805, 2015, doi: 10.1002/marc.201500270.
- [50] Y. Zhang and S. Jin, “Recent advancements in the synthesis of covalent triazine frameworks for energy and environmental applications,” *Polymers (Basel)*, vol. 11, no. 1, p. 31, 2018.
- [51] H. Chen, H. S. Jena, X. Feng, K. Leus, and P. Van Der Voort, “Engineering covalent organic frameworks as heterogeneous photocatalysts for organic transformations,” *Angew. Chemie Int. Ed.*, vol. 61, no. 47, p. e202204938, 2022.
- [52] M. Sachs *et al.*, “Understanding structure-activity relationships in linear polymer photocatalysts for hydrogen evolution,” *Nat. Commun.*, vol. 9, no. 1, p. 4968, 2018.
- [53] J. He, C. Wu, Y. Li, and C. Li, “Design of pre-catalysts for heterogeneous CO₂ electrochemical reduction,” *J. Mater. Chem. A*, vol. 9, no. 35, pp. 19508–19533, 2021.
- [54] P. Kumar, R. Boukherroub, and K. Shankar, “Sunlight-driven water-splitting using two-dimensional carbon based semiconductors,” *J. Mater. Chem. A*, vol. 6, no. 27, pp. 12876–12931, 2018.
- [55] W. J. Ong, L. L. Tan, Y. H. Ng, S. T. Yong, and S. P. Chai, “Graphitic Carbon Nitride (g-C₃N₄)-Based Photocatalysts for Artificial Photosynthesis and Environmental Remediation: Are We a Step Closer to Achieving Sustainability?,” *Chem. Rev.*, vol. 116, no. 12, pp. 7159–7329, 2016, doi: 10.1021/acs.chemrev.6b00075.
- [56] Y.-N. Liu *et al.*, “g-C₃N₄ hydrogen-bonding viologen for significantly enhanced visible-light photocatalytic H₂ evolution,” *ACS Catal.*, vol. 7, no. 12, pp. 8228–8234, 2017.
- [57] Y.-D. Wang, T.-W. Lee, Y.-C. Lo, W.-J. Hong, and C. Chen, “Insights into photochemical stability of graphitic carbon nitride-based photocatalysts in water treatment,” *Carbon N. Y.*, vol. 175, pp. 223–232, 2021.
- [58] D. H. Wang *et al.*, “A pure organic heterostructure of μ -oxo dimeric iron (iii) porphyrin and graphitic-C₃N₄ for solar H₂ reduction from water,” *J. Mater. Chem. A*, vol. 4, no. 1, pp. 290–296, 2016.
- [59] J. Xu, Y. Wang, and Y. Zhu, “Nanoporous graphitic carbon nitride with enhanced photocatalytic performance,” *Langmuir*, vol. 29, no. 33, pp. 10566–10572, 2013.
- [60] Y. Li, H. Zhang, P. Liu, D. Wang, Y. Li, and H. Zhao, “Cross-linked g-C₃N₄/rGO nanocomposites with tunable band structure and enhanced visible light photocatalytic activity,” *Small*, vol. 9, no. 19, pp. 3336–3344, 2013.

- [61] A. Yarahmadi and S. Sharifnia, "Dye photosensitization of ZnO with metallophthalocyanines (Co, Ni and Cu) in photocatalytic conversion of greenhouse gases," *Dye. Pigment.*, vol. 107, pp. 140–145, 2014.
- [62] Z. Peng *et al.*, "Homologous metal-free electrocatalysts grown on three-dimensional carbon networks for overall water splitting in acidic and alkaline media," *J. Mater. Chem. A*, vol. 4, no. 33, pp. 12878–12883, 2016.
- [63] J. Ren, X. Liu, L. Zhang, Q. Liu, R. Gao, and W.-L. Dai, "Thermal oxidative etching method derived graphitic C₃N₄: highly efficient metal-free catalyst in the selective epoxidation of styrene," *RSC Adv.*, vol. 7, no. 9, pp. 5340–5348, 2017.
- [64] Y. Feng *et al.*, "Facile synthesis of highly reactive and stable Fe-doped g-C₃N₄ composites for peroxymonosulfate activation: a novel nonradical oxidation process," *J. Hazard. Mater.*, vol. 354, pp. 63–71, 2018.
- [65] F. Qi, Y. Li, Y. Wang, Y. Wang, S. Liu, and X. Zhao, "Ag-Doped gC₃N₄ film electrode: fabrication, characterization and photoelectrocatalysis property," *Rsc Adv.*, vol. 6, no. 84, pp. 81378–81385, 2016.
- [66] K. Wang, Q. Li, B. Liu, B. Cheng, W. Ho, and J. Yu, "Sulfur-doped g-C₃N₄ with enhanced photocatalytic CO₂-reduction performance," *Appl. Catal. B Environ.*, vol. 176–177, pp. 44–52, 2015, doi: 10.1016/j.apcatb.2015.03.045.
- [67] J. Wei, W. Shen, J. Zhao, C. Zhang, Y. Zhou, and H. Liu, "Boron doped g-C₃N₄ as an effective metal-free solid base catalyst in Knoevenagel condensation," *Catal. Today*, vol. 316, pp. 199–205, 2018.
- [68] L. Zhou *et al.*, "Recent advances in non-metal modification of graphitic carbon nitride for photocatalysis: a historic review," *Catal. Sci. Technol.*, vol. 6, no. 19, pp. 7002–7023, 2016.
- [69] J. Zhang *et al.*, "Synthesis of a carbon nitride structure for visible-light catalysis by copolymerization," *Angew. Chemie*, vol. 2, no. 122, pp. 451–454, 2009.
- [70] J. Wen, J. Xie, X. Chen, and X. Li, "A review on g-C₃N₄-based photocatalysts," *Appl. Surf. Sci.*, vol. 391, pp. 72–123, 2017.
- [71] L. Ge *et al.*, "Synthesis and efficient visible light photocatalytic hydrogen evolution of polymeric g-C₃N₄ coupled with CdS quantum dots," *J. Phys. Chem. C*, vol. 116, no. 25, pp. 13708–13714, 2012.
- [72] X. Wang *et al.*, "Polymer semiconductors for artificial photosynthesis: Hydrogen evolution by mesoporous graphitic carbon nitride with visible light," *J. Am. Chem. Soc.*, vol. 131, no. 5, pp. 1680–1681, 2009, doi: 10.1021/ja809307s.
- [73] R. C. Pawar, S. Kang, S. H. Ahn, and C. S. Lee, "Gold nanoparticle modified graphitic carbon nitride/multi-walled carbon nanotube (gC₃N₄/CNTs/Au) hybrid

- photocatalysts for effective water splitting and degradation,” *Rsc Adv.*, vol. 5, no. 31, pp. 24281–24292, 2015.
- [74] G. Yanalak *et al.*, “Ternary nanocomposites of mesoporous graphitic carbon nitride/black phosphorus/gold nanoparticles (mpg-CN/BP-Au) for photocatalytic hydrogen evolution and electrochemical sensing of paracetamol,” *Appl. Surf. Sci.*, vol. 557, p. 149755, 2021.
- [75] M. Benaglia, A. Puglisi, and F. Cozzi, “Polymer-supported organic catalysts,” *Chem. Rev.*, vol. 103, no. 9, pp. 3401–3429, 2003, doi: 10.1021/cr010440o.
- [76] S. Busuiocanu, “CORPORAL IMMOBILIZATION REASSESSMENT ACCOUNTANCY AND TAX ALTERNATIVES,” *Bull. Transilv. Univ. Brasov. Econ. Sci. Ser. V*, vol. 5, no. 1, p. 147, 2012.
- [77] S. Naskar, S. A. Pillay, and M. Chanda, “Photocatalytic degradation of organic dyes in aqueous solution with TiO₂ nanoparticles immobilized on foamed polyethylene sheet,” *J. Photochem. Photobiol. A Chem.*, vol. 113, no. 3, pp. 257–264, 1998, doi: 10.1016/S1010-6030(97)00258-X.
- [78] A. Gu, G. Liang, and L. Lan, “Modification of polyaralkyl–phenolic resin and its copolymer with bismaleimide,” *J. Appl. Polym. Sci.*, vol. 59, no. 6, pp. 975–979, 1996.
- [79] P. C. LeBaron, Z. Wang, and T. J. Pinnavaia, “Polymer-layered silicate nanocomposites: an overview,” *Appl. Clay Sci.*, vol. 15, no. 1–2, pp. 11–29, 1999.
- [80] R. R. Tekade and S. G. Vidhale, “Advancement in Polymer Blends and Composites: A Comprehensive Review of Structural, Optical, Thermal and Electrical Attributes for Multifaceted Applications,” *Tuijin Jishu/Journal Propuls. Technol.*, vol. 44, no. 4, pp. 7190–7201, 2023.
- [81] D. V Rosato, *Plastics engineered product design*. Elsevier, 2003.
- [82] Y. Tian and G. Zhu, “Porous Aromatic Frameworks (PAFs),” *Chem. Rev.*, vol. 120, no. 16, pp. 8934–8986, 2020, doi: 10.1021/acs.chemrev.9b00687.
- [83] A. Lopez-Magano, A. Jimenez-Almarza, J. Aleman, and R. Mas-Balleste, “Metal–organic frameworks (MOFs) and covalent organic frameworks (COFs) applied to photocatalytic organic transformations,” *Catalysts*, vol. 10, no. 7, p. 720, 2020.
- [84] S. Kuecken, J. Schmidt, L. Zhi, and A. Thomas, “Conversion of amorphous polymer networks to covalent organic frameworks under ionothermal conditions: A facile synthesis route for covalent triazine frameworks,” *J. Mater. Chem. A*, vol. 3, no. 48, pp. 24422–24427, 2015, doi: 10.1039/c5ta07408h.
- [85] M. Liu, L. Guo, S. Jin, and B. Tan, “Covalent triazine frameworks: synthesis and applications,” *J. Mater. Chem. A*, vol. 7, no. 10, pp. 5153–5172, 2019.

- [86] P. Puthiaraj, Y.-R. Lee, S. Zhang, and W.-S. Ahn, "Triazine-based covalent organic polymers: design, synthesis and applications in heterogeneous catalysis," *J. Mater. Chem. A*, vol. 4, no. 42, pp. 16288–16311, 2016.
- [87] R. Ruppert, S. Herrmann, and E. Steckhan, "Very efficient reduction of NAD(P)⁺ with formate catalysed by cationic rhodium complexes," *J. Chem. Soc. Chem. Commun.*, vol. 1, no. 17, pp. 1150–1151, 1988, doi: 10.1039/C39880001150.
- [88] K. Ogawa, K. Suzuki, O. Mitsuharu, K. Yamazaki, and S. Shinkai, "The association of elevated reactive oxygen species levels from neutrophils with low-grade inflammation in the elderly," *Immun. Ageing*, vol. 5, pp. 1–8, 2008, doi: 10.1186/1742-4933-5-13.
- [89] A. Woźniacka, A. Sysa-Jędrzejowska, J. Adamus, and J. Gębicki, "Topical application of NADH for the treatment of rosacea and contact dermatitis," *Clin. Exp. Dermatol.*, vol. 28, no. 1, pp. 61–63, 2003, doi: 10.1046/j.1365-2230.2003.01118.x.
- [90] M. Kirsch and H. D. E. Groot, "NAD (P) H , a directly operating antioxidant ?," *FASEB J.*, pp. 1569–1574.
- [91] B. Halliwell and J. M. C. Gutteridge, "Role of free radicals and catalytic metal ions in human disease: An overview," *Methods Enzymol.*, vol. 186, no. C, pp. 1–85, 1990, doi: 10.1016/0076-6879(90)86093-B.
- [92] J. Alegre, J. M. Rosés, C. Javierre, A. Ruiz-Baqués, M. J. Segundo, and T. Fernández De Sevilla, "Nicotinamida adenina dinucleótido (NADH) en pacientes con síndrome de fatiga crónica," *Rev. Clin. Esp.*, vol. 210, no. 6, pp. 284–288, 2010, doi: 10.1016/j.rce.2009.09.015.
- [93] G. F. Rush, J. R. Gorski, M. G. Ripple, J. Sowinski, P. Bugelski, and W. R. Hewitt, "Organic hydroperoxide-induced lipid peroxidation and cell death in isolated hepatocytes," *Toxicol. Appl. Pharmacol.*, vol. 78, no. 3, pp. 473–483, 1985, doi: 10.1016/0041-008X(85)90255-8.
- [94] M. Rumayor, A. Dominguez-Ramos, and A. Irabien, "Formic Acid manufacture: Carbon dioxide utilization alternatives," *Appl. Sci.*, vol. 8, no. 6, p. 914, 2018.
- [95] N. Gelus, C. Bailly, F. Hamy, T. Klimkait, W. D. Wilson, and D. W. Boykin, "Inhibition of HIV-1 Tat-TAR interaction by diphenylfuran derivatives: Effects of the terminal basic side chains," *Bioorganic Med. Chem.*, vol. 7, no. 6, pp. 1089–1096, 1999, doi: 10.1016/S0968-0896(99)00041-3.
- [96] M. Delamar, G. Désarmot, O. Fagebaume, R. Hitmi, J. Pinson, and J. M. Savéant, "Modification of carbon fiber surfaces by electrochemical reduction of aryl diazonium salts: Application to carbon epoxy composites," *Carbon N. Y.*, vol. 35, no. 6, pp. 801–807, 1997, doi: 10.1016/S0008-6223(97)00010-9.

- [97] M. T. Konieczny *et al.*, “Synthesis of isomeric, oxathiolone fused chalcones, and comparison of their activity toward various microorganisms and human cancer cells line,” *Chem. Pharm. Bull.*, vol. 55, no. 5, pp. 817–820, 2007.
- [98] L. D. S. Yadav, R. K. Tripathi, R. Dwivedi, and H. Singh, “Chemoselective heterocyclizations of (4-oxo-2-thioxothiazolidin-5-yl) N-aryldithiocarbamates to antifungal 1, 3-dithiolo-, 1, 3-oxathiolo-, and thiazolothiazoles,” *J. Agric. Food Chem.*, vol. 40, no. 9, pp. 1700–1702, 1992.
- [99] H. R. Nace, “The Preparation of Olefins by the Pyrolysis of Xanthates. The C hugaev Reaction,” *Org. React.*, vol. 12, pp. 57–100, 2004.
- [100] K. M. Harmon and A. B. Harmon, “Carbonium Ion Salts. I. Tropenium and Trityl Bromoborates¹,” *J. Am. Chem. Soc.*, vol. 83, no. 4, pp. 865–871, 1961.
- [101] I. Dini, G. C. Tenore, and A. Dini, “S-alkenyl cysteine sulfoxide and its antioxidant properties from *Allium cepa* var. *tropeana* (red onion) seeds,” *J. Nat. Prod.*, vol. 71, no. 12, pp. 2036–2037, 2008.
- [102] A. A. Dar, N. Enjamuri, M. Shadab, N. Ali, and A. T. Khan, “Synthesis of unsymmetrical sulfides and their oxidation to sulfones to discover potent antileishmanial agents,” *ACS Comb. Sci.*, vol. 17, no. 11, pp. 671–681, 2015.
- [103] J. Weijlard, M. Tishler, and A. E. Erickson, “Sulfaquinoxaline and some related compounds,” *J. Am. Chem. Soc.*, vol. 66, no. 11, pp. 1957–1959, 1944.
- [104] S. W. Meyer, T. F. Mordhorst, C. Lee, P. R. Jensen, W. Fenical, and M. Köck, “Penilumamide, a novel lumazine peptide isolated from the marine-derived fungus, *Penicillium* sp. CNL-338,” *Org. Biomol. Chem.*, vol. 8, no. 9, pp. 2158–2163, 2010.
- [105] Y. Yamaguchi *et al.*, “Sulfuric odor precursor S-allyl-L-cysteine sulfoxide in garlic induces detoxifying enzymes and prevents hepatic injury,” *Antioxidants*, vol. 8, no. 9, p. 385, 2019.
- [106] R. Tiwari, P. A. Miller, S. Cho, S. G. Franzblau, and M. J. Miller, “Syntheses and antituberculosis activity of 1, 3-benzothiazinone sulfoxide and sulfone derived from BTZ043,” *ACS Med. Chem. Lett.*, vol. 6, no. 2, pp. 128–133, 2015.
- [107] P. Zhang *et al.*, “Photoenzymatic catalytic cascade system of a pyromellitic diimide/g-C₃N₄ heterojunction to efficiently regenerate NADH for highly selective CO₂ reduction toward formic acid,” *ACS Appl. Mater. Interfaces*, vol. 13, no. 39, pp. 46650–46658, 2021.
- [108] Z. Yang *et al.*, “State-of-the-art advancements in photo-assisted CO₂ hydrogenation: recent progress in catalyst development and reaction mechanisms,” *J. Mater. Chem. A*, vol. 8, no. 47, pp. 24868–24894, 2020.

- [109] Y. Liu, K. Ai, and L. Lu, "Polydopamine and its derivative materials: synthesis and promising applications in energy, environmental, and biomedical fields," *Chem. Rev.*, vol. 114, no. 9, pp. 5057–5115, 2014.
- [110] S. Cao, B. Fan, Y. Feng, H. Chen, F. Jiang, and X. Wang, "Sulfur-doped g-C₃N₄ nanosheets with carbon vacancies: General synthesis and improved activity for simulated solar-light photocatalytic nitrogen fixation," *Chem. Eng. J.*, vol. 353, pp. 147–156, 2018.
- [111] P. Xia, M. Liu, B. Cheng, J. Yu, and L. Zhang, "Dopamine modified g-C₃N₄ and its enhanced visible-light photocatalytic H₂-production activity," *ACS Sustain. Chem. Eng.*, vol. 6, no. 7, pp. 8945–8953, 2018.
- [112] X. Yang *et al.*, "Facile fabrication of acidified g-C₃N₄/g-C₃N₄ hybrids with enhanced photocatalysis performance under visible light irradiation," *Appl. Catal. B Environ.*, vol. 193, pp. 22–35, 2016.
- [113] B. Wang, J. Zhang, and F. Huang, "Enhanced visible light photocatalytic H₂ evolution of metal-free g-C₃N₄/SiC heterostructured photocatalysts," *Appl. Surf. Sci.*, vol. 391, pp. 449–456, 2017.
- [114] X. Dai *et al.*, "Metallic cobalt encapsulated in bamboo-like and nitrogen-rich carbonitride nanotubes for hydrogen evolution reaction," *ACS Appl. Mater. Interfaces*, vol. 8, no. 10, pp. 6439–6448, 2016.
- [115] X. Guan, Y. Wang, P. Luo, Y. Yu, D. Chen, and X. Li, "Incorporating N atoms into SnO₂ nanostructure as an approach to enhance gas sensing property for acetone," *Nanomaterials*, vol. 9, no. 3, p. 445, 2019.
- [116] T. W. Kim *et al.*, "Ultrafast charge transfer coupled with lattice phonons in two-dimensional covalent organic frameworks," *Nat. Commun.*, vol. 10, no. 1, 2019, doi: 10.1038/s41467-019-09872-w.
- [117] Z. Fan *et al.*, "Dual Dopamine Derived Polydopamine Coated N-Doped Porous Carbon Spheres as a Sulfur Host for High-Performance Lithium–Sulfur Batteries," *Chem. Eur. J.*, vol. 25, no. 45, pp. 10710–10717, 2019.
- [118] B. Kumru, M. Antonietti, and B. V. K. J. Schmidt, "Enhanced Dispersibility of Graphitic Carbon Nitride Particles in Aqueous and Organic Media via a One-Pot Grafting Approach," *Langmuir*, vol. 33, no. 38, pp. 9897–9906, 2017, doi: 10.1021/acs.langmuir.7b02441.
- [119] P. Singh, A. Kumar, A. P. Singh, and R. K. Yadav, "In-situ Prepared 2D Covalent Organic Framework as a Photocatalyst in the Photocatalytic-Biocatalytic Attached System for Highly Selective L-Glutamate Production under Solar Light," *Adv. Mater. Lett.*, vol. 11, no. 9, pp. 1–4, 2020, doi: 10.5185/amlett.2020.091556.
- [120] C. B. Park, S. H. Lee, E. Subramanian, B. B. Kale, S. M. Lee, and J. O. Baeg,

- “Solar energy in production of L-glutamate through visible light active photocatalyst - Redox enzyme coupled bioreactor,” *Chem. Commun.*, no. 42, pp. 5423–5425, 2008, doi: 10.1039/B808256A.
- [121] D. Huisingh, Z. Zhang, J. C. Moore, Q. Qiao, and Q. Li, “Recent advances in carbon emissions reduction: Policies, technologies, monitoring, assessment and modeling,” *J. Clean. Prod.*, vol. 103, no. May, pp. 1–12, 2015, doi: 10.1016/j.jclepro.2015.04.098.
- [122] G. P. Peters *et al.*, “The challenge to keep global warming below 2C,” *Nature Climate Change*, vol. 3, no. 1. Nature Publishing Group, pp. 4–6, Dec. 2013. doi: 10.1038/nclimate1783.
- [123] S. Sultana, P. Chandra Sahoo, S. Martha, and K. Parida, “A review of harvesting clean fuels from enzymatic CO₂ reduction,” *RSC Adv.*, vol. 6, no. 50, pp. 44170–44194, 2016, doi: 10.1039/c6ra05472b.
- [124] P. Huang *et al.*, “Selective CO₂ Reduction Catalyzed by Single Cobalt Sites on Carbon Nitride under Visible-Light Irradiation,” *J. Am. Chem. Soc.*, vol. 140, no. 47, pp. 16042–16047, 2018, doi: 10.1021/jacs.8b10380.
- [125] Y. Tamaki, T. Morimoto, K. Koike, and O. Ishitani, “Photocatalytic CO₂ reduction with high turnover frequency and selectivity of formic acid formation using Ru(II) multinuclear complexes,” *Proc. Natl. Acad. Sci. U. S. A.*, vol. 109, no. 39, pp. 15673–15678, Sep. 2012, doi: 10.1073/pnas.1118336109.
- [126] J. Barber and P. D. Tran, “From natural to artificial photosynthesis,” *J. R. Soc. Interface*, vol. 10, no. 81, p. 20120984, Apr. 2013, doi: 10.1098/rsif.2012.0984.
- [127] S. Fukuzumi, Y. M. Lee, and W. Nam, “Artificial Photosynthesis for Production of ATP, NAD(P)H, and Hydrogen Peroxide,” *ChemPhotoChem*, vol. 2, no. 3, pp. 121–135, 2018, doi: 10.1002/cptc.201700146.
- [128] M. E. El-Khouly, E. El-Mohsnawy, and S. Fukuzumi, “Solar energy conversion: From natural to artificial photosynthesis,” *J. Photochem. Photobiol. C Photochem. Rev.*, vol. 31, pp. 36–83, 2017, doi: 10.1016/j.jphotochemrev.2017.02.001.
- [129] C. Singh *et al.*, “Self-assembled carbon nitride/cobalt (III) porphyrin photocatalyst for mimicking natural photosynthesis,” *Diam. Relat. Mater.*, vol. 101, no. Iii, p. 107648, 2020, doi: 10.1016/j.diamond.2019.107648.
- [130] M. Yuan, M. J. Kummer, R. D. Milton, T. Quah, and S. D. Minteer, “Efficient NADH regeneration by a redox polymer-immobilized enzymatic system,” *ACS Catal.*, vol. 9, no. 6, pp. 5486–5495, 2019.
- [131] S. Choudhury, J.-O. Baeg, N.-J. Park, and R. K. Yadav, “A Photocatalyst/Enzyme Couple That Uses Solar Energy in the Asymmetric Reduction of Acetophenones,” *Angew. Chemie*, vol. 124, no. 46, pp. 11792–11796, 2012, doi:

10.1002/ange.201206019.

- [132] X. Yang and D. Wang, "Photocatalysis: From Fundamental Principles to Materials and Applications," *ACS Appl. Energy Mater.*, vol. 1, no. 12, pp. 6657–6693, 2018, doi: 10.1021/acsaem.8b01345.
- [133] S. Choudhury, J. O. Baeg, N. J. Park, and R. K. Yadav, "A solar light-driven, eco-friendly protocol for highly enantioselective synthesis of chiral alcohols via photocatalytic/biocatalytic cascades," *Green Chem.*, vol. 16, no. 9, pp. 4389–4400, 2014, doi: 10.1039/c4gc00885e.
- [134] R. K. Yadav *et al.*, "A photocatalyst-enzyme coupled artificial photosynthesis system for solar energy in production of formic acid from CO₂," *J. Am. Chem. Soc.*, vol. 134, no. 28, pp. 11455–11461, Jul. 2012, doi: 10.1021/JA3009902.
- [135] K. A. Brown, M. B. Wilker, M. Boehm, H. Hamby, G. Dukovic, and P. W. King, "Photocatalytic Regeneration of Nicotinamide Cofactors by Quantum Dot-Enzyme Biohybrid Complexes," *ACS Catal.*, vol. 6, no. 4, pp. 2201–2204, 2016, doi: 10.1021/acscatal.5b02850.
- [136] C. Chen *et al.*, "Ambient-Stable Black Phosphorus-Based 2D/2D S-Scheme Heterojunction for Efficient Photocatalytic CO₂ Reduction to Syngas," *ACS Appl. Mater. Interfaces*, vol. 13, no. 17, pp. 20162–20173, May 2021, doi: 10.1021/ACSAMI.1C03482.
- [137] M. Sayed *et al.*, "Sustained CO₂-photoreduction activity and high selectivity over Mn, C-codoped ZnO core-triple shell hollow spheres," *Nat. Commun.*, vol. 12, no. 1, Dec. 2021, doi: 10.1038/S41467-021-25007-6.
- [138] L. Wang, B. Cheng, L. Zhang, and J. Yu, "In situ Irradiated XPS Investigation on S-Scheme TiO₂@ZnIn₂S₄ Photocatalyst for Efficient Photocatalytic CO₂ Reduction," *Small*, vol. 17, no. 41, pp. 1–9, 2021, doi: 10.1002/sml.202103447.
- [139] D. Yadav, R. K. Yadav, A. Kumar, N. Park, and J. Baeg, "Functionalized graphene quantum dots as efficient visible-light photocatalysts for selective solar fuel production from CO₂," *ChemCatChem*, vol. 8, no. 21, pp. 3389–3393, 2016.
- [140] R. A. Salih, "Synthesis, identification and study of electrical conductivity of the doped copolymer carbazole-phenol formaldehyde," *Arab. J. Chem.*, vol. 7, no. 5, pp. 747–751, 2014, doi: 10.1016/j.arabjc.2010.12.013.
- [141] W. S. E. Solyman, H. M. Nagiub, N. A. Alian, N. O. Shaker, and U. F. Kandil, "Synthesis and characterization of phenol/formaldehyde nanocomposites: Studying the effect of incorporating reactive rubber nanoparticles or Cloisite-30B nanoclay on the mechanical properties, morphology and thermal stability," *J. Radiat. Res. Appl. Sci.*, vol. 10, no. 1, pp. 72–79, Jan. 2017, doi: 10.1016/j.jrras.2016.12.003.

- [142] C. Singh, T. W. Kim, R. K. Yadav, K. Kumar, and B. C. Yadav, "Anthracene-based g-C₃N₄ photocatalyst for regeneration of NAD(P)H and sulfide oxidation based on Z-scheme nature," *Int. J. Energy Res.*, vol. 45, no. 9, pp. 13117–13129, 2021, doi: 10.1002/er.6638.
- [143] R. K. Yadav, A. Kumar, N. J. Park, K. J. Kong, and J. O. Baeg, "A highly efficient covalent organic framework film photocatalyst for selective solar fuel production from CO₂," *J. Mater. Chem. A*, vol. 4, no. 24, pp. 9413–9418, 2016, doi: 10.1039/c6ta01625a.
- [144] T. Shah, T. Gul, and K. Saeed, "Photodegradation of bromophenol blue in aqueous medium using graphene nanoplates-supported TiO₂," *Appl. Water Sci.*, vol. 9, no. 4, pp. 1–7, 2019, doi: 10.1007/s13201-019-0983-z.
- [145] R. Raj and B. Tiwari, "Spectroscopic Investigation of Manganese (II) Bakelite Composite," *ICRTIET-2014 Conf. Proceeding*, vol. 2, no. August, pp. 66–68, 2014.
- [146] K. T. Oppelt *et al.*, "Rhodium-coordinated poly(arylene-ethynylene)- alt - Poly(arylene-vinylene) copolymer acting as photocatalyst for visible-light-powered NAD⁺/NADH reduction," *J. Am. Chem. Soc.*, vol. 136, no. 36, pp. 12721–12729, Sep. 2014, doi: 10.1021/ja506060u.
- [147] R. K. Yadav, G. H. Oh, N. J. Park, A. Kumar, K. J. Kong, and J. O. Baeg, "Highly selective solar-driven methanol from CO₂ by a photocatalyst/biocatalyst integrated system," *J. Am. Chem. Soc.*, vol. 136, no. 48, pp. 16728–16731, 2014, doi: 10.1021/ja509650r.
- [148] M. E. El-Khouly, E. El-Mohsnawy, and S. Fukuzumi, "Solar energy conversion: From natural to artificial photosynthesis," *J. Photochem. Photobiol. C Photochem. Rev.*, vol. 31, pp. 36–83, 2017, doi: 10.1016/j.jphotochemrev.2017.02.001.
- [149] C. Singh *et al.*, "Self-assembled carbon nitride/cobalt (III) porphyrin photocatalyst for mimicking natural photosynthesis," *Diam. Relat. Mater.*, vol. 101, no. Iii, p. 107648, 2020, doi: 10.1016/j.diamond.2019.107648.
- [150] M. Yuan, M. J. Kummer, R. D. Milton, T. Quah, and S. D. Minter, "Efficient NADH regeneration by a redox polymer-immobilized enzymatic system," *ACS Catal.*, vol. 9, no. 6, pp. 5486–5495, 2019.
- [151] S. Choudhury, J.-O. Baeg, N.-J. Park, and R. K. Yadav, "A Photocatalyst/Enzyme Couple That Uses Solar Energy in the Asymmetric Reduction of Acetophenones," *Angew. Chemie*, vol. 124, no. 46, pp. 11792–11796, 2012, doi: 10.1002/ange.201206019.
- [152] X. Yang and D. Wang, "Photocatalysis: From Fundamental Principles to Materials

- and Applications,” *ACS Appl. Energy Mater.*, vol. 1, no. 12, pp. 6657–6693, 2018, doi: 10.1021/acsaem.8b01345.
- [153] S. Choudhury, J. O. Baeg, N. J. Park, and R. K. Yadav, “A solar light-driven, eco-friendly protocol for highly enantioselective synthesis of chiral alcohols via photocatalytic/biocatalytic cascades,” *Green Chem.*, vol. 16, no. 9, pp. 4389–4400, 2014, doi: 10.1039/c4gc00885e.
- [154] R. K. Yadav *et al.*, “A photocatalyst-enzyme coupled artificial photosynthesis system for solar energy in production of formic acid from CO₂,” *J. Am. Chem. Soc.*, vol. 134, no. 28, pp. 11455–11461, Jul. 2012, doi: 10.1021/JA3009902.
- [155] K. A. Brown, M. B. Wilker, M. Boehm, H. Hamby, G. Dukovic, and P. W. King, “Photocatalytic Regeneration of Nicotinamide Cofactors by Quantum Dot-Enzyme Biohybrid Complexes,” *ACS Catal.*, vol. 6, no. 4, pp. 2201–2204, 2016, doi: 10.1021/acscatal.5b02850.
- [156] C. Chen *et al.*, “Ambient-Stable Black Phosphorus-Based 2D/2D S-Scheme Heterojunction for Efficient Photocatalytic CO₂ Reduction to Syngas,” *ACS Appl. Mater. Interfaces*, vol. 13, no. 17, pp. 20162–20173, May 2021, doi: 10.1021/ACSAMI.1C03482.
- [157] M. Sayed *et al.*, “Sustained CO₂-photoreduction activity and high selectivity over Mn, C-codoped ZnO core-triple shell hollow spheres,” *Nat. Commun.*, vol. 12, no. 1, Dec. 2021, doi: 10.1038/S41467-021-25007-6.
- [158] L. Wang, B. Cheng, L. Zhang, and J. Yu, “In situ Irradiated XPS Investigation on S-Scheme TiO₂@ZnIn₂S₄ Photocatalyst for Efficient Photocatalytic CO₂ Reduction,” *Small*, vol. 17, no. 41, pp. 1–9, 2021, doi: 10.1002/smll.202103447.
- [159] D. Yadav, R. K. Yadav, A. Kumar, N. Park, and J. Baeg, “Functionalized graphene quantum dots as efficient visible-light photocatalysts for selective solar fuel production from CO₂,” *ChemCatChem*, vol. 8, no. 21, pp. 3389–3393, 2016.
- [160] R. A. Salih, “Synthesis, identification and study of electrical conductivity of the doped copolymer carbazole-phenol formaldehyde,” *Arab. J. Chem.*, vol. 7, no. 5, pp. 747–751, 2014, doi: 10.1016/j.arabjc.2010.12.013.
- [161] W. S. E. Solyman, H. M. Nagiub, N. A. Alian, N. O. Shaker, and U. F. Kandil, “Synthesis and characterization of phenol/formaldehyde nanocomposites: Studying the effect of incorporating reactive rubber nanoparticles or Cloisite-30B nanoclay on the mechanical properties, morphology and thermal stability,” *J. Radiat. Res. Appl. Sci.*, vol. 10, no. 1, pp. 72–79, Jan. 2017, doi: 10.1016/j.jrras.2016.12.003.
- [162] C. Singh, T. W. Kim, R. K. Yadav, K. Kumar, and B. C. Yadav, “Anthracene-based g-C₃N₄ photocatalyst for regeneration of NAD(P)H and sulfide oxidation based

- on Z-scheme nature,” *Int. J. Energy Res.*, vol. 45, no. 9, pp. 13117–13129, 2021, doi: 10.1002/er.6638.
- [163] R. K. Yadav, A. Kumar, N. J. Park, K. J. Kong, and J. O. Baeg, “A highly efficient covalent organic framework film photocatalyst for selective solar fuel production from CO₂,” *J. Mater. Chem. A*, vol. 4, no. 24, pp. 9413–9418, 2016, doi: 10.1039/c6ta01625a.
- [164] T. Shah, T. Gul, and K. Saeed, “Photodegradation of bromophenol blue in aqueous medium using graphene nanoplates-supported TiO₂,” *Appl. Water Sci.*, vol. 9, no. 4, pp. 1–7, 2019, doi: 10.1007/s13201-019-0983-z.
- [165] R. Raj and B. Tiwari, “Spectroscopic Investigation of Manganese (II) Bakelite Composite,” *ICRTIET-2014 Conf. Proceeding*, vol. 2, no. August, pp. 66–68, 2014.
- [166] K. T. Oppelt *et al.*, “Rhodium-coordinated poly(arylene-ethynylene)- alt - Poly(arylene-vinylene) copolymer acting as photocatalyst for visible-light-powered NAD⁺/NADH reduction,” *J. Am. Chem. Soc.*, vol. 136, no. 36, pp. 12721–12729, Sep. 2014, doi: 10.1021/ja506060u.
- [167] K. T. Oppelt, E. Wöß, M. Stifinger, W. Schöfberger, W. Buchberger, and G. Knör, “Photocatalytic reduction of artificial and natural nucleotide co-factors with a chlorophyll-like tin-dihydroporphyrin sensitizer,” *Inorg. Chem.*, vol. 52, no. 20, pp. 11910–11922, 2013, doi: 10.1021/ic401611v.
- [168] R. K. Yadav, G. H. Oh, N. J. Park, A. Kumar, K. J. Kong, and J. O. Baeg, “Highly selective solar-driven methanol from CO₂ by a photocatalyst/biocatalyst integrated system,” *J. Am. Chem. Soc.*, vol. 136, no. 48, pp. 16728–16731, 2014, doi: 10.1021/ja509650r.
- [169] Nguyen, H. L.; Alzamly, A. Covalent Organic Frameworks as Emerging Platforms for CO₂ Photoreduction. *ACS Catal.* **2021**, *11*, 9809–9824.
- [170] Rangappa, A. P.; Kumar, D. P.; Wang, J.; Do, K. H.; Kim, E.; Reddy, D. A.; Ahn, H. S.; Kim, T. K. In situ growth of Ag₂S quantum dots on SnS₂ nanosheets with enhanced charge separation efficiency and CO₂ reduction performance. *J. Mater. Chem. A*, **2022**, *10*, 7291-7299.
- [171] Wang, J.; Kim, E.; Kumar, D. P.; Rangappa, A. P.; Kim, Y.; Zhang, Y.; Kim, T. K. Highly Durable and Fully Dispersed Cobalt Diatomic Site Catalysts for CO₂ Photoreduction to CH₄. *Angew. Chem. Int. Ed.* **2022**, *61*, e202113044.
- [172] (a) Tian, J.; Han, R.; Guo, Q.; Zhao, Z.; Sha, N. Direct Conversion of CO₂ into Hydrocarbon Solar Fuels by a Synergistic Photothermal Catalysis. *Catalysts* **2022**, *12*, 612; (b) Kondratenko, E. V.; Mul, G.; Baltrusaitis, J.; Larrazábal, G. O.; Pérez-Ramírez, J. Status and perspectives of CO₂ conversion into fuels and chemicals by

- catalytic, photocatalytic and electrocatalytic processes. *Energy Environ. Sci.* 2013, 6, 3112-3135.
- [173] Yadav, R. K.; Kumar, A.; Yadav, D.; Park, N.-J.; Kim, J.Y.; Baeg, J.-O. In situ prepared flexible 3D polymer film photocatalyst for highly selective solar fuel production from CO₂. *ChemCatChem*, **2018**, 10, 2024–2029.
- [174] Yadav, D.; Kumar, A.; Kim, J.Y.; Park, N.-J.; Baeg, J.-O. Interfacially synthesized 2D COF thin film photocatalyst: efficient photocatalyst for solar formic acid production from CO₂ and fine chemical synthesis. *J. Mater. Chem. A.* **2021**, 9, 9573–9580.
- [175] Cauwenbergh, R.; Das, S. Photochemical reduction of carbon dioxide to formic acid. *Green. Chem.* **2021**, 23, 2553–2574. 138 | Page
- [176] Riduan, S.N.; Zhang, Y.; Ying, J.Y. Conversion of carbon dioxide into methanol with silanes over N-heterocyclic carbene catalysts, *Angew. Chem. Int. Ed.* **2009**, 48, 3322–3325.
- [177] Ménard, G.; Stephan, D.W. Room temperature reduction of CO₂ to methanol by Al-based frustrated Lewis pairs and ammonia borane. *J. Am. Chem. Soc.* **2010**, 132, 1796–1797.
- [178] (a) Huff, C. A.; Sanford, M. S. Cascade catalysis for the homogeneous hydrogenation of CO₂ to methanol. *J. Am. Chem. Soc.* **2011**, 133, 18122–18125; (b) Jessop, P.G.; Joó, F.; Tai, C.-C. Recent advances in the homogeneous hydrogenation of carbon dioxide. *Coord. Chem. Rev.* 2004, 248, 2425–2442.
- [179] Wesselbaum, S.; Vom Stein, T.; Klankermayer J.; Leitner, W. Hydrogenation of carbon dioxide to methanol by using a homogeneous ruthenium–phosphine catalyst. *Angew. Chem. Int. Ed.* **2012**, 51, 7499–7502.
- [180] Wang, W.; Wang, S.; Ma, X.; Gong, J. Recent advances in catalytic hydrogenation of carbon dioxide. *Chem. Soc. Rev.* **2011**, 40, 3703–3727.
- [181] Ding, M.; Flaig, R. W.; Jiang, H. L.; Yaghi, O. M. Carbon Capture and Conversion using Metal-Organic Frameworks and MOF-Based Materials. *Chem. Soc. Rev.* **2019**, 48, 2783–2828.
- [182] Costentin, C.; Robert, M.; Saveant, J. M. Catalysis of the Electrochemical Reduction of Carbon Dioxide. *Chem. Soc. Rev.* **2013**, 42, 2423–2436.
- [183] Fisher B. J.; Eisenberg, R. Electrocatalytic Reduction of Carbon Dioxide by Using Macrocycles of Nickel and Cobalt. *J. Am. Chem. Soc.* **1980**, 102, 7361–7363.
- [184] Benson, E. E.; Kubiak, C. P.; Sathrum, A. J.; Smieja, J. M. Electrocatalytic and Homogeneous Approaches to Conversion of CO₂ to Liquid Fuels, *Chem. Soc. Rev.* **2009**, 38, 89–99.

- [185] Habisreutinger, S. N.; Mende L. S.; Stolarczyk, J. K. Photocatalytic Reduction of CO₂ on TiO₂ and Other Semiconductors. *Angew. Chem. Int. Ed.* **2013**, *52*, 7372-7408.
- [186] Hernandez-Alonso, M. D.; Fresno, F.; Surez, S.; Coronado, J. M. Development of Alternative Photocatalysts to TiO₂: Challenges and Opportunities. *Energy Environ. Sci.* **2009**, *2*, 1231–1257. 139 | Page
- [187] Yu, J. G.; Wang, K.; Xiao, W.; Cheng, B. Photocatalytic Reduction of CO₂ into Hydrocarbon Solar Fuels over g-C₃N₄–Pt Nanocomposite Photocatalysts. *Phys. Chem. Chem. Phys.* **2014**, *16*, 11492-11501.
- [188] Yadav, R. K.; Baeg, J.-O.; Oh, G. H.; Park, N.-J.; Kong, K.-J.; Kim, J.; Hwang, D. W.; Biswas, S. K. A Photocatalyst–Enzyme Coupled Artificial Photosynthesis System for Solar Energy in Production of Formic Acid from CO₂. *J. Am. Chem. Soc.* **2012**, *134*, 11455–11461.
- [189] Yadav, R. K.; Baeg, J. O.; Kumar, A.; Kong, K. J.; Oh, G. H.; Park, N. J. Graphene–BODIPY as a photocatalyst in the photocatalytic–biocatalytic coupled system for solar fuel production from CO₂. *J. Mater. Chem. A* **2014**, *2*, 5068-5076.
- [190]. Lee, S. H.; Nam, D. H.; Kim, J. H.; Baeg, J.O.; Park, C. B. Eosin Y-Sensitized Artificial Photosynthesis by Highly Efficient Visible-Light-Driven Regeneration of Nicotinamide Cofactor. *ChemBioChem.* **2009**, *10*, 1621-1624.
- [200] Yang, M-Q.; Gao, M.; Hong, M.; Ho, G. W. Visible-to-NIR Photon Harvesting: Progressive Engineering of Catalysts for Solar-Powered Environmental Purification and Fuel Production. *Adv. Mater.* 2018, *30*, 1802894.
- [201] Yadav, R.K.; Lee, J.O.; Kumar, A.; Park, N-J.; Yadav, D.; Kim, J. Y.; Baeg, J-O. Highly Improved Solar Energy Harvesting for Fuel Production from CO₂ by a Newly Designed Graphene Film Photocatalyst. *Sci Rep.* **2018**, *8*, 16741.
- [202] Choudhury, S.; Baeg, J-O.; Park, N-J.; Yadav, R. K. A solar light-driven, eco-friendly protocol for highly enantioselective synthesis of chiral alcohols via photocatalytic/biocatalytic cascades. *Green Chem.* **2014**,*16*, 4389-4400.
- [203] (a) Smith, B. H. Formic Acid as a Preservative. *J. Am. Chem. Soc.* **1907**, *29*, 1236–1241. (b) Hietala, J.; Vuori, A.; Johnsson, P.; Pollari, I.; Reutemann, W.; Kieczka, H. Formic Acid. *Ullmann's encycl. ind. chem.* **2016**, 1–22. (c) Marchetti, M.; Fois, M.; Ibos, L.; Dumoulin, J.; Bourson, P.; Piau, J.-M. Comparative Study in the identification of Liquid to Solid Transition Phase with DSC, Raman Spectra Analysis and Chemiometrics Methods Applied to Phase Change Materials used for Icing-Delay in Civil Engineering Infrastructures. *Appl. Therm. Eng.* **2018**, *130*, 49–61.

- [204] Reutemann, W.; Kieczka, H.; Formic Acid. *Ullmann's encycl. ind. chem.* **2012**, *16*, 13-33.
- [205] Yu, X.; Yang, Z.; Qiu, B.; Guo, S.; Yang, P.; Yu, B.; Zhang, H.; Zhao, Y.; Yang, X.; Han, B.; Liu, Z. Eosin Y-Functionalized Conjugated Organic Polymers for Visible-Light-Driven CO₂ Reduction with H₂O to CO with High Efficiency. *Angew. Chem. Int. Ed.* **2019**, *58*, 632–636.
- [206] Jiang, J-X.; Li, Y.; Wu, X.; Xiao, J.; Adams, D. J.; Cooper, A. I. Conjugated Microporous Polymers with Rose Bengal Dye for Highly Efficient Heterogeneous Organo-Photocatalysis, *Macromolecules* **2013**, *46*(22), 8779–8783.
- [207] Singh, P.; Yadav, R. K.; Kumar, K.; Lee, Y.; Gupta, A. K.; Kumar, K.; Yadav, B. C.; Singh, S. N.; Dwivedi, D. K.; Nam, S.-H.; Singh, A. P.; Kim, T. W. Eosin-Y and Sulfur-Codoped g-C₃N₄ Composite for Photocatalytic Applications: Regeneration of NADH/NADPH and Oxidation of Sulfide to Sulfoxide. *Catal. Sci. Technol.*, **2021**, *11*, 6401-6410.
- [209] Kumru, B.; Antonietti, M.; Schmidt, B.V.K.J. Enhanced dispersibility of graphitic carbon nitride particles in aqueous and organic media via a one-pot grafting approach. *Langmuir* **2017**, *33*, 9897–9906.
- [210] Dodd, A.C.; McKinley, A.J.; Saunders, M.; Tsuzuki, T. Effect of particle size on the photocatalytic activity of nanoparticulate zinc oxide. *J. Nanopart. Res.* **2006**, *8*, 43.
- [211] Yusuke Tamakia, Tatsuki Morimotoa, Kazuhide Koikeb, and Osamu Ishitania,c,1 Photocatalytic CO₂ reduction with high turnover frequency and selectivity of formic acid formation using Ru(II) multinuclear complexes, 109 (39) 15673-15678
- [212] V. Kumaravel, J. Bartlett, and S.C. Pillai, “Photoelectrochemical Conversion of Carbon Dioxide (CO₂) into Fuels and Value-Added Products,” *ACS Energy Letters*, 2020, v. 5, pp. 486–519.
- [213] M. R. Raupach, G. Marland, P. Ciais, C. Le Que´re, J. G. Canadell, G. Klepper, and C. B. Field, “Global and Regional Drivers of Accelerating CO₂ Emissions,” *Proceedings of the National Academy of Sciences of the United States of America*, 2007, v. 104, pp. 10288-10293.
- [214] M. Mikkelsen, M. Jørgensen, and F.C. Krebs, “The Teraton Challenge. A Review of Fixation and Transformation of Carbon Dioxide,” *Energy and Environmental Science*, 2010, v. 3, pp. 43–81.
- [215] J. Yu, J. Low, W. Xiao, P. Zhou, and M. Jaroniec, “Enhanced Photocatalytic CO₂-Reduction Activity of Enhanced Photocatalytic CO₂ -Reduction Activity of Anatase TiO₂ by Co-exposed and Facets,” *Journal of the American Chemical*

Society, 2014, v. 136, pp. 8839–8842.

- [216] E. J. Maginn, “What to do with CO₂,” *Journal of Physical Chemistry Letters*, 2010, v. 1, pp. 3478–3479.
- [217] Z. Sun, T. Ma, H. Tao, Q. Fan, and B. Han, “Fundamentals and Challenges of Electrochemical CO₂ Reduction Using Two-Dimensional Materials,” *Chem*, 2017, v. 3, pp. 560–587.
- [218] N. Zhang, R. Long, C. Gao, and Y. Xiong, “Recent progress on Advanced Design for Photoelectrochemical Reduction of CO₂ to fuels,” *Science China Materials*, 2018, v. 61, pp. 771–805.
- [219] Benson, E. E.; Kubiak, C. P.; Sathrum, A. J.; Smieja, J. M. *Chem.Soc. Rev.* 2009, 38, 89., Electrochemical and homogeneous approaches to conversion of CO₂ to liquid fuels.
- [220] D. Yang, H. Yu, T. He, S. Zuo, X. Liu, H. Yang, B. Ni, H. Li, L. Gu, D. Wang, and X. Wang, “Visible-Light-Switched Electron Transfer Over Single Porphyrin-Metal Atom Enter For Highly Selective Electroreduction of Carbon Dioxide,” *Nature Communications*, 2019, v. 10, pp. 1–10.
- [221] X. Liu, F. Kang, C. Hu, L. Wang, Z. Xu, D. Zheng, W. Gong, Y. Lu, Y. Ma and J. Wang, “A Genetically Encoded Photosensitizer Protein Facilitates The Rational Design of A Miniature Photocatalytic CO₂-Reducing Enzyme,” *Nature Chemistry*, 2018, v. 10, pp. 1201–1206.
- [222] J. Huang and R. Buonsanti, “Colloidal Nanocrystals as Heterogeneous Catalysts for Electrochemical CO₂ Conversion,” *Chemistry of Materials*, 2019, v. 31, pp. 13–25.
- [223] R. Currie, S. Mottaghi-Tabar, Y. Zhuang, and D.S.A. Simakov, “Design of an Air-Cooled Sabatier Reactor for Thermocatalytic Hydrogenation of CO₂: Experimental Proof-of-Concept and Model-Based Feasibility Analysis,” *Industrial and Engineering Chemistry Research*, 2019, v. 58, pp. 12964-12980.
- [224] L. Xu, Y. Xiu, F. Liu, Y. Liang, and S. Wang, “Research Progress In Conversion Of CO₂ to Valuable Fuels,” *Molecules*, 2020, v. 25, pp. 3653.
- [225] J. Barber, “Photosynthetic Energy Conversion: Natural And Artificial,” *Chemical Society Reviews*, 2009, v. 38, pp. 185–196.
- [226] T. Sagawa, R. Sueyoshi, M. Kawaguchi, M. Kudo, H. Ihara, and K. Ohkubo, “Photosensitized NADH Formation System with Multilayer TiO₂ Film,” *Chemical Communications*, 2004, v. 4, pp. 814–815.
- [227] N.L. and I. W. Z. Goren, “Photocatalysed Regeneration of Nad(P)H by Cds And

- TiO₂, Semiconductors: Applications In Enzymatic Synthesis,” *Journal of Molecular Catalysis*, 1988, v. 47, pp. 21–32.
- [228] Y. Amao and T. Watanabe, “Photochemical and Enzymatic Synthesis of Methanol from Formaldehyde with Alcohol Dehydrogenase from *Saccharomyces Cerevisiae* and Water-Soluble Zinc Porphyrin,” *Journal of Molecular Catalysis B: Enzymatic*, 2007, v. 44, pp. 27–31.
- [229] L. Yuan and Y.J. Xu, “Photocatalytic Conversion of CO₂ into Value-Added and Renewable Fuels,” *Applied Surface Science*, 2015, v. 342, pp. 154–167.
- [230] A. Dhakshinamoorthy, A.M. Asiri, and H. García, “Metal-Organic Framework (MOF) Compounds: Photocatalysts for Redox Reactions and Solar Fuel Production,” *Angewandte Chemie - International Edition*, 2016, v. 55, pp. 5414–5445.
- [231] D. Gust, T. A. Moore, and A. L. Moore, “Realizing Artificial Photosynthesis,” *Faraday Discussions*, 2012, v. 155, pp. 9–26.
- [232] Y. Tachibana, L. Vayssieres, and J. R. Durrant, “Artificial Photosynthesis for Solar Water-Splitting,” *Nature Photonics*, 2012, v. 6, pp. 511–518.
- [233] D. Gust, T. A. Moore, and A. L. Moore, “Realizing Artificial Photosynthesis,” *Faraday Discussions*, 2012, v. 155, pp. 9–26.
- [234] D. Gust, T.A. Moore, and A.L. Moore, “Fullerenes Linked to Photosynthetic Pigments,” *Research on Chemical Intermediates*, 1997, v. 23, pp. 621–651.
- [235] G. D. Scholes, G.R. Fleming, A. Olaya-Castro, and R. Van Grondelle, “Lessons from Nature About Solar Light Harvesting,” *Nature Chemistry*, 2011, v. 3, pp. 763–774.
- [236] (a) J. Su, L. Zhu, P. Geng and G. Chen, *J. Hazard. Mater.*, 2016, 316, 159–168. (b) X. Gao, H. B. Wu, L. Zheng, Y. Zhong, Y. Hu and X. W. Lou, *Angew. Chem. Int. Ed.*, 2014, 126, 6027–6031
- [237] Y. Wang, B. Gao, Q. Yue and Z. Wang, *J. Mater. Chem. A.*, 2020, 8, 19133-19155.
- [238] P. Babu, S. Mohanty, B. Naik and K. Parida, *ACS Appl. Energy Mater.*, 2018, 1, 5936–5947.
- [239] S. Ye, R. Wang, M.-Z. Wu and Y.-P. Yuan, *Appl. Surf. Sci.*, 2015, 358, 15-27.
- [240] K. Wang, Q. Li, B. Liu, B. Cheng, W. Ho and J. Yu, *Appl. Catal. B*, 2015, 176-177, 44–52.
- [241] Pooja Singh, Rajesh K. Yadav, Krishna Kumar, Yubin Lee,^b Abhishek K. Gupta,^c Kuldeep Kumar,^d B. C. Yadav,^d S. N. Singh,^e D. K. Dwivedi,^c Sang-Ho Nam,^{b,f} Atul P. Singh,^g and Tae Wu Kim,^{b,f,*} Eosin-Y and sulfur-codoped g-C₃N₄

composite for photocatalytic applications: the regeneration of NADH/NADPH and the oxidation of sulfide to sulfoxide

- [242] Fu, Q.; Ruan, Q.; McKenzie, T. G.; Reyhani, A.; Tang, J.; Qiao, G. G. Development of a robust PET-RAFT polymerization using graphitic carbon nitride (g-C₃N₄). *Macromolecules* 2017, 50, 7509–7516.
- [242] Dadashi-Silab, S.; Tasdelen, M. A.; Kiskan, B.; Wang, X.; Antonietti, M.; Yagci, Y. Photochemically mediated atom transfer radical polymerization using polymeric semiconductor mesoporous graphitic carbon nitride. *Macromol. Chem. Phys.* 2014, 215, 675–681.
- [243] Kumru, B.; Barrio, J.; Zhang, J.; Antonietti, M.; Shalom, M.; Schmidt, B. V. K. J. Robust carbon nitride-based thermoset coatings for surface modification and photochemistry. *ACS Appl. Mater. Interfaces* 2019, 11, 9462–9469.
- [244] Pan Zhang,^a Rui Li,^a Jian Huang,^a Boyu Liu,^a Mingjiong Zhou,^{*a} Bizheng Wen, Yonggao Xia^c and Shigeto Okada, Flexible poly(vinylidene fluoride-cohexafluoropropylene)- based gel polymer electrolyte for high-performance lithium-ion batteries.
- [245] Qian Cao, Baris Kumru, Markus Antonietti, and Bernhard V. K. J. Schmidt, Grafting Polymers onto Carbon Nitride via Visible-Light-Induced Photofunctionalization.
- [246] R. Ruppert, S. Herrmann, E. Steckhan, *Journal of the Chemical Society, Chemical Communications*, 1988, 17, 1150.
- [247] R. K. Yadav, J.-O. Baeg, G. H. Oh, N.-J. Park, K. Kong, J. Kim, D. W. Hwang, S. K. Biswas, *Journal of the American Chemical Society*, 2012, 134(28), 11455–11461.
- [248] B. Park, S. H. Lee, E. Subramanian, B. B. Kale, S. M. Lee, J.-O Baeg, *Chemical Communications* 2008, **42**, 5423.
- [249] Optical and structural properties of polyvinylidene fluoride (PVDF) / reduced graphene oxide (RGO) nanocomposites, A.M. Ismail, M.I. Mohammed, S.S. Fouad.
- [250] Wei Guan Gaoge Sun Lei Yin Zhenghua Zhang Shichao TianTi4O7/g-C₃N₄ Visible Light Photocatalytic Performance on Hypophosphite Oxidation: Effect of Annealing Temperature, *Front. Chem.*, 6 - 2018. |
- [251] Valentine Chikaodili Anadebe Vitalis, Ikenna Chukwuike Vinoth Selvaraj Alagarsamy Pandikumar Rakesh Chandra Barik Sulfur-doped graphitic carbon nitride (S-g-C₃N₄) as an efficient corrosion inhibitor for X65 pipeline steel in CO₂- saturated 3.5% NaCl solution: Electrochemical, XPS and Nanoindentation Studies,

- [252] Saha S, Sarkar P. Differential pulse anodic stripping voltammetry for detection of As (III) by Chitosan-Fe (OH)₃ modified glassy carbon electrode: a new approach towards speciation of arsenic. *Talanta*. 2016;158:235-245. Process Safety and Environmental Protection.
- [253] Synergistic effects of phosphorous/sulfur co-doping and morphological regulation for enhanced photocatalytic performance of graphitic carbon nitride nanosheets Xiaoxue Han¹, Aili Yuan¹, Chengkai Yao¹, Fengna Xi¹, Jiyang Liu¹, and Xiaoping Dong¹, *J Mater Sci* (2019) 54:1593–1605
- [254] Riyajuddin S, Tarik Aziz SK, Kumar S, Nessim GD, Ghosh K. 3D-graphene decorated with g-C₃N₄/Cu₃P composite: a Noble metal-free bifunctional electrocatalyst for overall water splitting. *ChemCatChem*. 2020;12:1394-1402
- [255] Capacitive and Sensing Responses of Biomass Derived Silver Decorated Graphene (Rabina Bhujel, Sadhna Rai, Khanindram Baruah, Utpal Deka, Joydeep Biswas & Bibhu P. Swain).
- [256] Poly(vinylidene fluoride) grafted polystyrene (PVDF-g-PS) membrane based on in situ polymerization for solvent resistant nanofiltration, Fang Yuan, Yi Yang, Rui Wang and Dongju Chen.
- [257] High performance dye sensitized solar cell based on electrospun poly(vinylidene fluoride-co-hexafluoropropylene)/Cobalt sulfidene nanocomposite membrane electrolyte).
- [258] MUKTA TRIPATHI, SANTOSH M BOBADE and ANUJ KUMAR, Preparation of polyvinylidene fluoride-co-hexafluoropropylene-based polymer gel electrolyte and its performance evaluation for application in EDLCs, *Bull. Mater. Sci.* (2019) 42:27.
- [259] Uniform distribution of low content BaTiO₃ nanoparticles in poly(vinylidene fluoride) nanocomposite: Toward high dielectric breakdown strength and energy storage density, Yafang Hou, Yao Wang and HongLi Gao, *RSC Adv.*, 2015,5, 72090-72098.
- [260] Raj Mohan Balakrishnan Batch and continuous studies on the removal of heavy metals from aqueous solution using biosynthesised melanin coated PVDF membranes, *Environmental Science and Pollution*, 2020, 27,3.
- [261] Hydroxyapatite deposition study through polymeric process on commercially pure Ti surfaces modified by laser beam irradiation.
- [262] Spin-coated polyvinylidene fluoride/graphene nanocomposite thin films with improved β-phase content and electrical conductivity, aryam Khosravi¹, Javad Seyfi², Ardeshir Saeidi¹, and Hossein Ali Khonakdar, *J Mater Sci* 55, 6696–6707

(2020). <https://doi.org/10.1007/s10853-020-04435-7>.

[263] B. Kumru, M. Antonietti, B. V. K. J. Schmidt, *Langmuir*, 2017, 33(38), 9897–9906.

[264] D. Li, H. Song, X. Meng, T. Shen, J. Sun, W. Han, Wang, X. *Nanomaterials*, 2020, 10(3), 546.

{Bibliography

List of Publications

- ❖ **Sandeep Kumar**, Rajesh K. Yadav, Seung Yeon Choi, Pooja Singh, and Tae Wu Kim, " An efficient polydopamine modified sulphur doped GCN photocatalyst for generation of HCOOH from CO₂ under sun ray irradiation." **Journal of Photochemistry and Photobiology A: Chemistry** 439 (2023): 114591. <https://doi.org/10.1016/j.jphotochem.2023.114591> Impact Factor: 5.141 (Published)
- ❖ **Sandeep Kumar**, Rajesh K. Yadav, Shivani Gupta, Seung Yeon Choi, and Tae Wu Kim. "A spherical photocatalyst to emulate natural photosynthesis for the production of formic acid from CO₂." *Journal of Photochemistry and Photobiology A: Chemistry* 438 (2023): 114545. <https://doi.org/10.1016/j.jphotochem.2023.114545> Impact Factor: 5.141 (Published)
- ❖ **Sandeep Kumar**, Rajesh K. Yadav, Chanadni Singh, Seung Yeon Choi, and Tae Wu Kim. " Fully π -conjugated Yne-linked Eosin-Y Based Photocatalyst for the Photoreduction of CO₂ to HCOOH." *ACS Applied Energy Materials*. Impact Factor: 6.959 (Under Review)
- ❖ **Sandeep Kumar**, Rajesh K. Yadav, Seung Yeon Choi, Pooja Singh, and Tae Wu Kim. " Nature-Inspired CO₂ Fixation Through Photopolymer Modified Sulphur Doped Graphitic Carbon Nitride Photocatalyst RSC, Catalysis Science Technology Impact Factor: 6.177(Under Review)

Curriculum Vitae

M.M.M. University of Technology Gorakhpur

Sandeep Kumar
C/O Prof. Rajesh Kumar Yadav
Professor
Artificial Photosynthesis Group
Madan Mohan Malaviya University of Technology
Gorakhpur- 273010
Contact No.: +91-9354451930
Email: sksanday@gmail.com



❖ Ph.D. Recapitulation

1. Ph.D. (Thesis submitted) under the supervision of **Prof. Rajesh Kumar Yadav** (*2% scientists listed by Stanford University in Stanford, California*)
2. Ph.D. (Chemistry): Thesis entitled “**Synthesis and Characterisation of Visible Light Responsive Photocatalysts for Solar Fuel Production and Synthesis of Fine Chemicals**” MMMUT, Gorakhpur, India.
3. Total Research Experience – 03 years

❖ Area of Research

Selective formation of Solar Fuels (HCOOH, CH₃OH), Synthesis of Ultra-responsive Covalent organic framework (COF), Polymer, Composite, Graphene quantum dots (GQDS) Photocatalyst, Organic Transformation (C-H bond Activation, C-S bond activation, Sulfoxidation, amines to Imines), Dye degradation.

❖ Academics Qualifications

Examination	Board / University	Year	Subject / Specialization	Percentage/ CGPA
Ph.D.	Madan Mohan Malaviya University of Technology	2020	Artificial Photosynthesis	7.87 CGPA
B.Ed	Ganpati Science and Technology Sahibabad Gaziabad C C S University Meerut	2007		60%

M. Sc.	J.V College Baraut Baghpat C C S University Meerut	2004	Chemistry	60.0 %
B. Sc.	J.V College Baraut Baghpat C C S University Meerut	2002	Physics & Chemistry	62.6 %
XII	D.N.Inter College Khatta Prahladpur Baghpat	1999	Physics, Chemistry & Maths	51%
X	D.A.V Inter College Tatiri Baghpat	1997	Science	56%

Technical Skills & Skills

Familiar with spectroscopic techniques such as **XRD, FTIR, UV-Vis Spectrophotometer, DRS, FTIR, ¹H NMR, ¹³C NMR, XPS spectroscopy, TGA, DSC, Zeta Potential, Particle Size, Cyclic Voltammetry, EIS, Muffle furnace Centrifuge, & Rota Vapour, etc.** for the characterization of organic derivatives.

Familiar with Windows 2007 and Windows 11, Applications, MS Word, MS Excel, MS PowerPoint, Mercury, Discovery, Chem Draw 15.0, M NOVA, Origin 2015, Chem draw 3Detc.

❖ Brief Description of Ph.D. work

During my Ph.D. at Madan Mohan Malaviya University of Technology in Gorakhpur, I focused on “**Synthesis and Characterisation of Visible Light Responsive Photocatalysts for Solar Fuel Production and Synthesis of Fine Chemicals**”. These studies were centered around the field of artificial photosynthesis and organic transformations.

In the Tenure of my research, I concentrated on synthesizing solar light-harvesting photocatalyst such as graphitic carbon nitride, graphene and covalent organic based frameworks. Additionally, I synthesized solar light-harvesting different ratio polymer

based photocatalysts through the application of key organic reactions like Sonogashira coupling, Friedel-Craft, condensation, and calcination processes. I played a key role in developing a versatile approach for synthesizing solar light-active photocatalysts via dry chemistry. These photocatalysts were covalently bonded to light-harvesting molecules.

Throughout my Ph.D. research, I am dedicated to crafting a comprehensive method for creating light-absorbing, exceptionally effective photocatalysts. These catalysts serve to regenerate NAD(P)H for solar-driven chemical processes, enabling organic transformations under solar light exposure. These transformations encompass various reactions including C-H and C-S bond activations, sulfoxidation, as well as the oxidative coupling of amines etc.

❖ List of Publications

- ❖ **Sandeep Kumar**, Rajesh K. Yadav, Seung Yeon Choi, Pooja Singh, and Tae Wu Kim, " An efficient polydopamine modified sulphur doped GCN photocatalyst for generation of HCOOH from CO₂ under sun ray irradiation." **Journal of Photochemistry and Photobiology A: Chemistry** 439 (2023): 114591. <https://doi.org/10.1016/j.jphotochem.2023.114591> Impact Factor: 5.141 (Published)
- ❖ **Sandeep Kumar**, Rajesh K. Yadav, Shivani Gupta, Seung Yeon Choi, and Tae Wu Kim. "A spherical photocatalyst to emulate natural photosynthesis for the production of formic acid from CO₂." *Journal of Photochemistry and Photobiology A: Chemistry* 438 (2023): 114545. <https://doi.org/10.1016/j.jphotochem.2023.114545> Impact Factor: 5.141 (Published)
- ❖ **Sandeep Kumar**, Rajesh K. Yadav, Chanadni Singh, Seung Yeon Choi, and Tae Wu Kim. " Fully π -conjugated Yne-linked Eosin-Y Based Photocatalyst for the Photoreduction of CO₂ to HCOOH." *ACS Applied Energy Materials*. Impact Factor: 6.959 (Under Review)
- ❖ **Sandeep Kumar**, Rajesh K. Yadav, Seung Yeon Choi, Pooja Singh, and Tae Wu Kim. " Nature-Inspired CO₂ Fixation Through Photopolymer Modified Sulphur Doped Graphitic Carbon Nitride Photocatalyst RSC, *Catalysis Science Technology* Impact Factor: 6.177(Under Review)

❖ PERSONAL DETAILS

Date of Birth	:	01 st March 1983
Gender	:	Male
Father's Name	:	Sri Subhash Chandra
Mother Name	:	Smt. Kamlesh Devi
Citizenship	:	Indian

Languages Known : Hindi & English
Religion : Hindu
Category : General

❖ REFERENCES

Prof. Rajesh Kumar Yadav Professor Madan Mohan Malaviya University of Technology Gorakhpur-273010 (INDIA) Mobile : +91- 6394483351 E-mail : rajeshkr_yadav2003@yahoo.co.in	Prof. Tae Wu Kim Professor Mokpo National University Muan-gun, Jeollanam-do, 58554 South Korea Mob. No. +82-10-6243-2565 Email: twkim@mokpo.ac.kr
---	--

Declaration: I hereby declare that the above-mentioned particulars are true to the best of my knowledge & belief.

Date: 27th January 2024

Sandeep Kumar